5-2008

Application and Optimization of Bioluminescence Resonance Energy Transfer (BRET) for Real Time Detection of Protein-Protein Interactions in Transgenic *Arabidopsis* as well as Structure-Based Functional Studies on the Active Site of Coelenterazine-dependent Luciferase from *Renilla* and its Improvement by Protein Engineering

Jongchan Woo
University of Tennessee - Knoxville

To the Graduate Council:

I am submitting herewith a dissertation written by Jongchan Woo entitled "Application and Optimization of Bioluminescence Resonance Energy Transfer (BRET) for Real Time Detection of Protein-Protein Interactions in Transgenic *Arabidopsis* as well as Structure-Based Functional Studies on the Active Site of Coelenterazine-dependent Luciferase from *Renilla* and its Improvement by Protein Engineering." I have examined the final electronic copy of this dissertation for form and content and recommend that it be accepted in partial fulfillment of the requirements for the degree of Doctor of Philosophy, with a major in Plant Sciences.

Albrecht von Arnim, Major Professor

We have read this dissertation and recommend its acceptance:

Beth Mullin, Andreas Nebenfuhr, Dan Roberts, Liz Howell

Accepted for the Council:
Dixie L. Thompson

Vice Provost and Dean of the Graduate School

(Original signatures are on file with official student records.)

To the Graduate Council:

I am submitting herewith a dissertation written by Jongchan Woo entitled “Application and Optimization of Bioluminescence Resonance Energy Transfer (BRET) for Real Time Detection of Protein-Protein Interactions in Transgenic *Arabidopsis* as well as Structure-Based Functional Studies on the Active Site of Coelenterazine-dependent Luciferase from *Renilla* and its Improvement by Protein Engineering.” I have examined the final electronic copy of this dissertation for form and content and recommend that it be accepted in partial fulfillment of the requirements for the degree of Doctor of Philosophy, with a major in Botany.

Albrecht von Arnim, Major Professor

We have read this dissertation

And recommend its acceptance:

Beth Mullin

Andreas Nebenführ

Dan Roberts

Liz Howell

Accepted for the Council:

Carolyn R. Hodges, Vice Provost and

Dean of the Graduate School

(Original signatures are on file with official student records.)

APPLICATION AND OPTIMIZATION OF BIOLUMINESCENCE RESONANCE ENERGY TRANSFER (BRET) FOR REAL TIME DETECTION OF PROTEIN-PROTEIN INTERACTIONS IN TRANSGENIC *ARABIDOPSIS* AS WELL AS STRUCTURE-BASED FUNCTIONAL STUDIES ON THE ACTIVE SITE OF COELENTERAZINE-DEPENDENT LUCIFERASE FROM *RENILLA* AND ITS IMPROVEMENT BY PROTEIN ENGINEERING

A Dissertation

Presented for the

Doctor of Philosophy Degree

The University of Tennessee, Knoxville

Jongchan Woo

May, 2008

ACKNOWLEDGEMENTS

I would like to thank all the people who have encouraged me and the Botany department as well as the BCMB department for supporting me during my Ph.D training. Most important of all, I have been amazingly fortunate to have an excellent advisor. I wish to thank my mentor Dr. Albrecht von Arnim for giving me a lot of opportunities able to study different areas of biology and for his excellent guidance. I am also grateful to my committee members, Dr. Andreas Nebenführ, Dr. Beth Mullin, Dr. Dan Roberts, and Dr. Liz Howell for sharing their knowledge and experience. Again, I deeply appreciate wonderful mentoring of all committee members. My deepest gratitude is to my mother and family since none of this would have been possible without endless love, concern, and patience of my family. Especially, I would like to thank Eunsook Park who is my colleague and wife for having been always there to listen and to give advice. Finally, I would like to express my heart-felt gratitude to my father in heaven for encouraging me throughout my life.

ABSTRACT

Bioluminescence resonance energy transfer (BRET) is a biological phenomenon in some marine organisms such as *Renilla reniformis* and *Aequorea victoria*. In BRET, resonance energy from decarboxylation of coelenterazine, a substrate of *Renilla* luciferase (RLUC), is transferred to its acceptor such as green fluorescent protein (GFP) or yellow fluorescent protein (YFP), dependent on a distance of around 5 nm between the energy donor (RLUC) and its acceptor. The activation of the energy acceptor results in a spectral change in luminescence emission. The BRET system allows investigation of *in vivo* protein-protein interactions in real time. This was demonstrated with two heterodimeric interactions in transgenic *Arabidopsis*.

In an attempt to optimize the activity and to address the reaction mechanism of the RLUC enzyme, a homology model of RLUC was obtained using a haloalkane dehalogenase, LinB, as a template. Furthermore, the homology model and the crystal structures of RLUC were docked with coelenterazine. The computational analyses suggested potential roles of catalytic triad residues (Asp120, Glu144, and His285) and substrate binding residues (N53, W121, and P220) in the active site. Mutagenesis, spectroscopy, and expression in *E. coli* were carried out to elucidate the reaction mechanism of RLUC and the possible roles of the residues. Moreover, the catalytic triad was probed using pharmacological tests. Using random mutagenesis, a new triple mutant was isolated, which showed increased k_{cat}, increased half-life, and higher resistance to substrate inhibition. These results establish enzymatic characteristics of RLUC and, furthermore, suggest that the triple mutant may result in potentially advantageous properties for BRET assays, including imaging routines in *Arabidopsis*.

TABLE OF CONTENTS

Page

LIST OF TABLES

LIST OF FIGURES

Page

Page

LIST OF ABBREVIATIONS

ABA	abscisic acid
BiFC	bimolecular fluorescence complementation
BL	blue light
BR	basic region
BRET	bioluminescence resonance energy transfer
bZIP	basic leucine zipper
CAB	chlorophyll a/b binding protein
CCD	charge-coupled device
CFP	cyan fluorescent protein
CHS	chalcone synthase
CL	continuous light
CLS	cytoplasmic localization signal
CLZ	coelenterazine
CO	CONSTANS
COP1	CONSTITUITVE PHOTOMORPHOGENIC 1
cry1 and 2	cryptochrome 1 and 2
DAPI	4’, 6-diamidino-2-phenylindole
DEPC	diethypyrocarbonate
FEDA	ferredoxin A
EF 1	elongation factor 1
FKF 1	flavin-binding, kelch repeat, F-box 1

FLUC	firefly luciferase
FR	far-red light
FRET	fluorescence resonance energy transfer
GFP	green fluorescent protein
GI	GIGANTEA
GUS	β-glucuronidase
hRLUC	humanized RLUC
HY5	elongated hypocotyl 5
HYH	HY5 homolog
LBP	luciferin binding protein
LH_2	dinoflagellate luciferin
LOV	light, oxygen, and voltage
LZIP	leucine zipper
NLS	nuclear localization signal
phot1 and 2	phototropin 1 and 2
phyA-E	phytochrome A-E
PIL5	phytochrome-interacting basic helix-loop-helix protein 5
PMSF	phenylmethanesulfonylfluoride
RBCS	rubisco small subunit
RL	red light
RLU	relative light units
RLUC	*Renilla* luciferase
rmsd	root mean square deviation

RrGFP	*Renilla reniformis* green fluorescent protein
RrLBP	*Renilla reniformis* luciferin binding protein
SCF	Skp1-Cul1-F-box
SPT	SPATULA
STH	STO homolog
STO	SALT TOLERANCE
TOC 1	timing of cab expression 1
Woodward reagent K	N-ethyl-5-phenylisoxazolium-3’-sulphonate
YFP	yellow fluorescent protein
ZTL	ZEITLUPE

CHAPTER I.

INTRODUCTION

I-1. Light impact on development of *Arabidopsis* seedlings

Since plants are non-mobile living organisms, they spend their entire lives at the spot where the seed was settled. Plants have little opportunity to select a favorable habitat but have evolved “seed dormancy” to choose a favorable time point for their birth. Although seed dormancy allows plants to avoid unfavorable environmental conditions at germination, they need to continuously monitor environmental changes from germination to death to increase the chance of survival and propagation. Misinformation about the environmental conditions may result in abnormal growth, even premature death of the plant. Environmental signals are divided into two categories; abiotic stimuli generally include light quantity/quality, temperature, water availability, air quality (CO_2 and O_2 availability), and salt concentration in the soil; biotic stimuli include signals from pathogens, herbivores, and microbial agents. Plants have evolved specific recognition systems to respond to individual stimuli and the recognition pathways appear to be interconnected, reflecting the fact that plants in nature are exposed to more than one stimulus at any given time. For example, light and cold stratification are important to break seed dormancy, and this interaction is evolutionarily conserved in some species. Plant seeds germinate more frequently under both light and cold treatment compared to either under light or under cold treatment alone, supporting the notion that individual external signal recognition events may interact (Penfield *et al*., 2005). This section reviews examples of communication between the perception cascades that process light and other external stimuli in *Arabidopsis*.

Plants have evolved several kinds of photoreceptors to continuously monitor the

light environment. *Arabidopsis* has three kinds of photoreceptors that are well characterized; 5 phytochromes (phyA-E), which are responsible for absorbing red and far red light, and cryptochromes (cry1 and 2) and phototropins (phot1 and 2), which absorb UV-A and blue light. UV-B receptors have not been identified yet. In addition, confirmed but less well-characterized photoreceptors include FKF1 (flavin-binding, kelch repeat, F-box 1) and ZTL (ZEITLUPE). The reason that FKF1 and ZTL are considered to be photoreceptors is that they have the LOV (Light, Oxygen, and Voltage) domain, which is a flavin chromophore-binding motif in the phototropin blue light photoreceptors. FKF1 may regulate flowering time of *Arabidopsis* through the regulation of the *CO* (CONSTANS) expression (Sawa *et al*., 2007). FKF1 and ZTL are also both F-box proteins, which function in the context of SCF E3 ubiquitin ligase complexes to direct the ubiquitination of specific target proteins. Both can directly interact with the light and circadian clock-regulatory GI (GIGANTEA) protein, although GI is not known to be ubiquitinated in this process. Recently, it has been found that the SCF^{ZTL} complex can recruit the central component, TOC1 (TIMING OF CAB EXPRESSION 1), indicating that ZTL may control the circadian rhythm by regulating the stability of the clock protein (Kim *et al*., 2007).

Arabidopsis can recognize light intensity, direction, duration, and wavelength through coordination between these specialized photoreceptors (Gyula *et al*., 2003). Light information absorbed by these specialized photoreceptors is transmitted through downstream signaling intermediates that play a key role in translating the acquired information into appropriate responses in plant development and physiology.

I-1-1. Light suppression of hypocotyl elongation

Light is one of the most important environmental stimuli to govern the body plan of plants. The regulatory mechanisms are complex processes mediated by transcriptional and/or posttranslational controls. In the posttranslational control mechanisms, protein-protein interactions are a common regulatory way for the relay of light stimuli from specialized photoreceptors to downstream components. In this section, it will be discussed how light signal information is translated to a response such as the inhibition of hypocotyl elongation.

Young plants that germinate under a layer of soil drive their stem growth to penetrate the soil. The genetically imprinted developmental program is to escape from darkness to reach the light, which is required for conversion of carbon dioxide to glucose and other derivative carbohydrates. For this process, hypocotyl growth of young seedlings under soil is developmentally important strategy to reach the light but this developmental program is generally shut down after the young seedlings start to harvest the light for photosynthesis. Light-mediated inhibition of hypocotyl elongation can be easily quantified due to the drastic morphological difference between light and dark germinated seedlings. In *Arabidopsis*, all known photoreceptors are involved in this response although individual receptors contribute differentially with respect to the timing and extent of the inhibition (Neff and Chory, 1998; Kang *et al*., 2008). In dark grown *Arabidopsis*, the hypocotyl elongation is maximized in comparison with any light treatment (Neff and Chory, 1998). The developmental program that is executed in darkness is termed skotomorphogenesis (synonymous with etiolation). Skoto-

morphogenic plants have a long hypocotyl, undeveloped cotyledons, and an unopened apical hook.

Comparing a seedling grown in monochromatic light with one grown in darkness, most monochromatic light treatments can inhibit hypocotyl elongation of *Arabidopsis*. At equal fluence rate, far-red light causes the strongest inhibition of hypocotyl growth, followed by blue light. Red light shows the mildest effect (Fig. I-1; Neff and Chory, 1998). Because constant monochromatic red light is perceived primarily through phyB, phyB appears to play a weaker role than other photoreceptors in the inhibition of hypocotyl elongation. Concerning blue light-specific hypocotyl inhibition, cryptochromes and phototropins are involved in this response with different inhibition kinetics (Folta and Spalding, 2001a and b). The flavin-binding cryptochromes are a homolog of type I photolyase enzymes, yet do not have photolyase activity. An extended C-terminal domain that shares homology with tropomyosin is necessary for cry signal transduction (Ahmad *et al*., 1995). Blue light-mediated phosphorylation of cryptochromes at the C-terminal end may induce the conformational change from the closed state to the open state of cryptochromes, causing recruitment of their substrates for the activation of blue light signal transduction (Yu *et al*., 2007).

Phototropin1 (phot1) is responsible for the early inhibition of hypocotyl elongation, acting within 30 min, and cryptochromes mediate a later response. This was concluded because the growth rate of the *phot1* mutant is perturbed within 30 min after blue light irradiation while *cry1* and *cry2* mutants showed a defect in growth inhibition after 30 min (Folta and Spalding, 2001a). Blue light-mediated hypocotyl growth inhibition is regulated through membrane depolarization. Additionally, the plasma membrane depolarization is

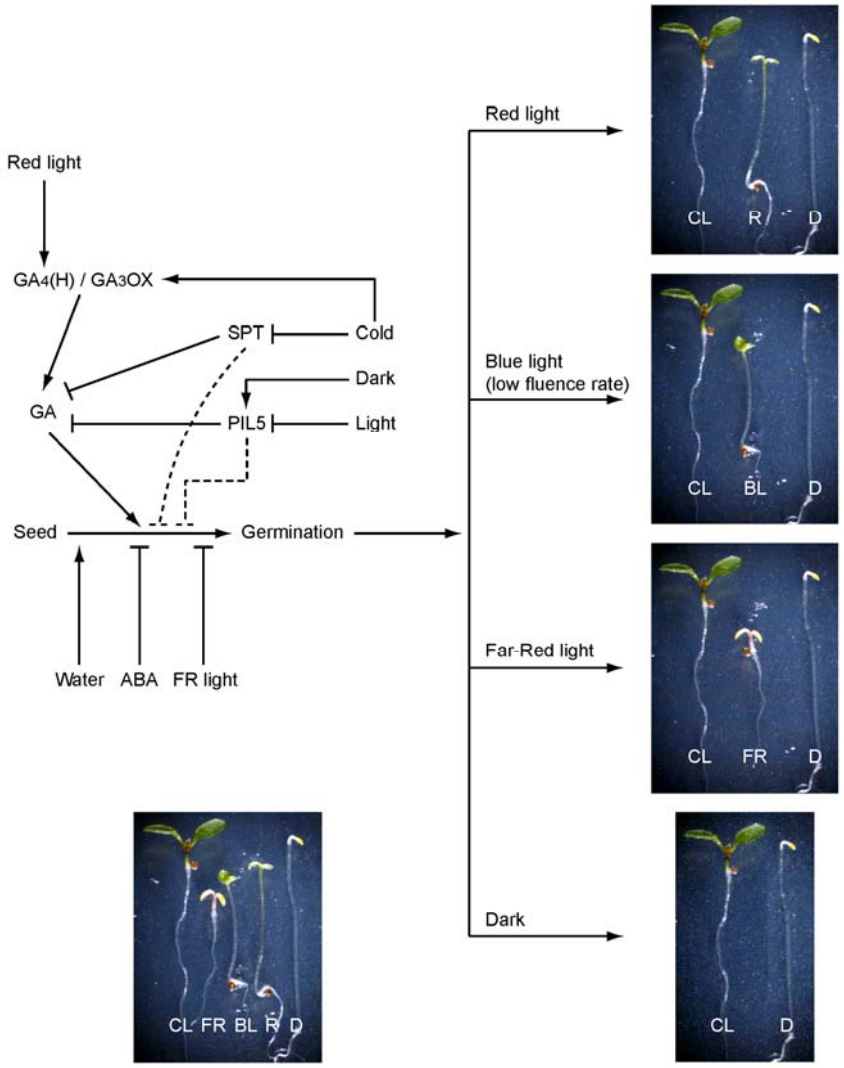

Figure I-1. Light regulation of seedling development

Red light and cold stratification activate seed germination through enhancing gibberellic acid (GA) biosynthesis, which induces a break in seed dormancy. The abiotic signals also inhibit negative regulators such as SPT and PIL5 in the GA synthetic pathway. In contrast to red light and GA, far-red light and ABA inhibit the seed germination independently. After germination, every monochromatic light inhibits hypocotyl growth (Hypocotyl length; D, Dark; R, Red light; B, Blue light; FR, Far-red light; CL, continuous white light). Seedlings shown are all 6 days old.

activated by the far-red photoreceptor, phyA, since the surface potential of the plasma membrane is dramatically reduced by a genetic lesion in phyA. However, the red light photoreceptor, phyB, does not influence this response (Folta and Spalding, 2001b). In conclusion, for the photoreceptor-mediated inhibition of hypocotyl elongation, regulation of anion channels by blue light photoreceptors and phyA, leading to plasma membrane depolarization, appears to be a critical component, notwithstanding that regulation of gene expression via phy and cry photoreceptors is likely to contribute as well. Regulation of gene expression occurs as a result of both cry and phy-mediated pathways, with phy-triggered events being far better understood. Transcription factors involved in this response include the phytochrome-interacting basic helix-loop-helix proteins of the PIF family, as well as the basic leucine zipper (bZIP) proteins, HY5 and HYH (Oyama *et al*., 1997).

Towards the goal of understanding the transition between skotomorphogenic and photomorphogenic growth, the *cop1* (constitutive photomorphogenic 1) and *det1* (deetiolated 1) mutants were striking discoveries. Both mutants showed photomorphogenic phenotypes such as a short hypocotyl as well as opened and enlarged cotyledons in the absence of light. Furthermore, transcripts of light-inducible genes such as *RBCS* (rubisco small subunit), *CAB* (chlorophyll a/b binding protein), *CHS* (chalcone synthase), and *FEDA* (ferredoxin A) were highly accumulated in the dark grown *cop1* seedling (Deng *et al*., 1991). COP1 (675 amino acids) has an N-terminal zinc-binding Ring finger motif (von Arnim and Deng, 1993), which is the hallmark motif of a subclass of E3 ubiquitin ligases, a coiled coil domain that mediates COP1 dimerization (Torii *et al*., 1998) and a WD-40 repeat domain in the C-terminus (Deng *et al*., 1992).

According to a genetic analysis, *cop1-5* was epistatic over a mutation in *HY5* that has an elongated hypocotyl in the light (Ang and Deng, 1994). *HY5* codes for a bZIP transcription factor that can bind and activate the promoter of light regulated genes such as chalcone synthase (CHS; Oyama *et al*., 1997; Ang *et al*., 1998). The genetic interaction suggested that COP1 functions as an inhibitor of photomorphogenesis and specifically, an inhibitor of HY5-mediated photomorphogenesis (Deng *et al*., 1991; Ang *et al*., 1998). In agreement with the genetic relationship, the physical interaction between COP1 and HY5 was confirmed by yeast two hybrid assay (Ang *et al*., 1998; Torii *et al*., 1998). Moreover, enhanced protein turnover of HY5 specifically under dark conditions was dependent on COP1 (Osterlund *et al*., 2000). These data underscore that COP1 is a direct inhibitor of light regulatory proteins, such as HY5. The N-terminus of HY5 (amino acids 1-77) was sufficient for the interaction with the C-terminal WD-40 domain of COP1 (Ang *et al*., 1998) through the HY5 sequence motif V-P-E/D-Φ-G (Φ: hydrophobic residue) (Ang *et al*., 1998; Holm *et al*., 2002). COP1 could ubiquitinate HY5 (Saijo *et al*., 2003) and LAF1, a myb transcription factor (long after far-red light 1; Seo *et al*., 2003). HYH (HY5 homolog) is another target for the COP1-mediated ubiquitination. Like HY5, HYH is a bZIP transcription factor, which is a positive regulator in photomorphogenesis. HYH has partially functional redundancy with HY5 but also plays a predominant role in blue light signaling (Holm *et al*., 2002). The COP1 interactive motif in HY5 is also conserved in HYH (Holm *et al*., 2002). COP1 tagged with beta-glucuronidase (GUS-COP1) is relocalized toward the nucleus upon exposure of seedlings to darkness and is preferentially excluded from the nucleus in the light (von Arnim and Deng, 1994; von Arnim *et al*., 1997). Nuclear localization signals and nuclear exclusion signals have been

delineated in the central domain of COP1 (Stacey *et al*., 1999; Subramanian *et al*., 2006). Consistent with previous observations of the genetic interaction among COP1, HY5, and HYH, the etiolation program is regulated by interactions among the COP1 repressor, and the HY5 and HYH activator proteins. In the skotomorphogenic seedlings, the transcriptional activators, HY5 and HYH, are bound to COP1 in the nucleus and in turn, HY5 and HYH are ubiquitinated by COP1 that functions as an E3 ubiquitin ligase. As a consequence, the ubiquitinated HY5 and HYH are degraded by 26S proteasome (Osterlund *et al*., 2000; Holm *et al*., 2002). However, HY5 and HYH can escape from the ubiquitination attack of COP1 due to the different localization of COP1 in response to light. Thus, plants in the light undergo photomorphogenesis.

I-1-2. A few examples for the crosstalk between the light signal transduction and other signaling cascades

The red light photoreceptor, phyB, can activate gibberellic acid (GA) biosynthesis, which stimulates germination, whereas far-red light inhibits seed germination, suggesting that red light-mediated seed germination is activated through GA biosynthesis (Fig. I-1; Yamaguchi *et al*., 1998 and 2004). As is the case with red and far-red light, light also interacts with abiotic stresses (cold, salt, and drought) to affect plant growth and development. After germination, plants must be prepared to adapt to a potentially harsh environment. To protect themselves from environmental stresses, plants have evolved elaborate control mechanisms that operate at the levels of cellular metabolism and gene expression. Interactions between light and stress signaling have recently attracted the

interest of researchers. For example, the possibility of crosstalk between light and cold signaling was highlighted by a paper showing that phyB could activate cold-inducible gene expression through the cold-regulatory C/DRE promoter sequence element (Kim *et al*., 2002). However, the components that play a key role as signal transducers between light signaling and cold stress signaling have not been identified. A second example involves the regulation of proline synthesis, which accumulates as an osmoprotectant under salt and drought stress in many species including *Arabidopsis* (Yoshiba *et al*., 1995). During proline biosynthesis, Δ^1-pyrroline-5-carboxylate synthase (P5CS) plays a dual role as both a kinase and a dehydrogenase (Hu *et al*., 1992). P5CS phosphorylates and reduces glutamate to glutamyl-5-semialdehyde (G5SA), which is converted to Δ^1-pyrroline-5-carboxylate (P5C). At the last step, P5C is reduced to proline by Δ^1-pyrroline-carboxylate reductase (P5CR). Interestingly, proline accumulation in the cell is regulated by light. In dark-adapted *Arabidopsis*, the transcription level of *P5CS* decreases, suggesting that P5CS may be a common component shared by both light signaling and stress signaling transduction (Ábrahám *et al*., 2003).

It has been suggested that plants and yeast may share a similar mechanism for resistance against salt stress. By heterologous complementation, it was demonstrated that a B-box protein, STO (salt tolerance) of *Arabidopsis*, could rescue the phenotype of the salt-sensitive yeast mutant, *cna* (calcineurin, Ca^{2+}/calmodulin-dependent Ser/Thr phosphoprotein phosphatase type 2B; Lippuner *et al*., 1996). Moreover, *Arabidopsis* plants expressing *STO* driven by the cauliflower mosaic virus 35S promoter (CaMV 35S) had longer roots than WT in high salinity media (over 50 mM NaCl), indicating that STO might be involved in the resistance to salt stress (Nagaoka and Takano, 2003). For the

function of STO in light signaling transduction, it was found that both the T-DNA insertion null mutant and the RNAi knockdown line had shorter hypocotyls than WT under red, far-red, and blue light. Furthermore, the null mutant also showed a defect in the transcriptional control of a light-inducible gene, *CHS*. In contrast, overexpressed STO could inhibit photomorphogenic characteristics such as a short hypocotyl and cotyledon expansion (Indorf *et al*., 2007). STO and a homolog, STH whose role in light signaling is less clear, could directly interact with COP1, and STO also showed interaction with HY5 (Holm *et al*., 2001; Subramanian *et al*., 2006; Datta *et al*., 2007). Taken together, the evidence strongly suggests that light signaling may be coupled with stress signal transduction.

I-2. Bioluminescence Resonance Energy Transfer (BRET)

Protein-protein interaction is one of the major ways by which biological information is transferred from signal receptors to downstream targets in the cell. Despite the importance of protein-protein interactions for signal transfer in the cell, no experimental method capable of easily investigating them *in vivo* and in real time exists. The BRET system is being developed toward this goal. Several methods have been developed to detect protein-protein interactions, such as the yeast two hybrid assay, bimolecular fluorescence complementation (BiFC), and fluorescence resonance energy transfer (FRET). Each method has some limitation. In case of the yeast two hybrid assay, the protein-protein interaction is investigated in a heterologous organism, yeast cells, and false-positives are another problem. In the BiFC system, GFP (green fluorescent

protein) is split into the N-terminal 155 or 173 residues and the remaining C-terminal part. Each half is translationally fused to one of the two candidate proteins that are to be examined for protein-protein interaction. Under spatially favorable conditions, namely, when the two halves of GFP are brought into close contact by the protein interaction between the candidates, the entire GFP can be reconstituted, and then GFP fluorescence is emitted in the presence of the excitation light source (Hu *et al*., 2002). However, after reconstitution, the functional GFP protein does not split again even when the interaction between the fused partner proteins is abolished. Due to the low dissociation constant of the GFP-halfmers, BiFC is not strictly a real-time assay (Villalobos *et al*., 2007).

The FRET assay also allows examination of protein interactions in authentic cells. Cyan fluorescent protein (CFP) and yellow fluorescent protein (YFP) are the best couple for FRET because the CFP emission spectrum is well matched with the absorption spectrum of YFP (Hink *et al*., 2002). In principle, if a protein interaction between a candidate and its partner takes place, the fluorescent tags fused to the candidates come close to each other. Upon absorption of blue light by CFP, the excitation energy can be transferred from the donor, CFP, to the acceptor, YFP. The efficiency of transfer drops with the 6^{th} power of the distance, and half-maximal transfer occurs at ~5 nm (Förster radius). FRET is a powerful technique because a protein-protein interaction can be investigated *in vivo.* However, to some degree, the external excitation light activates the resonance energy acceptor, YFP, directly, i.e. in the absence of the interaction, which is a potential source of artifacts.

Unlike FRET, the bioluminescence resonance energy transfer (BRET) system uses *Renilla* luciferase (RLUC) instead of CFP as a resonance energy donor (Xu *et al*., 1999; Subramanian *et al*., 2004a and b). Replacement of CFP with RLUC can eliminate the false-positive signal in FRET that is due to autofluorescence or excitation of YFP by the excitation light for CFP. Moreover, because no external light source is needed for activation of the energy donor, BRET can overcome another major pitfall of FRET, namely, phototoxicity. Instead, the resonance energy for activation of the energy acceptor, YFP (Xu *et al*., 1999), comes from the oxidative decarboxylation of a substrate, coelenterazine, by *Renilla* luciferase (RLUC) (Matthews *et al*., 1977a and b). The resonance energy transfer is dependent on several factors; (1) spectral overlap between the emission maximum of the energy donor and the absorption spectrum of the energy acceptor, (2) spatial configuration of tags, (3) distance between the donor and the acceptor, (4) quantum yield of the energy donor (Villalobos *et al*., 2007).

For the generation of the resonance energy, the native coelenterazine is first oxidized into a 2-hydroperoxy-coelenteramide. After abstraction of a hydrogen atom from the 2-hydroperoxy-coelenteramide, the highly reactive peroxide anion attacks a carbonyl group at the C3 carbon of the substrate, resulting in a dioxetanone intermediate (Fig. I-2B). The unstable dioxetanone luciferin converts to the excited state oxyluciferin monoanion under release of one molecule of carbon dioxide. Upon the relaxation from the excited state to the ground state, energy is released as one photon of blue bioluminescence (Deng *et al*., 2004). Alternatively, in BRET, if RLUC is brought into sufficiently close proximity to the YFP energy acceptor, the resonance energy is

Figure I-2. Different luciferins and their catalytic cascades

(A) Dinoflagellate luciferin (LH_2) is turned over in two different ways. The bioluminescence reaction of dinoflagellate luciferase is quite different from other luminescence reactions. The oxidized luciferin is converted to the electronically excited state and then the bioluminescence is emitted without a decarboxylation. The hydroxylation of dinoflagellate luciferin is a non-enzymatic reaction, resulting in weak light emission (B) Bioluminescence reactions of coelenterazine-like substrates, which are common in marine organisms. Oxidation of luciferin triggers formation of a dioxetanone intermediate, followed by decarboxylation of luciferin and light emission. (C) Firefly luciferin reaction. Firefly luciferin is adenylated, and then a peroxide anion intermediate is made by breakdown of a bond between AMP and the carboxyl group, resulting in a dioxetanone intermediate. Bioluminescence is emitted after decarboxylation upon relaxation from the excited state to the ground state.

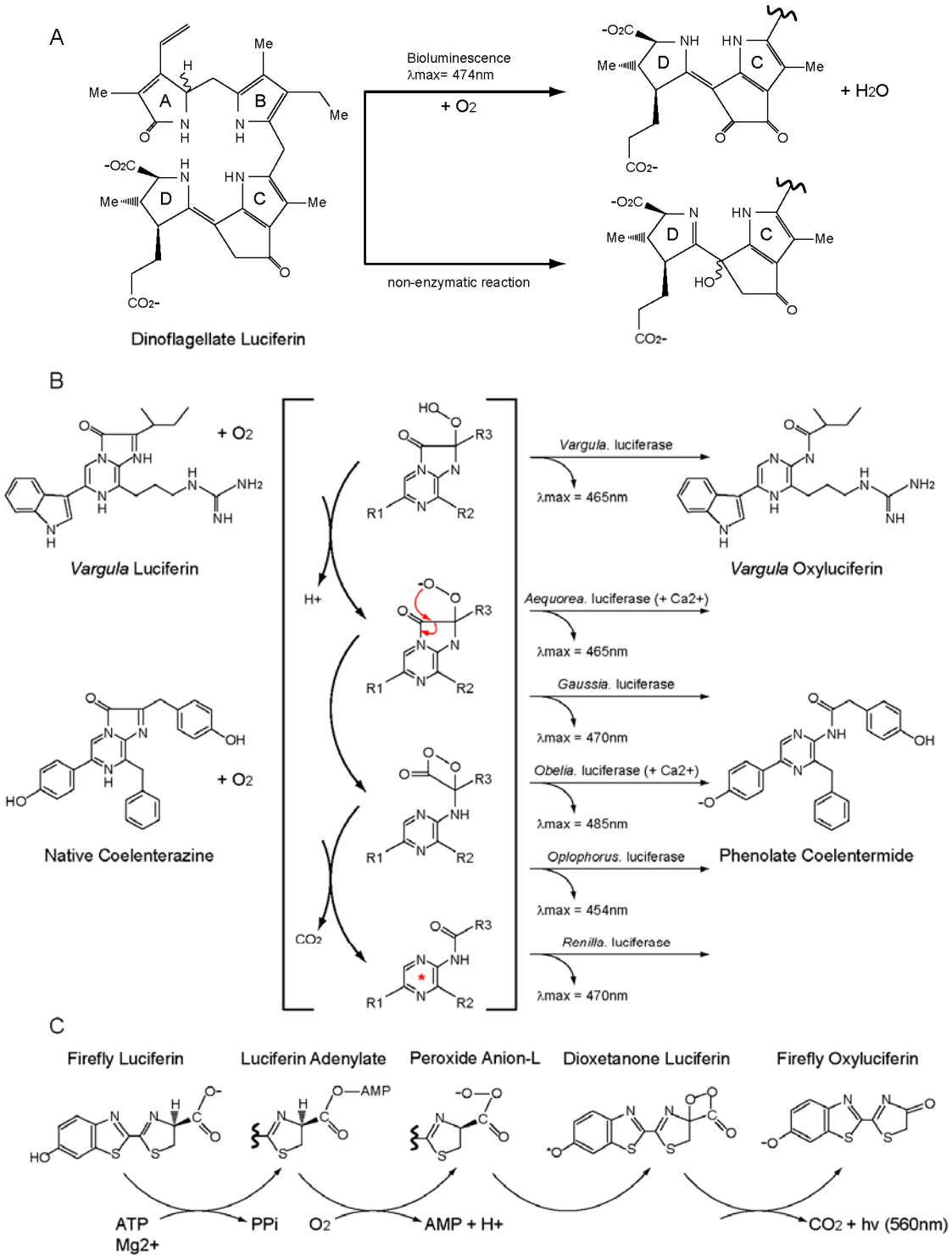

Figure I-2. Continued.

able to excite YFP (Fig. I-3). Thus, the short wavelength emission (~470 nm) from the decarboxylation by RLUC is changed to a longer wavelength (~530 nm) (Xu *et al*., 1999; Subramanian *et al*., 2006). The spectral change can be detected by a luminometer and then the ratio of yellow fluorescence to blue luminescence is calculated. The Y/B ratio in the BRET system is a variable that indicates whether a protein interaction between candidates is taking place. The Y/B ratio is not an absolute value. Therefore, it should be compared with that of positive and negative controls such as RLUC-YFP (RLUC is translationally fused to YFP; the resonance energy can be transferred optimally) and RLUC alone (no energy acceptor), respectively.

BRET has been applied to the investigation of protein interactions in the light signaling cascade of *Arabidopsis*. Two pairs of protein interactions have been tested transiently in onion epidermal cells and in stable transgenic *Arabidopsis*. One interaction is between the bZIP transcription factors HY5 and HYH and the other is between STH, which is a B-box transcription factor, and an E3 ubiquitin ligase, COP1 (See Chapter II; Subramanian *et al*., 2006). In the course of adapting BRET from bacteria to plants, the sensitivity of detection has been improved by using of a codon optimized version of RLUC, humanized RLUC (hRLUC). Furthermore, the resonance energy transfer within hRLUC-YFP was detected in subcellular organelles, indicating that coelenterazine is permeable across cell membranes (Subramanian *et al*., 2006). The next step would be to demonstrate the utility of the codon optimized cDNA for luminescence detection in *Arabidopsis*. Another goal pursued in this project was to engineer improved versions of the resonance energy donor. As will be described in Chapter III, new donors with increased stability, increased activity, or an altered emission spectrum may be useful for

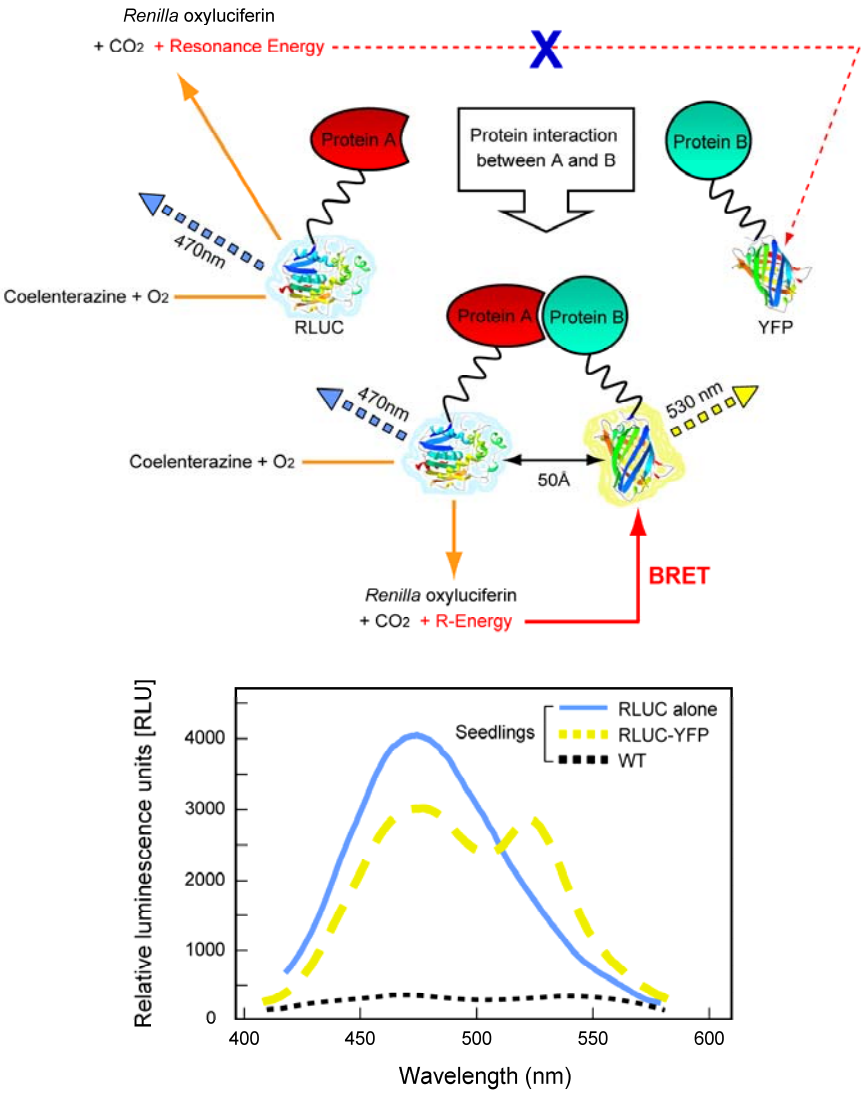

Figure I-3. Schematic diagram of BRET and the spectral shift mediated by BRET

The upper diagram shows that the resonance energy transfer from RLUC to YFP mainly depends on the distance between the BRET tags. Compared with the spectrum of an RLUC transgenic seedling, the spectrum of the RLUC-YFP seedling has an additional yellow emission peak, indicating BRET from RLUC to YFP (von Arnim, unpublished data). RLU of wild type seedling indicates background measurement. ~50Å represents Förster radius defined as the distance at which 50% of the energy generated by an energy donor can be transferred.

enhancing the sensitivity of the cuvette-based BRET assay and of BRET imaging.

I-3. Comparative enzymology of luciferases

Aside from its application as a resonance energy donor for *in vivo* protein-protein interactions (Xu *et al*., 1999; Subramanian *et al*., 2004a, b, and 2006), *Renilla* luciferase has formed the basis of protein interaction assays based on fragment complementation (split-RLUC). It is widely used as a reporter for gene expression. And, its utility has been further expanded as a probe for diagnoses of diseases such as herpes simplex virus type 1 (HSV-1) (Lucker *et al*., 2002) and tumors (Yu *et al*., 2003). Although RLUC has been popular, limited information about the enzymatic characteristics of RLUC is available. Thus, understanding the enzymatic reaction mechanisms and the structural characteristics of similar luciferases is necessary to elucidate the bioluminescence reaction of RLUC. The photoproteins aequorin and obelin are of particular interest in this respect because they utilize the same substrate, coelenterazine, as RLUC, suggesting that the turnover process of coelenterazine at the active site of RLUC may be similar with that of aequorin and obelin. Unlike aequorin and obelin, which are calcium activated, RLUC is insensitive to calcium ions, indicating that the protein structure of RLUC may be quite different from aequorin and obelin. Experiments to identify unique characteristics of RLUC should be preceded by a better understanding of the relationship between the structure, substrate turnover processes, and emission spectra of other luciferases, which may guide the formulation of testable hypotheses for characterization of RLUC.

I-3-1. Function and mechanism of bioluminescence

Luciferases are light emitting enzymes that catalyze the turnover of high-energy chemical compounds (luciferins) under production of a photon of visible light (bioluminescence). Luminescence is a natural phenomenon in which light but not heat is emitted accompanying the relaxation of a molecule from the excited state to the ground state. Bioluminescence is more common in marine organisms than in terrestrial organisms. Bioluminescence reactions have evolved from over 30 origins (Wilson and Hastings, 1998). Most luciferases share little sequence similarity, suggesting that the structures of individual luciferases may be quite distinct in a variety of organisms. The function of bioluminescence may be for communication, hunting, mating, and camouflage (Lloyd, 1965; Hastings, 1971). The regulation of the half-life of bioluminescence emission varies among different organisms in nature. Whereas most bacterial luciferases can emit bioluminescence continuously, many other organisms such as firefly and *Renilla* flash the luminescence (Wilson and Hastings, 1998). To turn bioluminescence on and off, a specialized mechanism is required. For example, bioluminescence of aequorin and obelin, which harbor calcium-binding motifs (EF-hands), is triggered when the luciferases are exposed to Ca^{2+} ions (Head *et al*., 2000; Liu *et al*., 2000; Vysotski *et al*., 2003; Deng *et al*., 2004). The dinoflagellate *Lingulodinium/Gonyaulax* has dedicated organelles known as scintillons, which contain luciferase, luciferin binding protein (LBP), and substrate. The blue bioluminescence is emitted from scintillons in response to mechanical stimuli. In the absence of the stimulus, *Gonyaulax* luciferase is inactive since LBP tightly binds to the substrate within the

scintillon at around pH 8. However, upon a rapid drop in pH to 5.7 in response to the stimulus, LBP releases the substrate, activating the luciferase. (Fogel and Hastings, 1972). Since the recombinant luciferase of the North American firefly, *Photinus pyralis*, was successfully expressed in the heterologous host, *E. coli* (de Wet *et al*., 1985), firefly luciferase has been popular in molecular biology. Moreover, firefly luciferases from other species have been isolated and characterized. Although all firefly luciferases use the same substrate, their emission maxima show considerable variability from 552 nm to 582 nm (Seliger and McElroy, 1964), indicating that the change of the emission peak might depend on the luciferase structure (de Wet *et al*., 1985), especially at the active site. Firefly luciferase requires ATP, luciferin, magnesium, and oxygen for the bioluminescence reaction (Wannlund *et al*., 1978). Due to the dependence on ATP and its relatively large size (~62 kDa), the utility of firefly luciferases is often restricted, especially in human, given that human serum normally contains ATP below 10 nM (Yegutkin *et al*., 2003). In this regard, the marine ostracod luciferases of *Vargula hilgendorfii* and *Cypridina noctiluca* are of interest because they are secreted outside of the organisms (Thompson *et al*., 1989; Nakajima *et al*., 2004). Extracellular luciferases may prove useful for cellular or biomedical applications such as the studies of the secretion pathway of insulin. *Vargula* and *Cypridina* luciferases share 83.1% amino acid similarity and their emission maxima are exactly the same at 465 nm (Nakajima *et al*., 2004). Two segments of the ~62 kDa *Vargula* luciferase showed similarity with a part of jellyfish aequorin, suggesting that these segments might be involved in the enzymatic function, while other segments might function in supporting the extracellular activity of these secreted luciferases in seawater although this needs to be confirmed

experimentally (Thompson *et al*., 1989). Unlike firefly luciferases, both *Vargula* and *Cypridina* luciferase require coelenterazine substrate and oxygen for the bioluminescence reaction (Fig. I-2B; Thompson *et al*., 1989; Nakajima *et al*., 2004). Another coelenterazine utilizing luciferase was isolated from the deep-sea shrimp, *Oplophorus gracilirostris* (Inouye *et al*., 2000). The secreted *Oplophorus* luciferase forms a heterotetrameric complex of 103 kDa molecular weight consisting of two 31 kDa and two 19 kDa subunits. The 19 kDa subunit alone has enzymatic activity with a 454 nm emission maximum (Nakamura *et al*., 1997). *Oplophorus* luciferase is attractive as a reporter molecule because it shows high activity, high quantum yield (~0.34 at 22°C), and high thermostability (active light emission up to 40°C) (Inouye *et al*., 2000). In addition, *Oplophorus* luciferase shows broad substrate specificity; a commercially available derivate of coelenterazine, *bisdeoxycoelenterazine* (DeepBlue C; Fig. I-4A), could be catalyzed more efficiently by *Oplophorus* luciferase (Nakamura *et al*., 1997) than by *Renilla* luciferase. Despite these potential advantages of the *Oplophorus* luciferase, its potential dimerization activity hampers its experimental application as an energy donor in the bioluminescence resonance energy transfer (BRET) for the study of protein-protein interactions.

The jellyfish, *Aequorea*, photoprotein (aequorin) has become increasingly popular as an intracellular calcium sensor since the first successful measurement of intracellular calcium concentration in the giant single muscle fiber of the acorn barnacle was performed (Ridgway and Ashley, 1967). Another calcium dependent photoprotein, obelin, from the hydroid *Obelia geniculata* showed stable activity from pH 5 to 8 at 3.5°C but inhibition by a dication, Mg^{2+} (Campbell, 1974). These two EF-hand photoproteins

Figure I-4. Coelenterazine variants and relative luciferase activities

(A) Structures of thirteen commercially available coelenterazine variants. *EnduRen* and *ViviRen* are especially used in animal experiments. The added side groups are meant to stabilize the substrate in the extracellular space, they are cleaved off by intracellular esterases (Otto-Duessel *et al*., 2006). (B) The normalized *in vitro* relative light units (RLU; wild type activity=100%) and the emission maxima of coelenterazine variants catalyzed by His-RLUC. Native coelenterazine shows the highest bioluminescence. Minor changes of substrates affect the enzyme activity of RLUC. Coelenterazine *hcp* and Deepblue C show blue shifted emission maxima (See Chapter III). Due to the broad range of the emission peak, the emission maximum of coelenterazine *e* has not been determined. Error bars denote standard deviations (n=3).

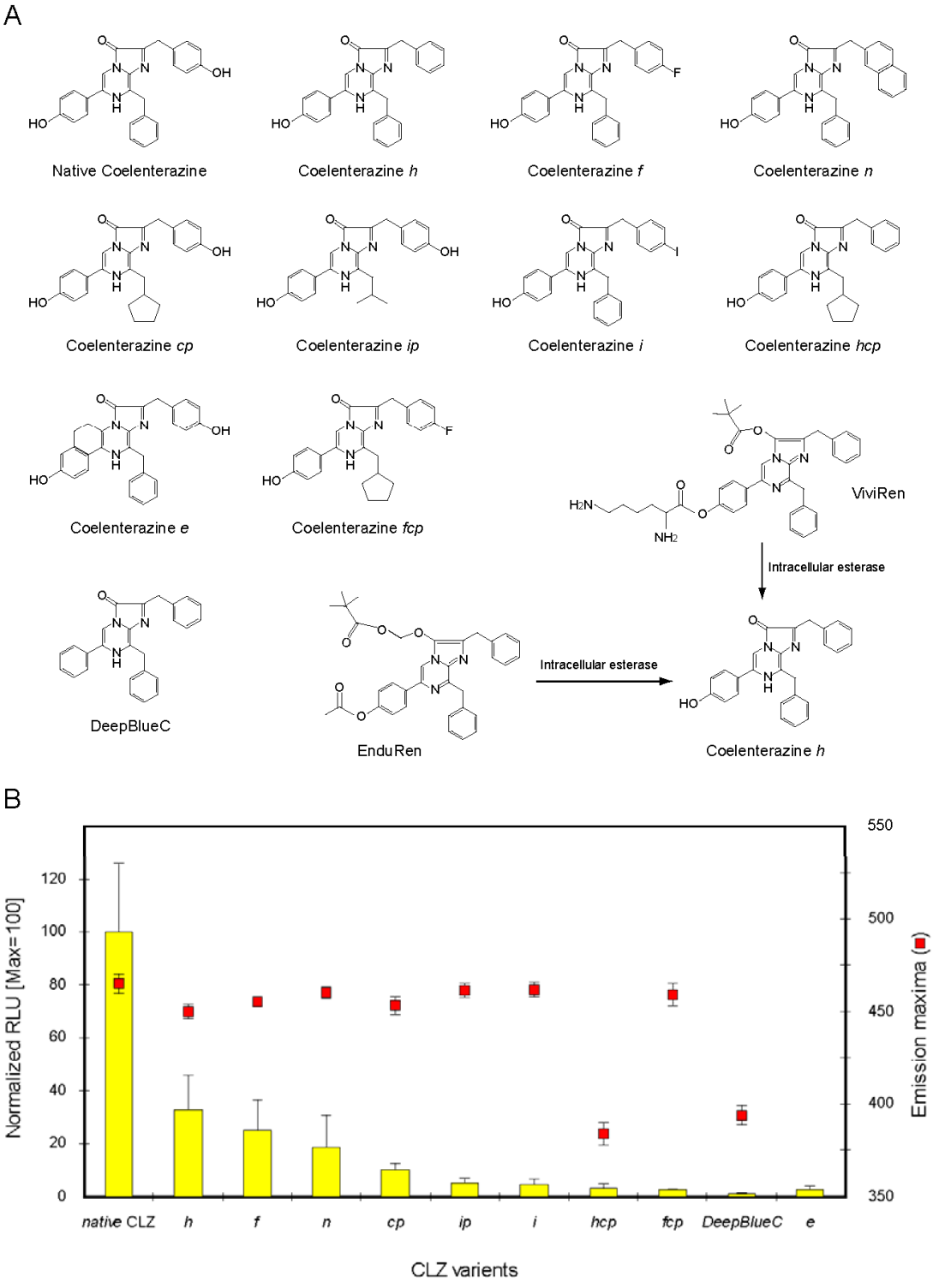

Figure I-4. Continued.

(Moncrief *et al*., 1990) are capable of oxidizing the same substrate, coelenterazine, and then releasing carbon dioxide, although the emission peak of the calcium-discharged obelin was longer (~485 nm) than that of aequorin (~465 nm) (Markova *et al*., 2002). According to the crystal structures of these two calcium-stimulated photoproteins in the presence or absence of the coelenterazine ligand, the two are structurally and functionally similar to each other (Head *et al*., 2000; Liu *et al*., 2000; Vysotski *et al*., 2003; Deng *et al*., 2004). In their active sites, coelenterazine reacts with molecular oxygen in a reaction coordinated by a catalytic triad of tyrosine (Y184 and Y190 in apo-aequorin and obelin, respectively), tryptophan (W173 and W179), and histidine (H169 and H175). In the sequential bioluminescence reaction of coelenterazine by obelin, a native coelenterazine (Fig. I-5A; R1, para-hydroxy-benzyl; R2, benzyl; R3, para-hydroxy-benzyl) reacts with oxygen at the C2 position to form a 2-hydroperoxy-coelenterazine (Fig. I-5B). H175 is kept protonated by Y190, and the side chain of W179 interacts with the carbonyl group at the C3 position. The 2-hydroxy-coelenterazine forms a hydrogen bond with the hydroxyl group of the nucleophilic Tyr190 of the catalytic triad, and this results in production of a peroxide anion (Fig. I-5C). A dioxetanone luciferin is produced by the attack of the peroxide anion (Fig. I-5D), and then the excited state coelenteramide is made after catalyzing the decarboxylation of the dioxetanone luciferin (Fig. I-5E). A photon of blue (~480 nm) light is emitted when the excited intermediate, the oxyluciferin monoanion (Fig. I-5E), is stabilized to the ground state oxyluciferin (Liu *et al*., 2006). Both obelin and aequorin crystal structures show Ca^{2+} binding EF-hand motifs, which are important to trigger the substrate catalysis (Head *et al*., 2000; Deng *et al.*, 2004).

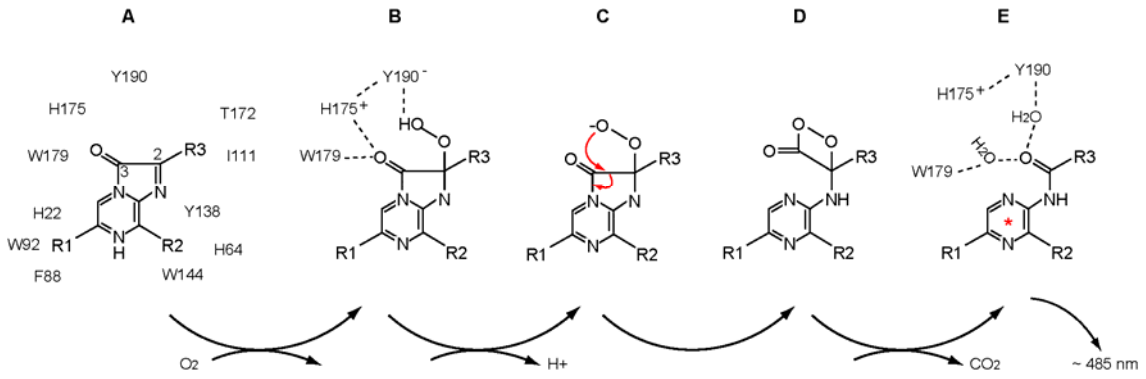

Figure I-5. Catalytic cascade of the substrate of obelin

(A) Native coelenterazine with para-hydroxy benzyl rings attached at the R1 and the R3 positions as well as a benzyl ring at the R2. Eleven residues near coelenterazine in the active site are presented. (B) Oxidized native coelenterazine is converted to 2-hydroperoxy-coelenterazine of which the hydroxyl group interacts with the deprotonated Y190 for abstraction of a proton from the 2-hydroperoxy group while protonated H175 and W179 interact with the C3 carbonyl in the active site. (C) After the deprotonation, a highly active peroxide anion intermediate is made, followed by an internal nucleophilic attack to the C3 carbon. (D) Unstable dioxetanone luciferin is produced. (E) The dioxetanone luciferin is converted to the excited state of the *Renilla* oxyluciferin by the decarboxylation. When the excited state of the *Renilla* oxyluciferin relaxes to the ground state, the energy is released as blue bioluminescence. The C2 carbonyl group of the final byproduct forms water-mediated hydrogen bonds with W179 and Y190 of the catalytic triad, causing the oxyluciferin byproduct to remain bound at the active site before charging new calcium ions into EF-hand motifs. Broken lines represent hydrogen bonds and red arrows indicate the nucleophilic attack. Red asterisk indicates the electronically excited coelenteramide (oxyluciferin) (Deng *et al*., 2004).

In obelin, the EF-hand IV is most important since the Ca^{2+} binding to the EF-hand IV results in the perpendicular repositioning of the imidazole ring of His175, which is a residue of the catalytic triad in the active site (Liu *et al*., 2006). Spent aequorin cannot trigger a new oxidation reaction of a second substrate molecule. It was confirmed *in vitro* that the removal of byproduct from the active site and the recruitment of a fresh substrate required the concomitant EF-hand modification by fresh calcium ions (Shimomura and Johnson, 1975). For controlling the emission maxima of the photoproteins, a second tryptophan in the active site in both aequorin and obelin is of importance for regulating the protonation status of the reaction intermediate, oxyluciferin (coelenteramide). W92 of obelin and W86 of aequorin have spatially identical positions in the active sites (Head *et al*., 2000; Liu *et al*, 2000) and are responsible for the regulation of a shoulder at 400 nm in the emission spectrum via abstraction of the hydrogen atom from para-hydroxyl on the RI side chain. Specifically, it was shown that W92F and W86F mutants, which increased hydrophobicity and inhibited the abstraction of the hydrogen atom near the para-hydroxyl of the R1 ring in coelenterazine, caused the enhanced emission at 400 nm (Ohmiya *et al*., 1992; Deng *et al*., 2001).

The octocorallian *Renilla reniformis* and *Renilla mülleri* are also known as “sea pansy” and live along the South Atlantic coast of the United States of America and in the southern tropical area, respectively. The polyps are distributed on the upper surface of the leaf-like frond, the color of which varies from red to purple (Fig. I-6). The 36 kDa anthozoan *Renilla* luciferase (RLUC; E.C. number 1.13.12.5, luciferin-2-monooxygenase, decarboxylating; Matthews *et al*., 1977a; Loening *et al*., 2007b) has been used as an energy donor for BRET (Xu *et al*., 1999; Subramanian *et al*., 2004a, b, and 2006) and as

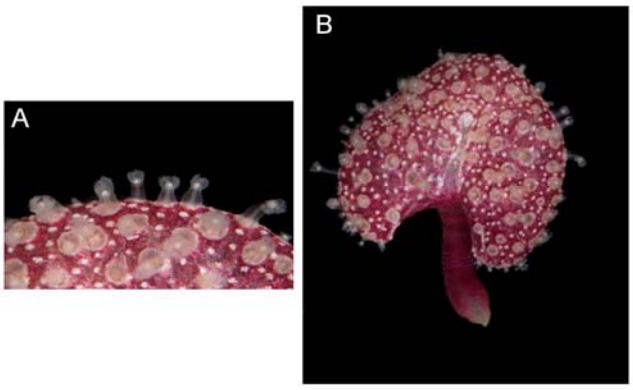

Figure I-6. *Renilla reniformis* and its polyps

(A) Polyps colonize the upper surface of the leaf-shaped frond. (B) *Renilla reniformis* consists of frond tissue, which bears the luminescing polyps, and a stalk for sticking to the surface on the ocean floor. Photographs used with permission from the Southeastern Regional Taxonomic Center/South Carolina Department of Natural Resources (www.dnr.sc.gov/.../Renilla%20_reniformis.htm).

a reporter for imaging in the mouse (Venisnik *et al*., 2006).

The subcellular organelle responsible for emitting bioluminescence has been investigated in both *R. reniformis* (Anderson and Cormier, 1973) and *R. mülleri* (Spurlock and Cormier, 1975). In blue light emitting cells of *Renilla reniformis*, “lumisomes” are intracellular membrane-bound vesicles with 0.2 - 0.4 μm width that resemble the scintillons of the dinoflagellate *Lingulodinium/Gonyaulax*, containing RLUC, a calcium activated coelenterazine (luciferin) binding protein (RrLBP), and a green fluorescent protein (RrGFP) (Anderson and Cormier, 1973). Luciferyl sulfate purified from the animals is a purportedly inactive substrate precursor that can be converted into the active luciferin by luciferin sulfokinase (Cormier *et al*., 1970; Hori and Cormier, 1972). Active luciferin is bound to RrLBP and released to RLUC in the presence of calcium. Upon oxidation of luciferin, resonance energy can be transferred from RLUC to the closely associated RrGFP, whose activation in turn, results in the emission of greenish light rather than the blue light that is typical of the bioluminescence reaction by RLUC alone. RLUC catalyzes the oxidative decarboxylation of coelenterazine (Matthews *et al*., 1977a and b). In detail, 1 mol oxygen is required to convert 1 mol coelenterazine to 2-hydroperoxy-coelenterazine, and then 1 mol carbon dioxide and 1 mol coelenteramide (oxyluciferin) are made as byproducts (Matthews *et al*., 1977a).

Because RLUC uses the same substrate, yields the same products, and emits a photon with similar spectral characteristics as aequorin and obelin, the reaction cascade of coelenterazine is expected to be similar (Matthews *et al*., 1977a and b). However, given the lack of significant sequence similarity between aequorin and RLUC, and according to the recently described RLUC crystal structures (PDB ID, 2PSD 2PSE, 2PSF,

2PSH, 2PSJ; Loening *et al*., 2007a) the RLUC structure is totally different from aequorin and obelin. These findings raise the question of how *Renilla* luciferase turns over its substrate, and how the enzymatic properties of RLUC might be modified to better support its application in BRET and other heterologous expression assays. These questions will be addressed in Chapter III.

I-3-2. Luciferase structures

I-3-2-1. Dinoflagellate *Lingulodinium polyedrum*

Dinoflagellate *Lingulodinium polyedrum,* previously called *Gonyaulax polyedra,* codes for a blue light emitting luciferase that shows circadian rhythmic flashing emitted from a group of intracellular membrane compartments, termed scintillons (Morse *et al*., 1989; Okamoto *et al*., 2001). The circadian rhythmic bioluminescence reaction is regulated by the expression of LBP, which is maximal at night (Morse *et al*., 1989). The ~130 kDa dinoflagellate luciferase catalyzes the turnover of a tetrapyrrole substrate (Fig. I-2A; dinoflagellate luciferin; LH_2), which originates from chlorophyll, and emits bluish light with a peak at 474 nm (Nakamura *et al*., 1989). The *Lingulodinium* luciferase has three structurally related functional subdomains (D1, D2, and D3), each of which shows bioluminescence activity (Li *et al*., 1997). According to the crystal structure of the 36 kDa D3 domain (Fig. I-7A), this unit is composed of seven α helices and sixteen β strands. There is a highly conserved portion between the α4 helix and the β12 strand, which is present in all subdomains (D1-D3), and among each of seven dinoflagellate luciferases

Figure I-7. Structures of luciferases

(A) The D3 subdomain of dinoflagellate luciferase (PDB ID, 1VPR). The triangular prism-shaped gateway consisting of α2, α5, and α6 is secured by hydrogen bonds to the β-barrel active site. The hydrogen bonds break down at acidic pH, resulting in increased flexibility of Gly-Gly (G-G) hinges at the bottom of the gateway. This causes the gateway to open. As a result, a linear substrate enters the active site. Blue broken arrows represent directions of α2, α5, and α6 helices for the open gateway at acidic pH. (B) The superimposed structures of aequorin (PDB ID, 1EJ3; blue) and obelin (PDB ID, 1S36; yellow). Note the red-colored substrate in the middle of the active site. Catalytic triads of aequorin and obelin are labeled by red and blue, respectively. (C) The superimposed structures of two firefly luciferases. The active sites are composed of α8, β12, β13, β14, an active site loop in the active site (D), and a C-loop in the C-terminus. The C-terminal domains of the American *Photinus* luciferase (*P*. FLUC; PDB ID, 1LCI) and the Japanese *Luciola* luciferase (*L*. FLUC; PDB ID, 2D1Q) are colored yellow and violet, respectively. The curved double-headed arrows indicate the rotation of the C-terminal part of FLUC for bioluminescence reaction. Blue AMP and red oxyluciferin are in the active site. 12.4Å represents the C-terminal difference between 1LCI and 2D1Q. (E) The crystallography of *Renilla* luciferase (PDB ID, 2PSD) shows structural similarity with an α/β hydrolase fold. Putative catalytic residues, D120, E144, and H285, are highlighted in the active site and a flexible loop on the cap domain may regulate the size of the substrate entrance (Loening *et al*., 2007a).

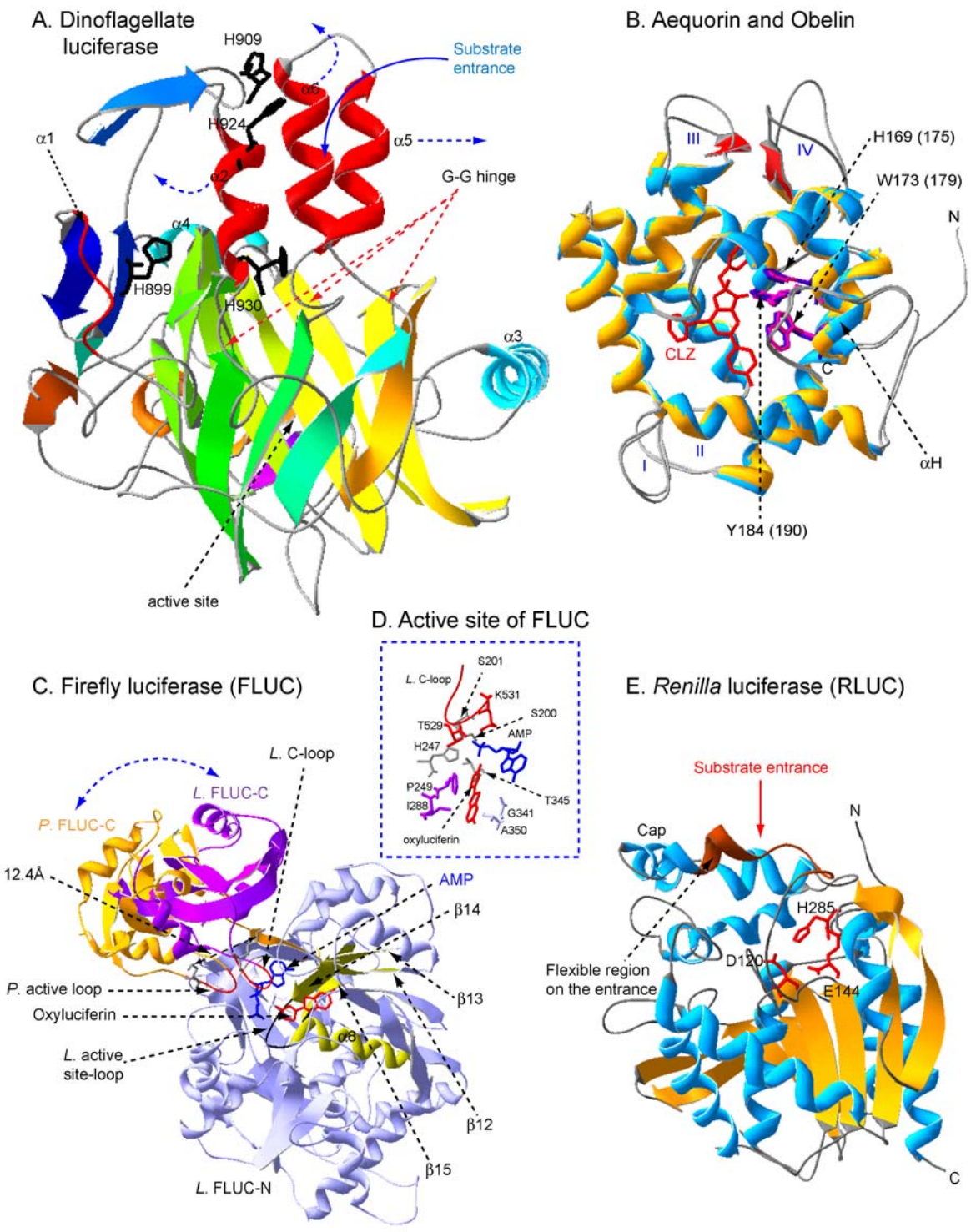

Figure I-7. Continued.

(Schultz *et al*., 2005). The active site is located at the bottom of the β barrel where L1072, V1083, R1095, W1097, E1105, W1117, R1142, Q1155, and Y1168 are coordinated by a hydrogen-bonding network. A helix-loop-helix motif in the N-terminus is connected with a β-barrel consisting of β5 to β14. The helix-loop-helix motif consisting of α2, α5, and α6 helices plays a role as a gateway to take up the linear tetrapyrrole substrate. The bottom of the triangular α helices is connected to the Gly-Gly (G-G) hinge responsible for structural flexibility. The gateway is of interest since four histidines (H899, H909, H924, and H930) are situated in the N-terminus. The four histidines function as a pH sensor. At pH 8.0, H899 forms hydrogen bonds with both Y925 and the carbonyl of V1087, which is located at the end of the N-terminus of the β barrel, H909 interacts with the carbonyl of L1050 and forms a van der Waals interaction with A1052, and H924 is within a hydrogen bonding distance with S921 and a van der Waals contact with I1045. In case of H930, it forms a hydrogen bond with Q1037 and is a component of a hydrophobic pocket coordinated with A1088, A1038, and M1070 (Schultz *et al*., 2005). The triangular prism-shaped gateway appears to be tightly secured by the hydrogen bonds and the van der Waals interactions. The optimal pH for bioluminescence of the *Lingulodinium* luciferase is around 6.3 but it loses the activity at pH 8 (Fogel and Hastings, 1972). In contrast, most coelenterazine catalyzing luciferases such as RLUC, aequorin, and obelin show their highest activity at weakly alkaline pH. It is thought that below the pKa of histidine (pH 6.3), the interactions between the protonated histidines and their counterparts in the D3 subdomain break down, leading to increased flexibility of the gateway, mostly the G-G hinge regions at the bottom of the gateway helices (Fig. I-7A). These conclusions were echoed by a molecular dynamics analysis; specifically,

the α helices were opened enough for the linear tetrapyrrole substrate to gain access to the active site at pH 6.3, but not pH 8.0 (Schultz *et al*., 2005).

I-3-2-2. Aequorin and Obelin

Aequorin, which shares high homology with obelin, possesses four EF-hands responsible for calcium ion recruitment (Head *et al*., 2000). Three of them have high calcium affinity while EF-hand II does not. Most oxygen atoms involved in the interaction with a calcium ion are contributed by the carboxyl groups of Asp and Glu in the three EF-hands, and both a water molecule and the hydroxyl of S163 are additionally engaged in the interaction, in case of the EF-hand IV. Comparing the apo-photoprotein with the calcium discharged photoprotein, the overall structure does not change much. However, a local conformational change of both the EF-hand IV and the C-terminus takes place before the bioluminescence reaction (Deng *et al*., 2004). After the recruitment of coelenterazine into the active site, the conformational change mediated by calcium binding may induce the C-terminal helix H to cap the hydrophobic active site, resulting in repositioning Y184 (Y190 in obelin) on the helix H in a distance for a hydrogen bond with H169 (H175) (Fig. 1-7B).

Maintaining a hydrophobic environment in the active site appears to be important for stabilizing the substrate-enzyme complex and for triggering the oxidation of coelenterazine. How calcium triggers the bioluminescent reaction has been investigated thoroughly for obelin. The calcium binding to the EF-hand IV results in an almost perpendicular repositioning of the imidazole ring of H175 in the catalytic triad, triggering

deprotonation of the hydroxyphenol ring of Y190 (Deng *et al*., 2004). Since deprotonated Y190 abstracts a proton from 2-hydroperoxy coelenterazine, Y190 (Y184) should position near H175 of obelin (H169 of aequorin) to be deprotonated before the bioluminescence reaction.

I-3-2-3. Firefly luciferase (FLUC)

A 6-hydroxyl-benzothiazole-4-carboxyl-thiazole (Fig. I-2C) is a firefly luciferin, which is adenylated by firefly luciferase (FLUC; EC 1.13.12.7, Photinus-luciferin 4-monooxygenase, ATP-hydrolyzing) in the presence of Mg^{2+} before the oxidation of firefly luciferin. Two oxygen atoms are attached on the C4 in the thiazole moiety, and the product, a peroxide anion intermediate, is converted to the dioxetanone luciferin by an intramolecular nucleophilic attack. Concomitantly, an adenosine monophophate (AMP) is released from the peroxide anion intermediate. As in other cases of luciferin decomposition, formation of a four-atom dioxetanone ring is followed by decarboxylation. After the release of carbon dioxide, bioluminescence is emitted when the electronically excited oxyluciferin relaxes to the ground state (Koo *et al*., 1978).

Crystal structures have been solved for the luciferases of the North American firefly, *Photinus pyralis,* and the Japanese *Luciola cruciata* (Conti *et al*., 1996; Franks *et al*., 1998; Nakatsu *et al*., 2006) (Fig. I-7C). *Photinus* FLUC (PDB ID, 1LCI and 1BA3) shares 82% sequence similarity with *Luciola* FLUC (PDB ID, 2DIQ and 2DIR) and the crystal structures are well aligned with each other. Firefly luciferase consists of a large N-terminal (amino acids 1-437) and a small C-terminal domain (443-548 in *Luciola*

luciferase). The secondary structure of *P*. FLUC is comprised of 15 α helices and 27 β strands, the latter forming 5 β sheets (A-E). The calculated rmsd (root mean square deviation) between PDB ID, 1BA3 and 2DIR is 1.16Å excluding the C-terminal 112 amino acids (418 selections of 539 residues). Interestingly, the rmsd of the alignment between the C-terminal parts is 0.78Å excluding the N-terminal 436 amino acids (100 selections of 108 residues of the C-terminal end). For the active site of *L*. FLUC, the hydrophobic binding pocket consists of α8, β12-β15, and an active site loop (343-350 a.a) in the middle of the N-terminus and a C terminal loop (C-loop; 526-531 a.a) in the flexible C-terminus (Fig. I-7D). According to the crystal structure with 5'-*O*-[*N*-(dehydroluciferyl)-sulfamoyl] adenosine (DLSA), the benzothiazole ring is in van der Waals interaction with P249 and I288 on the one side as well as G341 and A350 on the opposite side. The tight packing of the benzothiazole squeezes out water molecules near the oxidized reaction intermediate, resulting in the formation of the hydrophobic active site where the hydrophobic microenvironment is favorable for the electronically excited state of oxyluciferin (Nakatsu *et al*., 2006).

Photinus FLUC has a peroxisome-targeting signal, SKL, at the C-terminus (Conti *et al*., 1996). Due to the lack of substrate in the active site (PDB ID, 1LCI; Conti *et al*., 1996) (PDB ID, 1BA3; Frank *et al*., 1998), it is difficult to elucidate the mechanism of the bioluminescence reaction of the *P*. FLUC (Nakatsu *et al*., 2006). In contrast to *P*. FLUC, the crystal structure of *L*. FLUC was solved both with FLUC luciferin and with DLSA, a luciferyl•AMP intermediate analogue. Comparing the structure of *P*. FLUC lacking substrate with that of *L*. FLUC in the presence of DLSA, the *P*. FLUC structure appears to represent an opened state, as evidenced by the wide gap between K529 of *P*. FLUC

(PDB ID, 1BA3) and the corresponding K531 of *L*. FLUC (PDB ID, 2D1R) in the cap loop of the C-terminus (Fig. I-7C). Concerning the function of K529 of *P*. FLUC, it has been suggested that K529 may play a role in the adenylation reaction since the K529A mutant showed a 100 fold reduction of the adenylation rate of the native firefly luciferin (LH_2), but only a mild phenotype for oxidation of the adenylated intermediate (LH_2-AMP). Unlike K529, K443 in the C-terminus may function during the oxidation of the adenylated intermediate because the K443A mutant couldn't oxidize the LH_2-AMP, but did perform the adenylation of LH_2 (Branchini *et al*., 2005). Furthermore, a computer simulation for the oxidation reaction of *P*. FLUC showed that K443 located close to its adenylated intermediate, suggesting that the C-terminal FLUC may be rotated as its RLK residues (437-439 a.a) served as the hinge during the bioluminescence reaction (Branchini *et al*., 2005; Fraga, 2008). Since K529 is around 16Å away from K443 in the C-terminus (PDB ID, 1BA3) and both lysine residues are important for both step of the bioluminescence reaction, adenylation and oxidation, it has been suggested that K529 exists near the active site for the adenylation of firefly luciferin and then, the C-terminus rotates for K443 to be close to the active site, followed by the oxidation of the adenylated luciferin (Branchini *et al*., 2005).

A hydrophobic environment is required to avoid quenching of the luminescence by water molecules (Conti *et al*., 1996). The degree of packing of the benzothiazole ring by residues P249, I288, G341, and A350 in the active site, and the concomitant exclusion of water may affect the emission maximum. Evidence for this comes from the crystal structure of the S286N mutant of *Luciola* FLUC. It clearly showed the repositioning of I288, resulting in looser packing of the benzothiazole of DLSA (PDB ID, 2D1T; Nakatsu

et al., 2006). Meanwhile, the S286N mutant showed a red-shifted emission peak (~605 nm) compared to the wild type enzyme (~560 nm). It is plausible that in the S286N mutant some excitation energy may be rapidly quenched before it can be converted to bioluminescence, due to water molecules located near the crevasse between I228 and the benzothiazole ring, leading to a lower-energy emission maximum. Furthermore, the emission peaks of two related mutants, I288V and I288A, showed emission maxima in the orange and red, respectively. It also suggests that high hydrophobicity and exclusion of bulk water at I288 may be correlated with a short-wavelength emission maximum (Nakatsu *et al*., 2006).

There are three different light emitting species of the electronically excited state of firefly luciferin, dependent on the protonation status, such as the enolate, the enol, and the keto form, each of which emits 550, 590, and 620 nm, respectively (Ugarova *et al*., 2005). Protonation and deprotonation take place at two different positions such as C4 and C5 of the thiazole ring in the light emitters. Although pKa of the three light emitters is still unclear, the molar ratio of keto: enol: enolate was 8: 1.5: 0.5 at pH 6.0. However, the molar ratio among the light emitters could be changed to 2: 3: 5 at pH 8.0, indicating that certain equilibria among the light emitters might exist and could change in a pH-dependent manner (Ugarova *et al*., 2005). The protonation status of the light emitters appears to be correlated with the conformational flexibility or the solvent accessibility in the active site (Viviani *et al*., 2008). According to sequence alignments between pH sensitive and pH insensitive luciferases, a loop composed of R223-T235 residues in the pH sensitive *P*. FLUC shows lower hydrophobicity, suggesting less structural rigidity in comparison with the pH insensitive luciferases such as click beetle luciferase. Moreover,

mutagenesis of the loop region results in a red-shifted emission maximum, indicating the predominant keto form in the active site. Although the loop is not a part of the active site of FLUC, it covers the active site to face the benzothiazole moiety. A possibility to explain the relationship between pH and emission maximum of *P*. FLUC is that the loop together with another loop of 351-360 residues may play a role as a back door for water molecules or H^+ ions while the main gate is at the contact region between the N-terminus and the C-terminus. In detail, the hydrogen bonds between the loop 223-235 a.a and the loop 351-360 a.a may be disrupted at low pH and then the back door is opened, resulting in influx of water molecules or H^+ ions into the active site (Viviani *et al*., 2008). It is unclear whether the red-shifted emission peak of the pH sensitive FLUC results from water-mediated quenching or from the H^+-mediated formation of the keto form at pH 6. For the pH insensitive click beetle luciferases, strong hydrophobicity between the loop regions may be resistant for pH 6 in comparison with *P*. FLUC. As a result, a more hydrophobic microenvironment at the active site of click beetle luciferase may protect the quenching or inhibit the production of the keto form of the excited state luciferin, resulting in yellow-green luminescence instead of red at pH 6 (Viviani *et al*., 2008).

In summary, FLUC shows structural dynamics to catalyze firefly luciferin such as the rotation of the C-terminus for adenylation and oxidation as well as the flexibility of the N-terminal loops for sensing pH. These conformational changes are required for the catalysis of FLUC luciferin, which is correlated with emission maxima of bioluminescence. The relationship between the structural rearrangement of the active site and the emission spectrum has been discussed.

I-3-2-4. *Renilla* luciferase (RLUC)

Considering the functional similarities between RLUC and aequorin, in particular the ability to use the same substrate, coelenterazine, and to emit blue bioluminescence, it is likely that the reaction mechanism of RLUC may be similar with that of aequorin or obelin. However, the amino acid sequence of RLUC is most similar to that of LinB (~42% identity), a bacterial haloalkane dehalogenase from *Sphingomonas paucimobilis*, which is a member of the α/β hydrolase superfamily, despite the functional difference (Loening *et al*., 2006). In addition, the structure of RLUC may be quite different from the functionally similar photoproteins such as aequorin and obelin because RLUC is not calcium-dependent (Fig. I-7B and D).

Renilla luciferase has been applied as a molecular reagent in a number of different situations, apart from the BRET assay introduced earlier; (i) as a transcriptional or translational reporter in plants and mammalian cells (Minko *et al*., 1999; Bhaumik and Gambhir, 2002). Initially, *RLUC* was mostly used as the “reference gene”, but more often it is now being used as the primary reporter and FLUC is used as the reference (Holcik *et al*., 2005). (ii) RLUC also lends itself to reconstitution by fragment complementation (Paulmurugan and Gambhir, 2003; Stefan *et al*., 2007). Such fragment complementation assays can be adapted to score protein-protein interaction of fused partner proteins *in vivo* or *in vitro* (Paulmurugan and Gambhir, 2003). (iii) Another use of RLUC is as a beacon in small animal imaging studies (Bhaumik and Gambhir, 2002; De and Gambhir, 2005; RLUC expressing cells and their targeting to specific tissues in the mouse). For optimization of each of these and other applications, the enzymatic properties or RLUC

may need to be modified or at least better understood.

Early enzymatic studies of RLUC were performed prior to the molecular era using enzyme purified from *Renilla* by Milton Cormier and coworkers (Karkhanis and Cormier, 1971; Matthews *et al*., 1977a and b). These investigations established that RLUC has a relatively low quantum efficiency (~6%; Matthews *et al*., 1997a). Its pH optimum is around 8. While the K_m is low, suggesting high affinity for its substrate, the k_{cat} is poor. Characterization of competitive inhibitors suggested that the enzyme binds its substrate through interactions with each of three aromatic side chains, and the hydroxylation status of the R1 ring is particularly critical (See Chapter III). The coelenteramide product is a potent competitive inhibitor of the enzyme. It also became clear that RLUC is rapidly inactivated in the presence of substrate. However, whether this is due solely to the accumulation of the coelenteramide end product has not been established. It is evident that certain properties of the RLUC enzyme could be targeted for optimization in an attempt to generate a more effective molecular reagent. These include the low k_{cat}, low quantum efficiency, tight binding of the end product, and loss of activity in the presence of substrate.

CHAPTER II.

APPLICATION AND OPTIMIZATION OF BIOLUMINESCENCE RESONANCE ENERGY TRANSFER (BRET) FOR *IN VIVO* DETECTION OF PROTEIN-PROTEIN INTERACTIONS IN TRANSGENIC *ARABIDOPSIS*

Part of this chapter has been published in the *Plant Journal*.

Chitra Subramanian, Jongchan Woo, Xue Cai, Xiaodong Xu, Stein Servick, Carl H. Johnson, Andreas Nebenführ, and Albrecht G. von Arnim. 2006. A suite of tools and application notes for *in vivo* protein interaction assays using bioluminescence resonance energy transfer (BRET). *Plant Journal* 48, 138-152.

II-1. Abstract

Bioluminescence resonance energy transfer (BRET) is a natural phenomenon where resonance energy from the enzymatic reaction of a luciferase can excite a spectrally compatible energy acceptor located at a distance of ~5 nm, followed by spectrally shifted emission of light. A BRET system capable of monitoring protein interactions has been developed and optimized for *Arabidopsis*. In a typical experiment, a candidate protein is genetically fused with a resonance energy donor, *Renilla* luciferase (RLUC), and its putative interaction partner is fused to yellow fluorescent protein (YFP) as an energy acceptor. Resonance energy transfer was detected for a number of plant protein-protein interactions; the homo-dimerization of the bZIP protein, HY5, and the heterodimeric interactions between the B-box protein STH and the E3 ubiquitin ligase COP1, and also between the bZIP transcription factors, HY5 and HYH, in living seedlings. For *in vivo* BRET assays, generation of transgenic *Arabidopsis* plants was facilitated by simultaneous co-transformation with two different T-DNAs resident in a single agrobacterium strain. In summary, BRET is a promising tool for the precise

examination of dynamic signaling cascades that are controlled by protein-protein interactions.

II-2. Introduction

To grow and develop optimally, all living plants require specialized sensors to capture a variety of environmental signals. Light is one of the most important factors to control plant development. Plants have evolved at least 3 families of photosensory proteins. In *Arabidopsis*, there are five phytochromes (phy A to E), which absorb red/far-red light. Phototropins and cryptochromes are responsible for sensing UV-A or blue light while UV-B photoreceptors are still awaiting their discovery (Gyula *et al*., 2003; Castillon *et al*., 2007). A large number of gene products is involved in decoding the light signals in the process of adjusting plant development (photomorphogenesis). *Arabidopsis* has at least two distinct body plans in response to availability of light; one is photomorphogenesis (deetiolation) and the other is skotomorphogenesis (etiolation) (Fankhauser *et al*., 1997). Those plans are regulated by coordination of the central key regulators. Etiolated *Arabidopsis* has a long hypocotyl, a closed apical hook, and undeveloped cotyledons. One of the central components of skotomorphogenesis is *COP1* (constitutive photomorphogenic1), which acts as a repressor of photomorphogenesis. COP1 protein is responsible for etiolation responses by regulating the stabilities of light responsive gene products under the dark condition (Deng *et al*., 1991). At the molecular level, COP1 is an E3 ubiquitin ligase that can recruit bZIP transcription factors, HY5 and HYH (Osterlund *et al*., 2000; Holm *et al*., 2002; Saijo *et al*., 2003) and trigger their turnover by the ubiquitin-proteasome pathway. HY5 and HYH

have a common V-P-E/D-Φ-G motif (Φ: hydrophobic residue) in the N-terminus and a basic leucine zipper in the C-terminus. The V-P-E/D-Φ-G motif participates in the interaction with the WD-40 domain of COP1 (Holm *et al*., 2002). The deetiolation activators targeted by COP1 are destined for proteasome-mediated degradation in the nucleus. The COP1 protein has both a bipartite nuclear localization signal (NLS) and a cytoplasmic localization signal (CLS), modulating the subcellular localization of COP1 in response to light (Stacey *et al*., 1999 and 2000; Subramanian *et al*., 2004b). In darkness, COP1 can be translocated from the cytoplasmic inclusion bodies to the nuclei (von Arnim *et al*., 1994) where COP1 ubiquitinates HY5 and HYH. In part due to the decreased level of HY5 and HYH, *Arabidopsis* undergoes etiolation (Saijo *et al*., 2003). HY5 and HYH can interact with each other in the light whereas COP1 binds to either HY5 or HYH in the dark. Moreover, the heterodimer containing HY5 and HYH can bind to the G-box element in the *RBCS* promoter *in vitro*, indicating that the heterodimer may play a role as a transcriptional activator for deetiolation. Overexpressed HYH could suppress the long hypocotyl phenotype of the *hy5-215* allele, suggesting functional overlap between HY5 and HYH in the photomorphogenic development (Holm *et al*., 2002). Besides the complementation by HYH of the hypocotyl elongation of the *hy5* mutant, HYH appears to have its own function since the *hy5*/*hyh* double mutant has shorter roots and fewer lateral roots than either the *hy5* or the *hyh* single mutant. This idea is also supported by a transcriptome analysis. The transcriptional profile of most genes in either the *hy5* or the *hy5/hyh* mutant is quite similar, however, many auxin related genes are misregulated in the *hy5/hyh* double mutant, compared with those in the *hy5* mutant, suggesting the possibility that the complex of HY5 and HYH may have a

unique function to regulate transcription of some auxin responsive genes, independent of the HY5 monomer or possibly the HY5 dimer (Sibout *et al*., 2006).

Adapting to environmental changes is an important process for plants to change their body plans and metabolism for survival. A variety of cues from the abiotic or biotic environment can trigger a change in physiology, morphology, and development of plants. To respond to their surroundings, plants should reset their developmental and metabolic programs for optimal growth, generally through turning on and/or off certain signaling cascades.

The stress signal transduction appears to be connected to the light signal cascade in plants. For supportive evidence, two B-box proteins, STO and STH of *Arabidopsis* could complement the salt stress sensitive *cna* mutants of yeast (Lippuner *et al*., 1996) although it has not been tested whether the yeast *CNA* (calcineurin) could rescue the *sto* (or *sth*) mutant of *Arabidopsis*. In addition, *Arabidopsis* plants overexpressing *STO* showed stronger tolerance than wild type against salinity stress (Nagaoka *et al*., 2003). That said, the *sto* mutant didn't show any visible phenotype under salt stress (Datta *et al*., 2007; Indorf *et al*., 2007). Interestingly, the null mutant of *sto* was hypersensitive to light, suggesting that STO is also a negative regulator of photomorphogenesis in *Arabidopsis*. Additionally, a light and stress inducible gene, chalcone synthase (*CHS)* was misregulated in the *sto* mutant (Indorf *et al*., 2007). While STO appears to function as a negative regulator in photomorphogenesis, another homolog of STO, STH2, may play a role as an activator of the developmental process (Datta *et al*., 2007). Although the molecular function of STH in photomorphogenesis has not been investigated, there is an attractive scenario to explain a possible function of the

interaction between STH and COP1 if STH may play a role as an activator in photomorphogenesis. Upon exposure of light grown plants to high salinity environment, they are more resistant to the salt stress in comparison with dark grown plants in the same stress condition, as suggested in proline biosynthesis (See Chapter I-2). Since STH can escape from the COP1-mediated ubiquitination in light, light grown plants under salt stress can activate salt stress signaling via a B-box transcription factor STH.

Protein interactions among STO, STH and COP1 have been demonstrated by the yeast two hybrid assay (Holm *et al*., 2001). Interestingly, STO and STH proteins also contain and utilize the V-P-E/D-Φ-G (Φ=hydrophobic residue) motif that mediates the interaction between HY5 and COP1 (Holm *et al*., 2001). According to a site-directed mutagenesis study, when VP was converted to AA in the V-P-E/D-Φ-G (Φ=hydrophobic residue) motif in STH, the mutated STH could no longer bind to the WD40 domain of COP1 (Holm *et al*., 2001). Considering the protein interaction studies and the genetic analyses, it is possible that the light signaling cascade may share signal transducers with the stress signal transduction. The functional significance of this is unclear but might be founded on the notion that high salinity can be caused by high light or high temperature and a resulting low availability of water.

As described, the light information appears to be processed in various ways. From an input, for example, the photoreversible isomerization of the tetrapyrrole chromophores of the phytochromes (phytochromobilins), to an output, for example, the short hypocotyl, the light signal [decoded by converting inactive 15Z (Pr) to active 15E (Pfr)] flows through a variety of downstream signal transduction components. The decoding or amplification steps are mainly governed by transcriptional controls as well

as protein interactions. Although many of the physical components have been identified by extensive genetic approaches, much of the signal relay mechanisms are still awaiting discovery. The mechanistic steps often involve protein-protein interactions, and these interactions may well be conditional in space or in time. BRET can play a part in measuring such events in real time.

To study protein interactions in the cell, several techniques are available. The yeast two hybrid assay is a common method. The yeast two hybrid system has two components. The bait protein is fused to a promoter-binding domain for a reporter gene such as *LacZ* the product of which is β-galactosidase. The other is the prey part that is fused to a transcriptional activation domain of the reporter. If the protein interaction between candidates of this system occurs in the nucleus of yeast, this system activates transcription and translation of the reporter gene. The major benefit of the yeast two hybrid system is to allow large-scale screening for identification of interacting candidates. However, this powerful technique has some limitations. In the yeast two hybrid system, the protein interaction between candidates can often be investigated only if the interaction occurs in the nuclei. Therefore, an interaction that depends on cell specific processing, multi component complexes or compartmentalization will not be detected by this system. There are also a number of reasons for false-positive results.

A second method capable of detecting protein-protein interactions is bimolecular fluorescence complementation (BiFC) of GFP (green fluorescent protein). Here, candidates are fused to the split N-terminal half (1-155 or 173 a.a of GFP) and the C-terminal half, respectively. When the protein interaction between the candidates occurs, each half of GFP can be brought into close proximity and GFP is then reconstituted,

resulting in the emission of green fluorescence upon excitation of GFP (Hu *et al*., 2002). However, the reconstituted fluorophore is difficult to be dissociated for return to the halves, even upon termination of the protein interaction between the candidates. Because of strong interaction between the halves, BiFC is not suitable for real time detection of protein interactions (Villalobos *et al*., 2007).

A third advanced technique is fluorescence resonance energy transfer (FRET) for testing protein interactions in the cell. In case of the energy transfer from ECFP (enhanced cyan fluorescent protein) to EYFP (enhanced yellow fluorescent protein), the Förster radius (R_0), the interfluorophore distance when 50% energy is transferred from a donor to an acceptor, is 49-52Å (Tsien, 1998). For instance, the protein interaction between HYH (HY5 homolog), a bZIP transcription factor, and COP1 was found by the FRET assay (Holm *et al*., 2002). HYH translationally fused with green fluorescent protein (GFP) could bind to COP1 tagged with blue fluorescent protein (BFP) through the WD40 domain of COP1 (Holm *et al*., 2002). Additionally, intramolecular FRET took place between the cyan-emitting mutant *Aequorea* GFP and YFP to measure free Ca^{2+} concentration using calmodulin in the cell (Miyawaki *et al*., 1997). In FRET, one fluorophore as an energy donor transfers its excited-state energy to the other fluorophore, an energy acceptor, when two proteins tagged with the respective fluorophores interact with each other. After the energy acceptor absorbs the energy from the donor, the acceptor can generate fluorescence of a different color. This approach depends on the overlap between the absorption spectrum of the acceptor and the emission spectrum of the donor, the relative orientation between the emission dipoles of the donor and acceptor, and the distance between the two fluorophores. Unlike the yeast

two hybrid method, FRET allows protein interactions to be measured in the protein's native organism such that cell type specific-modifications are preserved and compartmentalization of the proteins can be visualized by microscopy. Although FRET gives spatial information where a protein-protein interaction takes place, FRET has a few drawbacks of its own such as photobleaching of the fluorophore, tissue damage by the excitation light, and a need to master quantitative imaging skills. Therefore, new advanced approaches are necessary to study protein interactions *in vivo* and in real time.

A new approach for studying protein interactions came from Dr. Johnson's group (Xu *et al*., 1999). The principle of Bioluminescence Resonance Energy Transfer (BRET) is similar to FRET. BRET relies on an energy donor and an energy acceptor like FRET. Typically, *Renilla* luciferase (RLUC), which is a blue (~470 nm) light emitting luciferase from the marine coelenterate *Renilla reniformis*, is used as the energy donor and YFP (yellow fluorescent protein) as the energy acceptor. RLUC cannot directly interact with YFP. When RLUC and YFP are brought together by an interaction between their translational fusion partners (Subramanian *et al*., 2004a and b), the resonance energy from the reaction of coelenterazine substrate may be transferred from RLUC to YFP and emitted according to the spectral characteristics of YFP (~530 nm). Thus, the BRET assay does not require an excitation light source, which could cause tissue damage and photobleaching of YFP. BRET is easily measured in living cells or tissues because of the membrane permeability of coelenterazine (Subramanian *et al*., 2006).

II-3. Results

II-3-1. The transient BRET assays in onion epidermal cells

In order to examine a possible heterdimerization between COP1 and the STH (Fig. II-1) in plant cells, translational fusion constructs harboring STH-RLUC and YFP-COP1 as one set as well as RLUC-STH and YFP-COP1 as the other were introduced into onion epidermal cells using biolistic co-transformation. At the same time, single constructs such as STH-RLUC and RLUC-STH were transformed. First of all, the localizations of STH and COP1 were examined. YFP-COP1 accumulated in cytoplasmic inclusion bodies and also in the nuclei (Fig. II-1B), as described (Stacey *et al*., 1999). STH-YFP accumulated in the nuclei and weakly in the cytoplasm. RLUC-YFP was highly accumulated in the cytoplasm as well as in the nuclei (Fig. II-1B). To investigate the *in vivo* interaction between STH and COP1, the interaction between STH-RLUC and YFP-COP1 was monitored by comparing the ratio of the yellow to blue luminescence units (Y/B ratio) with the Y/B ratios of other control combinations. Co-expression of STH-RLUC and YFP-COP1 resulted in an elevated Y/B ratio, as did co-expression of RLUC-STH and YFP-COP1 in comparison with negative controls such as STH-RLUC alone and RLUC-STH alone. Among the combinations tested, all Y/B ratios were lower than the ratio of RLUC-YFP, which served as a positive control (Fig. II-1C). Compared with the Y/B ratio of a corresponding negative control, the significantly increased ratios of co-expression combinations are indicative of BRET and therefore suggest an interaction between STH and COP1 (Fig II-1C).

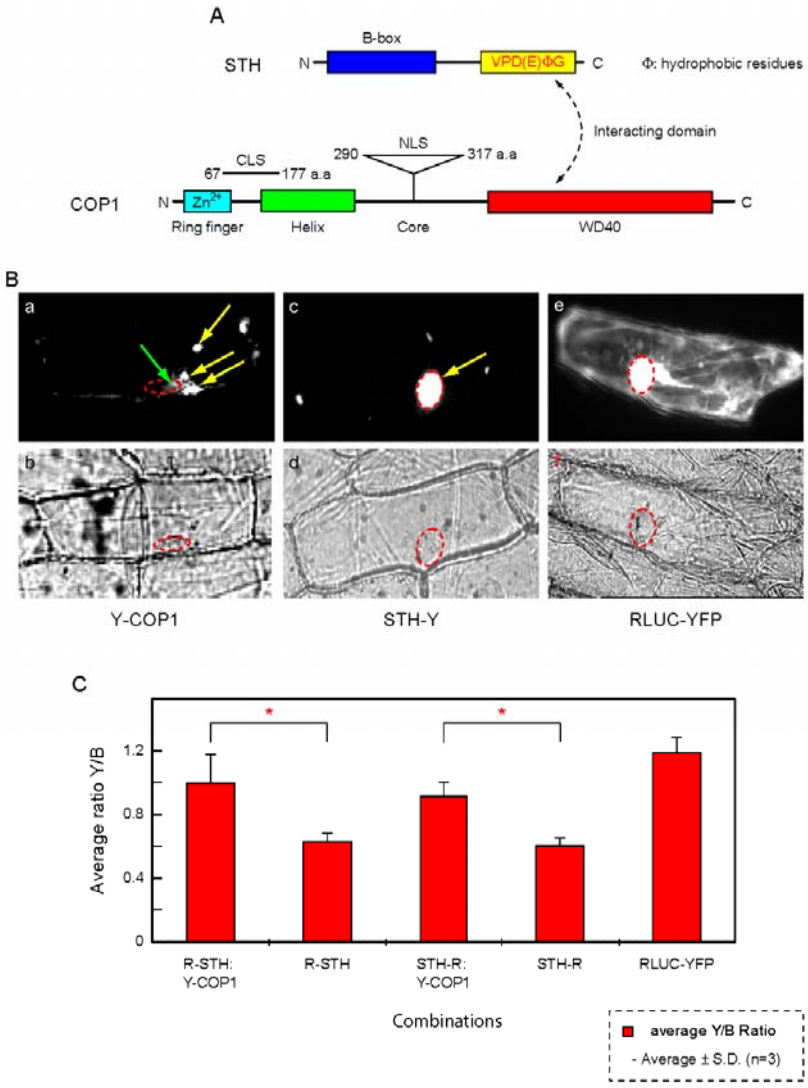

Figure II-1. The transient BRET study between STH-RLUC and YFP-COP1 in onion epidermal cells

(A) Primary structures of STH and COP1. Arrow indicates the interaction part. (B) The localizations of fusion proteins as indicated. The corresponding bright field images are at the bottom. Yellow arrows represent strong YFP signal and green indicates YFP in the nucleus. Nuclei are labeled by red circles. (C) The elevated Y/B ratios of RLUC-STH:YFP-COP1 as well as STH-RLUC:YFP-COP1 indicate *in vivo* protein-protein interactions. Asterisks represent significant difference ($P<0.05$).

Next, BRET was applied to the homodimer of the bZIP transcription factor, HY5. The HY5 dimer is formed primarily by salt bridges between leucine zippers, resulting in the parallel juxtaposition of HY5 monomers in the homodimer (Yoon, *et al*., 2007). To confirm the spatial configuration of the HY5 homodimer, four BRET combination constructs were made by the Gateway^{TM} cloning system (Landy, 1989; Subramanian *et al*., 2006). At this time, the Gateway BRET vectors containing hRLUC, a codon-optimized version, were used (Subramanian *et al*., 2006). Before the BRET measurement, the expression and the localization of the RLUC and the YFP fusion cassettes were confirmed. Strong yellow fluorescence was detected within nuclei in all co-expression combinations and high luciferase activity was measured. In case of YFP localization in the cell, neither the combinations with YFP alone nor hRLUC-YFP showed the specific nuclear localization, as expected. Among four BRET combinations to test the HY5 homodimerization, only the combination of HY5-hRLUC:HY5-YFP showed a significantly elevated Y/B ratio in comparisons with the negative control combinations. However, the other combinations didn't show a statistically significant increase in the Y/B ratios, suggesting that the spatial orientations or the distances between hRLUC and YFP might not be optimal for the resonance energy transfer in these cases (Fig. II-2). The leucine zipper-mediated homodimerization between HY5 proteins (Yoon *et al*., 2007) may allow the C-termini of HY5 to be close to each other. Thus, the C-terminal BRET tags in the HY5 dimer may be juxtaposed, acquiring an optimal configuration between the tags for BRET. As a result, the resonance energy may be transferred from HY5-hRLUC to HY5-YFP, indicating that the HY5 homodimerization takes place in the onion cell (Fig. II-2).

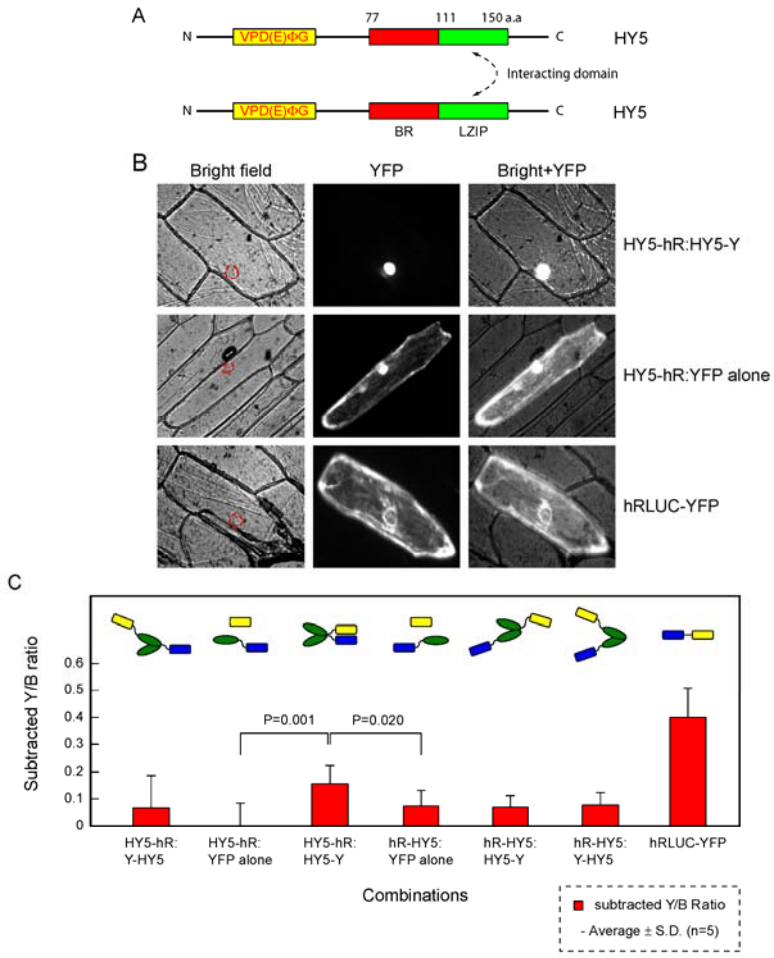

Figure II-2. The transient BRET assay for the HY5 homodimerization in onion cells

(A) Subdomains are labeled by different colors. Yellow, red, and green represent the interaction domain with COP1, the basic region (BR), and the leucine zipper (LZIP), respectively. (B) HY5 fusion protein localization in the onion cells. Image fields and co-bombarding combination are indicated at the top and at the right. (C) Transient BRET assay with all possible combinations shows that the Y/B ratio of HY5-hRLUC:HY5-YFP is significantly higher than the Y/B ratios of negative controls. Schematic diagram for the dimerization is in the box. Yellow, green, and blue represent YFP, HY5, and hRLUC, respectively. All BRET ratios represented are subtracted by the BRET ratio of the combination of HY5-hR:YFP alone.

II-3-2. Generating double transformants, STH-RLUC:YFP-COP1 and RLUC-HYH:YFP-HY5 as well as single transformants

For assaying the interaction between STH and COP1 in *Arabidopsis*, the STH and COP1 expression cassettes were cloned into T-DNA vectors. pPZP222, containing spectinomycin resistance and pBIN19 with the kanamycin marker for selection in agrobacteria were used for RLUC and YFP fusion constructs, respectively. Generating double transformants expressing both the RLUC fusion and the YFP fusion cassettes in *Arabidopsis* for the purpose of the BRET assay could be accomplished by a) genetic crossing, b) sequential transformation, and c) placing both cassettes onto the same T-DNA. Genetic crossing and sequential transformation methods generally take two generations to select double transformants expressing RLUC and YFP fusion proteins. Meanwhile, generating a single T-DNA harboring two individual reporter cassettes takes only one generation. However, one limitation of this method is that individual RLUC and YFP fusion cassettes are incorporated into the same locus in the plant genome, which means that they cannot be separated by meiotic recombination. Simultaneous dual-binary T-DNA transfer (Afolabi *et al*., 2004) involves introducing two separate T-DNA plasmids into the same agrobacterium cell. In this case, independent insertion events of two different T-DNAs into the plant genomes might occur upon plant transformation. For the generation of double transformants, agrobacterium strain GV3101 was co-electroporated simultaneously with both the STH-RLUC and the YFP-COP1 cassette, and then, double resistant clones were recovered on medium containing 100 μg/mL spectinomycin and 50 μg/mL kanamycin. The integrity of the T-DNA plasmids was

checked in two ways, first by PCR amplification of a part of the expression cassette (Fig. II-3B), and second by transformation of the plasmids back into *E. coli* and restriction analysis (Fig. II-3C; T-DNA shuttling). The latter was performed to rule out the possibility that recombination between the two different T-DNA plasmids might occur in agrobacterium. Restriction patterns of plasmids from the double transformant were exactly the same as from single transformants, indicating that double transformed agrobacterium contains two different binary vectors.

Confirmed double or single transformants were used for the agrobacterium-mediated floral dip transformation (Clough and Bent, 1998). After transformation of each construct into *Arabidopsis*, two individual homozygous lines of STH-RLUC, YFP-COP1, and double transformants were screened from the media containing kanamycin and gentamycin. In addition, the intact size of the RLUC expression cassette was analyzed by Southern blot. The intact expression cassette with the expected length of 3.2 kb was detected in a double transgenic line (Fig. II-4A). The transcript level of STH-RLUC in double transformed *Arabidopsis* was investigated by RT-PCR. The primer set for rubisco small subunit was used to estimate genomic DNA contamination because the 5' forward primer could anneal on the first exon of the rubisco small subunit gene (*rbcS*) and the 3' reverse primer could bind to the second exon. Additionally, elongation factor 1 (EF1) was used to normalize the amount of RNA for RT-PCR. cDNA fragments from RLUC messenger RNA were amplified in the double transformant seedlings as well as in control lines, confirming that each RLUC expression cassette integrated to the *Arabidopsis* genome could be transcribed (Fig. II-4B).

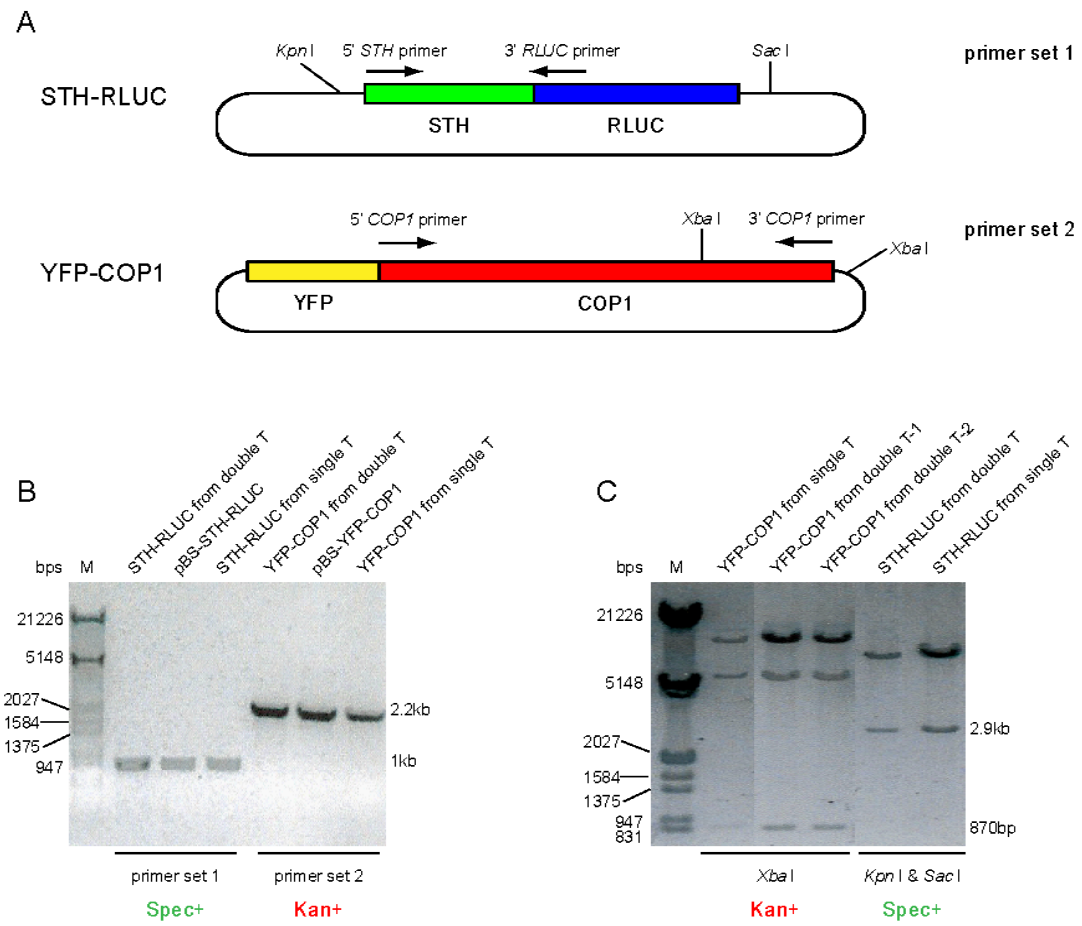

Figure II-3. T-DNA shuttling of the double transformed agrobacteria containing both the STH-RLUC and the YFP-COP1 expression cassette

(A) The expression cassettes of STH-RLUC and YFP-COP1. Primer sites are marked on the amplified target regions. (B) The expression cassettes were confirmed by PCR. Plasmids were isolated from the indicated agrobacteria and used as templates. (C) The expression cassettes were further confirmed by restriction digestion after back transformation into *E. coli*. Antibiotic selection markers are shown at the bottom of the gel pictures. Expected sizes of DNA fragments are at the right in (B) and (C). T and M characters stand for transformant and DNA size marker, respectively. pBS-STH-RLUC and pBS-YFP-COP1 are positive controls.

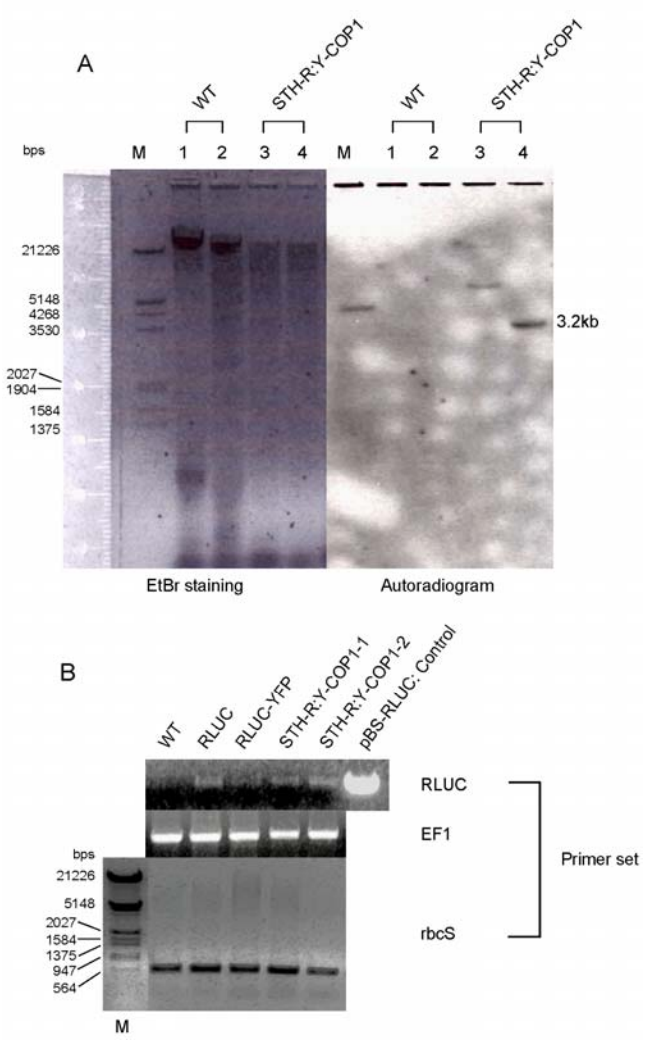

Figure II-4. Southern blotting and RT-PCR for the integration and the transcription of STH-RLUC

(A) Integration of the STH-RLUC expression cassette was confirmed by Southern blotting. 3.2 kb fragment indicates that the intact expression cassette of STH-RLUC is integrated in the genome of the BRET plant. The genomic DNA of lane 1 and 3 was digested by *Xho* I and lane 2 and 4 by *Pvu* II. (B) Transcripts of all foreign genes in the indicated transgenic plants are detected by RT-PCR. pBS-RLUC is used as a size control. EF1 and rbcS primer sets are used for normalization of transcript used for cDNA synthesis and detection of genomic DNA contamination, respectively.

II-3-3. Subcellular localizations of YFP-COP1 and YFP-HY5 in double transformed *Arabidopsis* expressing STH-RLUC:YFP-COP1 and RLUC-HYH:YFP-HY5

In the light-grown STH-RLUC:YFP-COP1 plant, the YFP-COP1 protein predominantly accumulated in the cytoplasmic inclusion bodies and also in the nucleus in the root hair, the trichome, and the whole seedling body (Fig. II-5), as observed in the transient bombardment assay (Fig. II-1B; von Arnim *et al*., 1997; Subramanian *et al*., 2004b). However, yellow fluorescence in the 35S-YFP plants was dispersed in the cytoplasm and the nuclei (Fig. II-5C and D). The bZIP transcription factors, HY5 and HYH were previously shown to be nuclear localized (Oyama *et al*., 1997; Holm *et al*., 2002). A previous transient bombardment assay showed strong nuclear accumulation of YFP-HY5 in onion cells (Fig. II-2B). In both the single and the double transformants expressing YFP-HY5, the yellow fluorescence of YFP-HY5 overlapped well with DAPI staining, indicating the nuclear localization of YFP-HY5 (Fig. II-6) whereas the transgenic plant expressing YFP alone emitted yellow fluorescence in the cytoplasm and in the nucleus (Fig. II-5C and D).

II-3-4. Determining *in vivo* interactions between STH and COP1 as well as between HY5 and HYH by BRET assay

The double transformed plants for BRET experiments, referred to as 'BRET plants', co-express pairs of BRET-tagged proteins in *Arabidopsis*. Initially, the optimal BRET tag positions for the efficient resonance energy transfer were confirmed in onion

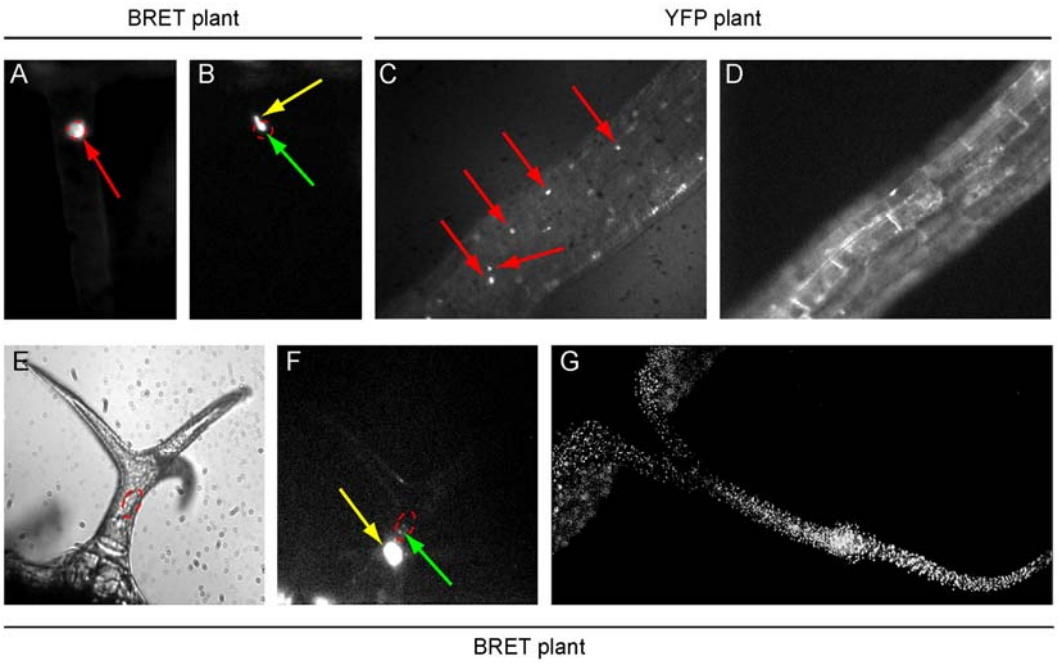

Figure II-5. YFP-COP1 localization of the BRET plant expressing STH-RLUC and YFP-COP1

(A) DAPI staining of a root hair. (B) YFP-COP1 expression at the cytoplasm in the corresponding cell of the root hair in (A). (C) DAPI staining of a primary root (D) YFP expression in the same root in (C). (E) Bright field image of a trichome on the leaf surface. (F) YFP-COP1 distribution in the cytoplasm as well as in the nucleus in the trichome. (G) YFP-COP1 expression in a 6-day old seedling of the BRET plant. (A) and (C) are DAPI staining and (B), (D), (F), and (G) are images taken at the YFP field. Red, yellow, and green represent the DAPI staining, the cytoplasmic YFP, and the nuclear YFP, respectively.

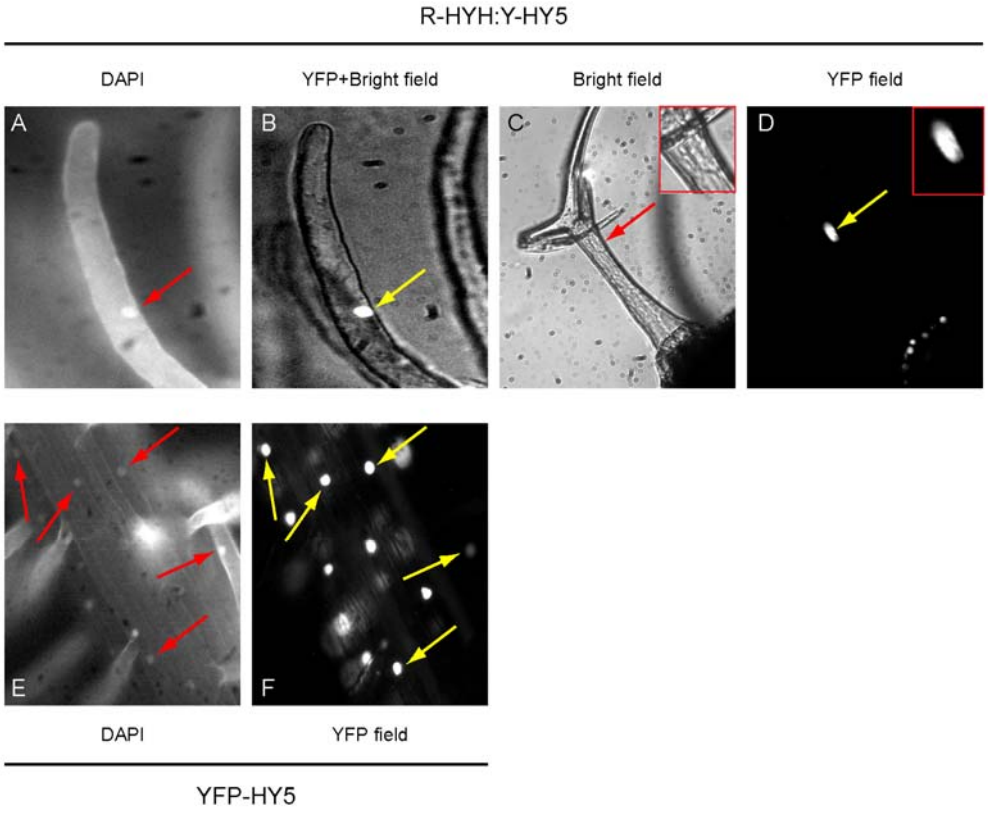

Figure II-6. YFP-HY5 expression in the single transgenic YFP-HY5 and the BRET plant containing the RLUC-HYH and the YFP-HY5 expression cassettes

(A-D) RLUC-HYH and YFP-HY5 double transgenic (E-F) YFP-HY5 single transgenic plant, (A) and (E) represent DAPI staining and the others are YFP signals in the nuclei. (A-B) Root hair; (C-D) Trichome. Inset images indicate the magnified nucleus and the YFP-HY5 in the nucleus, respectively; (E-F) Primary root. Red and yellow are the DAPI staining and the nucleic YFP, respectively.

epidermal cells by the transient BRET assays before generation of BRET plants. Based on the information about BRET tag orientations, two different BRET plants, namely STH-RLUC:YFP-COP1 and RLUC-HYH:YFP-HY5, were made by simultaneous dual-binary T-DNA transfer (Afolabi *et al*., 2004), as described before.

The interaction between STH and COP1 previously shown by the yeast two hybrid assay was further established by the BRET assay. Relative luminescence units of blue luminescence measured in the BRET plants were at least 20 times higher than the background, i.e. wild type plants in the presence of 2 μM coelenterazine (Fig. II-7A). Compared with the transgenic line expressing only STH-RLUC, plants co-expressing STH-RLUC and YFP-COP1 displayed an elevated yellow-to-blue luminescence ratio, as was measured in two independent lines, indicating *in vivo* protein interaction between STH and COP1 (Fig. II-7C). The heterodimer between bZIP transcription factors, HY5 and HYH was found by co-imunoprecipitation (Holm *et al*., 2002). In order to test the heterodimerization *in vivo*, the transient BRET assay was conducted and a positive BRET combination of RLUC-HYH:YFP-HY5 was pre-screened (Subramanian *et al*., 2006). Whereas no BRET was observed in the single transgenic controls without the energy acceptor such as RLUC-HYH and RLUC alone, the Y/B ratio of the positive BRET combination was elevated, suggesting that the resonance energy was efficiently transferred from RLUC-HYH to YFP-HY5 in stable transformed *Arabidopsis* (Fig. II-8C).

II-3-5. Improvement of BRET

Not all BRET fusion cassettes employing the regular RLUC sequence were

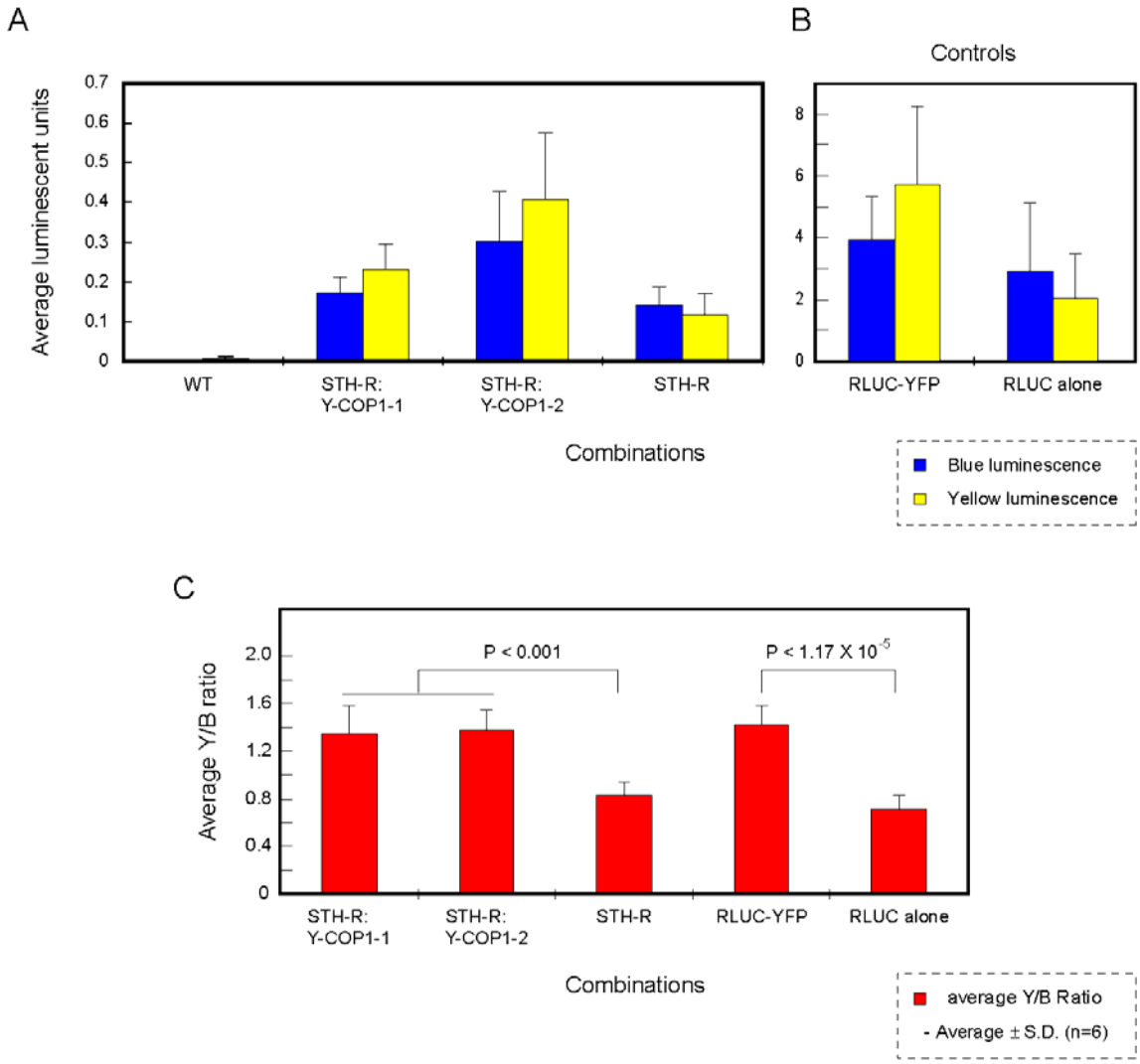

Figure II-7. *In vivo* BRET assay for the study of the protein-protein interaction between STH-RLUC and YFP-COP1

(A) and (B) represent luminescence measurement of transgenic plants. STH-RLUC and RLUC alone plants served as negative controls and RLUC-YFP is a positive control. Wild type seedlings are used for the background measurement. (C) Converted Y/B ratios from the LUC measurements. The BRET combinations show elevated BRET ratios, compared with those of negative contols. Blue and yellow bars indicate the measurement of blue and yellow luminescence and red represents average Y/B ratio.

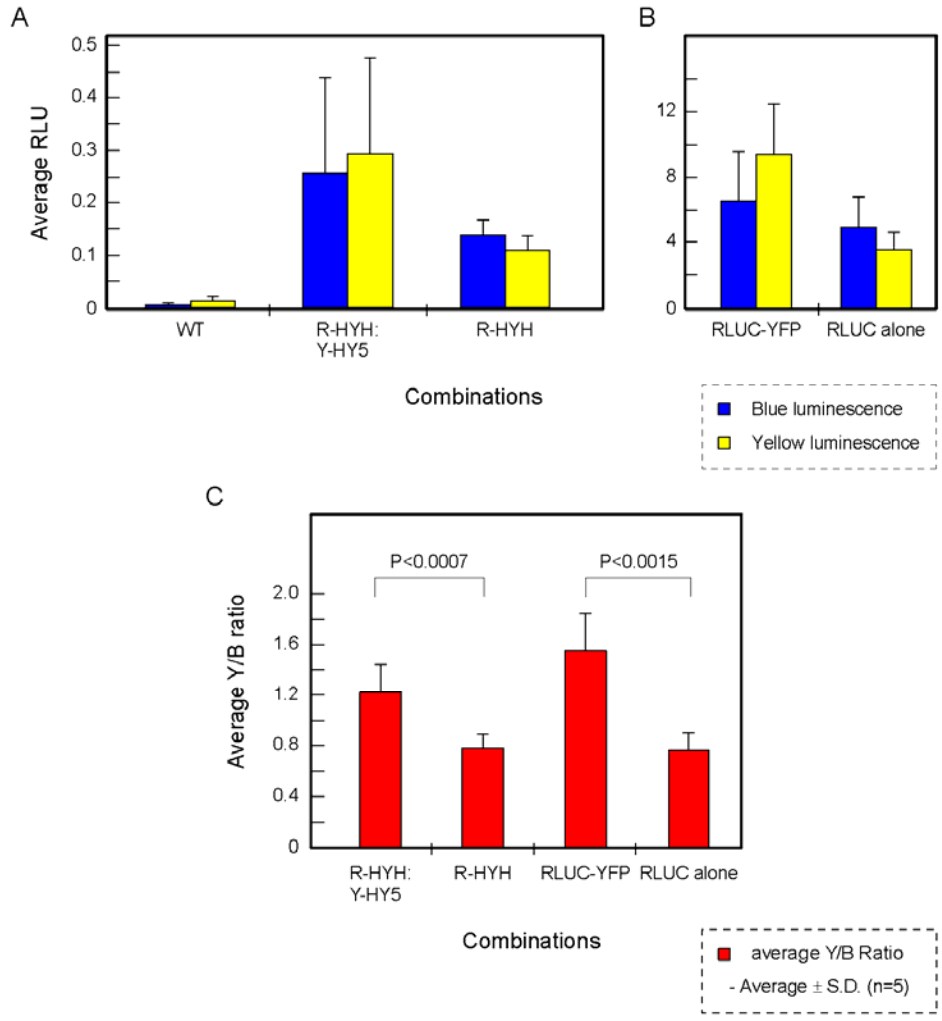

Figure II-8. *In vivo* BRET assay of the interaction between RLUC-HYH and YFP-HY5

The elevated Y/B ratio of the BRET combination indicates the interaction between bZIP transcription factors. Figure legends are same with Fig. II-7.

expressed in plants. To optimize and increase the expression of the BRET fusion cassettes, the regular RLUC cDNA was replaced with the hRLUC sequence, a codon optimized RLUC (Packard Biosignal Inc.). Transgenic lines expressing RLUC or hRLUC fused to HY5 were made and the RLUC activities were assayed. Alongside the RLUC or hRLUC fusion constructs driven by the strong 35S promoter, the native promoter versions of the expression constructs were also transformed to *Arabidopsis*. At least ten independent transgenic plants of each construct were tested. All plants containing the RLUC fusion constructs driven by the HY5 promoter luminesced at a low level, compared with corresponding constructs driven by the 35S promoter. The same trend was observed in the plants expressing the hRLUC fusion proteins. Comparing the luciferase activity of 35S-HY5-hR with 35S-RLUC, the emission level of the 35S-HY5-hR plants was sometimes two times higher (Fig. II-9A). The increased emission from the plants with the hRLUC fusion constructs were captured by the Hamamatsu intensified CCD (Fig. II-9B). The photon-counting image showed the blue photon emission from hypocotyls and roots where native HY5 is expressed (Oyama *et al*., 1997). However, the photons of the 35S RLUC plant were emitted from leaves, hypocotyls, and roots. Before the coelenterazine application, mock treated plants did not emit any photon (Fig. II-9B). Taken all together, the luminometry measurements and the photon-counting image suggest that hRLUC may be a better choice than the regular RLUC as the energy donor for the BRET application in *Arabidopsis*.

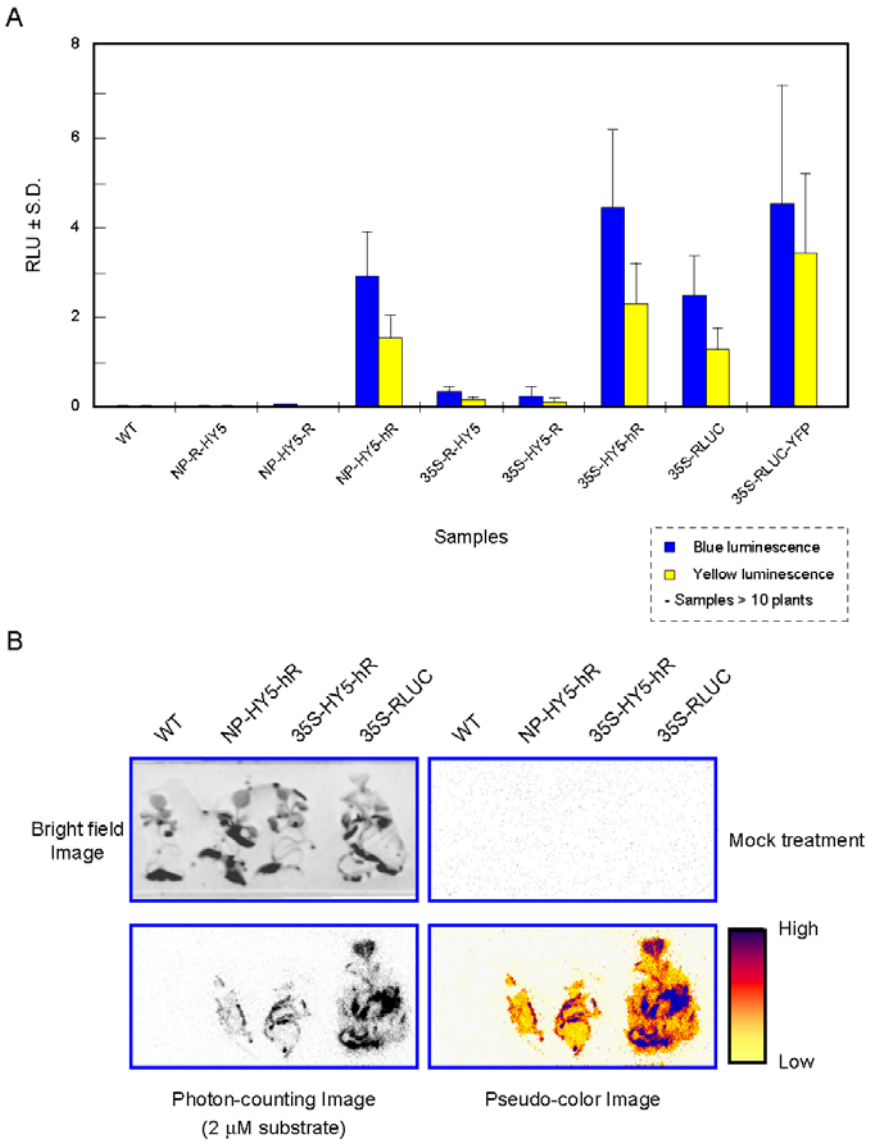

Figure II-9. Improvement of luciferase activity in *Arabidopsis*

(A) Comparison of *in vivo* hRLUC activity with the regular RLUC. Average RLU comes from the LUC measurement of over ten independent transgenic plants. S.D. represents standard deviation. (B) A photon-count image of HY5-hRLUC plants and RLUC plant. NP and 35S represent the native promoter of HY5 and the strong CaMV 35S promoter, respectively. hR indicates hRLUC, a codon optimized RLUC. Color scale of photon emission is at the pseudo-color image.

II-4. Discussion

Using the *in vivo* BRET assay, the heterodimeric interactions between STH and COP1 as well as between HY5 and HYH were confirmed by transient expression assay in onion cells, and further confirmed in stable transformed *Arabidopsis* generated by simultaneous agrobacterium-mediated transformation (Fig. II-7 and II-8). The dual-binary T-DNA delivery system (Afolabi *et al*., 2004) is a convenient method to generate BRET plants within a short period of time. Among seven different BRET plants, which have been made by the dual-binary T-DNA delivery system, two BRET plants presented in Chapter II shows detectable resonance energy transfer (Fig. II-7C and Fig. II-8C). Unlike single transformation with a T-DNA containing two expression cassettes to make BRET plants, individual transgenes are separable if necessary since the two foreign genes may be genetically unlinked.

In addition, a homodimerization between HY5 proteins was tested by the transient BRET assay. Among four possible BRET combinations, only one combination showed detectable resonance energy transfer, in agreement with a recent structural analysis (Yoon *et al*., 2007). This crystal structure showed the ZIP domain-mediated HY5 dimerization, indicating that the C-terminal BRET tags in the homodimer might have an optimal configuration for the resonance energy transfer. In the homodimerizations such as the COP1 (Subramanian *et al*., 2004b) and the HY5 dimer, it is predictable that certain self-competitions take place. For example, there are three possible pairs between the BRET tagged-HY5 proteins including HY5-hRLUC:HY5-hRLUC (the donor dimerization), HY5-YFP:HY5-YFP (the acceptor dimerization), and HY5-hRLUC:HY5-

YFP (the BRET pair) in the cell. The donor dimerization and the acceptor dimerization are predicted to cause a reduction in the abundance of the positive BRET pair (HY5-hRLUC:HY5-YFP), weakening the signal intensity of BRET from HY5-hRLUC to HY5-YFP. However, BRET from HY5-hRLUC to HY5-YFP is detectable even in the presence of competing, BRET–inactive interactions, indicating that the cuvette-based BRET assay is sensitive enough to detect the interaction in living cells (Fig. II-2).

Bioluminescence resonance energy transfer is a versatile technique suitable for examining *in vivo* protein-protein interactions in real time. Although early application of the BRET system has been successful to test protein-protein interactions in *Arabidopsis*, BRET needs to be optimized for enhancing RLUC activity in *Arabidopsis*. As a first step to improve BRET, the replacement of the regular RLUC sequence with a human codon optimized RLUC (hRLUC) yielded better expression efficiency (Subramanian *et al*., 2006). In the case of HY5, the hRLUC fusion protein was detectable when driven by the native promoter (Fig. II-9A). Although BRET is not an image-based technology like FRET, success with BRET imaging would be a tangible advance. Recently, the BRET image of the COP1 dimerization has been taken at the tissue level in tobacco seedlings (Xu *et al*., 2007). Subcellular BRET imaging has also been demonstrated in mammalian cells (Hoshino *et al*., 2007; Coulon *et al*., 2008). In order to enhance the resolution of the BRET image, advances should be made in the sensitivity of detection and in the robustness of the biological reagents, in particular by improving the enzymatic characteristics of RLUC, and by selecting BRET tags with better spectral overlap between the emission maximum of the energy donor and the absorption spectrum of the energy acceptor. Beside the importance of *Renilla* luciferase in the BRET system, RLUC

has become popular as a reporter for labeling cancerous implants in animal model studies (Bhaumik and Gambhir, 2002; De and Gambhir, 2005; Chan *et al*., 2008). Thus, the understanding of the enzymatic reaction mechanism of the energy donor is required for identification of new BRET donors and diagnostic reagents generated by protein engineering.

II-5. Materials and Methods

II-5-1. Plant growth condition and transgenic lines

Columbia WT and transgenic seedlings used for this research were germinated on 0.8% agar media containing MS, Murashige and Skoog salts (Sigma, St. Louis), and 1% sucrose without antibiotics. The transgenic plants expressing the RLUC cassette were grown on a selection MS media containing 100 μg/ml gentamycin and YFP expressing transgenic plants were on a MS media containing 50 μg/ml kanamycin. For the double transformed plants, the selection MS media contains both 100 μg/ml gentamycin and 50 μg/ml kanamycin. After 2 days cold treatment, all plants grew under continuous light at 22°C.

II-5-2. T-DNA constructs and T-DNA shuttling

STH cDNA (Salt tolerence homolog; GeneBank accession No. AF453477) was a gift from Dr. Magnus Holm. The cDNA was amplified with oligonucleotides using 5'-

cacctgagatctaccatggccaagatacaatgtg-3' containing a *Nco* I site and 5'-tatcaagcggccgcg cctaggtcggggactag-3' with a *Not* I site. Amplified *STH* cDNA was cloned into the pENTR TOPO vector (Invitrogen). After digestion of cloned *STH* with *Nco* I and *Not* I, the fragment was inserted to the 35S:RLUC vector (GeneBank accession No. AY189980; Subramanian *et al*., 2004a). The 35S:STH expression cassette C-terminally tagged with RLUC was restricted by *Kpn* I and *Sac* I. The digested expression cassette was inserted to the *Kpn* I and *Sac* I site (pPZP222-35S:STH-RLUC) on the pPZP 222 binary vector (GeneBank accession No. U10463). For making the YFP-COP1 construct, pT7RLUC•YFP (Xu *et al*., 1999) was used as a template to amplify YFP (yellow fluorescent protein) using 5'-ggagatctcgggatccccgggtaccg-3' and 5'-gagagatctcttgtacagc tcgtccat-3'. After the amplified fragments were cut by *Nco* I and *Bgl* II, the digested fragments were inserted to the pBluescript (Stratagene) with the 35S promoter. *COP1* cDNA (GeneBank accession No. L24437) was cloned to the *Bgl* II site on the pBluescript:35S with YFP. The 35S:YFP-COP1 expression cassette was moved to the *Sal* I and *Sma* I site (pBin-35S:YFP-COP1) on the pBin19 binary vector (GeneBank accession No. U12540). Both of them were transformed into agrobacterium competent cells by co-electroporation at the same time. In terms of the double transformant, single agrobacterium cell expresses two constructs. Also, each construct was transformed into agrobacterium cells separately. These strains are referred to as single transformants. After DNA isolation of single transformants and double transformants from agrobacteria, precipitated DNAs were used for transformation back to the *E*. *coli* competent cells. Each construct in *E*. *coli* was precipitated again and confirmed by restriction (Fig. II-10; T-DNA shuttling). Confirmed single transformants and double transformants containing

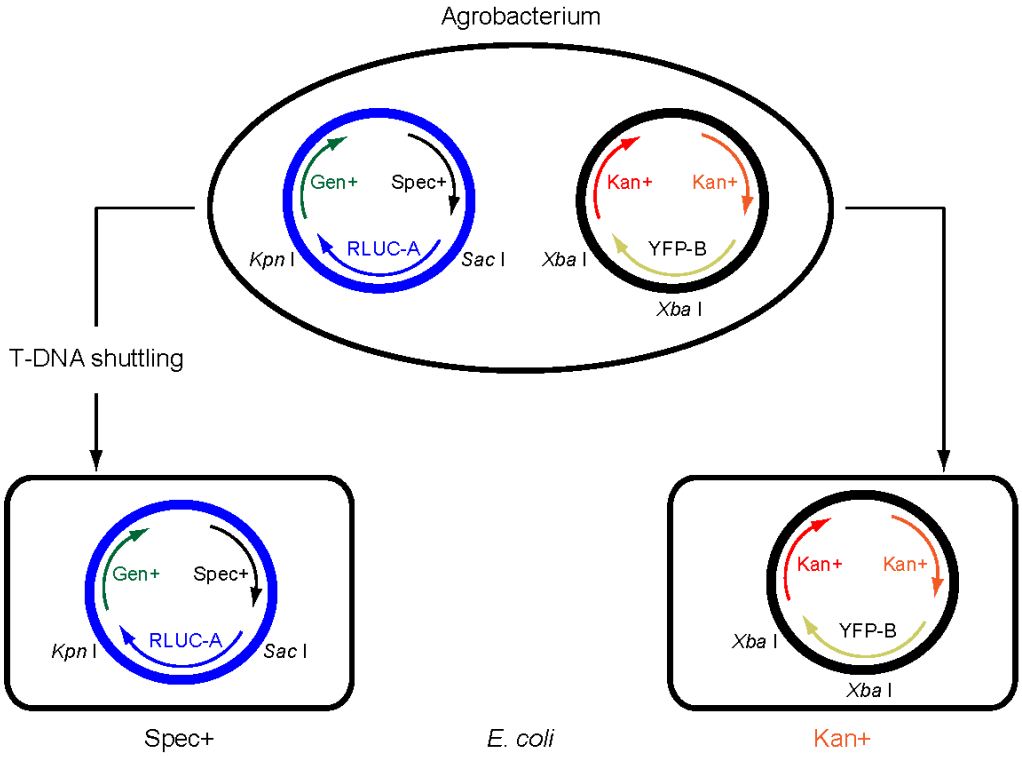

Figure II-10. Double transformation into agrobacterium single cell and T-DNA shuttling

Double transformed agrobacteria are generated by co-electroporation and then the isolated T-DNAs from the double transformants are used for back-transformation into *E. coli*. The RLUC fusion and the YFP fusion expression cassette carry the selection marker of spectinomycin and kanamycin resistance in *E. coli* and gentamycin and kanamycin resistance in the plant, respectively. Blue and black circles represent pPZP222 and pBIN19 binary vectors, respectively. Restriction enzyme sites used for T-DNA shuttling are marked on each construct.

BRET expression cassettes were used for plant transformation via the floral dip method. T1 transformed plants were selected on 1/2 MS medium containing 100 μg/ml gentamycin and 50 μg/ml kanamycin. RLUC-HYH and YFP-COP1 plant were constructed following the same procedure.

II-5-3. Transient expression assays in onion epidermal cells

Onion epidermal cells were transformed using PDS-1000 / He Biolistic Particle delivery System (Bio-Rad), and 1100 psi rupture discs were employed. The inner epidermis of an onion was peeled and placed in MS agar plates. After bombardment with 500 ng plasmids as indicated, onion layers were incubated in the darkness for 18 hours. Then, YFP expression was investigated by fluorescence microscopy after water mounting. For measuring RLUC activity, 2 μM coelenterazine was applied under the darkness for 20 min. RLUC activity or BRET was measured from onion layers using TD-20/20 luminometer with the dual BRET filter (Turner Designs, Sunnyvale, CA). Each measurement was carried out four times at 35% sensitivity (Integration time and delay time were 10 sec and 3 sec, respectively) in living cells.

II-5-4. Screening of transgenic plants

For single transformants expressing RLUC or RLUC fusion constrcuts, plants were selected on MS agar plates containing 100 μg/mL gentamycin. For YFP transgenic *Arabidopsis*, plants grew in 50 μg/mL kanamycin plates. Double transformants were

selected in agar MS plates containing both 100 μg/mL gentamycin and 50 μg/mL kanamycin.

II-5-5. *In vivo* BRET assay

Luminescence units were measured from 6 to 10 day-old seedlings in the presence of 2 μM coelenterazine (Biotium, Hayward, CA) in water using a TD-20/20 tube luminometer that is equipped with the dual-color filter. After adding 2 μM coelenterazine, samples were incubated in darkness for 10 min at room temperature to allow the substrate to penetrate into plants and to allow delayed chlorophyll autofluorescence to decay. Otherwise, methods were the same as for onion cells. The Y/B ratio, yellow luminescent units divided by blue luminescent units, was calculated for determining the protein interaction (Xu *et al*., 1999; Subramanian *et al*., 2006) between STH and COP1. BRET was measured from 3 seedlings of each family together.

CHAPTER III.

STRUCTURE BASED FUNCTIONAL STUDY OF *RENILLA* LUCIFERASE (RLUC) AND IMPROVEMENT OF ENZYMATIC PROPERTIES BY PROTEIN ENGINEERING

Part of this chapter has been published in the journal *Protein Science*.

Jongchan Woo, Matthew H. Howell, and Albrecht G. von Arnim. 2008. Structure-function studies on the active site of the coelenterazine-dependent luciferase from *Renilla*. *Protein Science* 17, 725-735.

III-1. Abstract

Renilla luciferase (RLUC) is a versatile tool for gene expression assays and *in vivo* biosensor applications, but its catalytic mechanism remains to be elucidated. RLUC is evolutionarily related to the α/β hydrolase family. Its closest known homologs are bacterial dehalogenases raising the question how a protein with a hydrolase fold can function as a decarboxylating oxygenase. In spite of limited information on RLUC properties, engineering of the native protein sequence for enhanced performance under heterologous expression conditions has just begun recently. Homology modeling of the protein structure and molecular docking simulations with the coelenterazine substrate were used to build hypotheses about functionally important residues, which were subsequently tested by site-directed mutagenesis, heterologous expression experiments, and bioluminescence emission spectroscopy. My site directed mutagenesis data and bioluminescence emission spectra of the mutants highlight two triads of residues that are critical for catalysis. For histidine 285, its role in catalysis was confirmed by inactivation with diethylpyrocarbonate. Multiple substitutions of N53, W121, and P220, three other residues implicated in product binding in the homologous dehalogenase, *Sphingomonas*

LinB, also supported their involvement in catalysis. Additional residues near the entrance to the active site may play a role in guiding the substrate into the substantially hydrophobic binding pocket. Mutations of proline 220 extended the half-life of photon emission, which yielded brighter signals when expressed in *E. coli*. Because D120, H285, and E144 bear only limited resemblance to the residues found in the active site of aequorin, the reaction scheme employed by RLUC probably differs substantially from the one established for aequorin. Instead, the panel of critical residues resembles that of the bacterial dehalogenase LinB, which served as the template for homology modeling. Random mutagenesis was employed to select new mutations that enhanced the intensity of photon emission, yet maintained an emission maximum near 470nm, and yielded more stable light emission over time. Integrated into an existing codon-optimized RLUC cDNA and combined with previously identified mutations, this advance may prove useful for adaptation of RLUC as a reporter protein, biosensor, or resonance energy donor in heterologous host cells.

III-2. Introduction

The blue-light emitting luciferase of the marine anthozoan *Renilla reniformis* (RLUC; E.C. number 1.13.12.5, luciferin-2-monooxygenase, decarboxylating) has become popular as a reporter enzyme for gene expression assays (Lorenz *et al*., 1991) and also serves as an energy donor for protein-interaction assays based on bioluminescence resonance energy transfer (Xu *et al*., 1999; Subramanian *et al*., 2006). Attempts to improve the enzymatic properties by protein engineering are hampered by

the fact that the enzymatic reaction mechanism of RLUC is not well understood, although mutagenesis approaches have nevertheless started to bear fruit (Loening *et al*., 2006; Hoshino *et al*., 2007). However, a better understanding of the enzymatic mechanism catalyzed by RLUC would be helpful. The substrate of *Renilla* luciferase, coelenterazine, is an aromatic imidazolo-pyrazinone, which is derivatized on three of its carbon ring atoms with p-hydroxy-phenyl (R1), benzyl (R2), and p-hydroxy-benzyl (R3) moieties. Coelenterazine is turned over in an oxidative decarboxylation reaction during which the imidazole ring is opened and carbon dioxide is released (Matthews *et al*., 1977a and b; Ohmiya and Hirano, 1996). The primary product, an electronically excited state of coelenteramide, relaxes to its ground state by emission of a photon of blue (~470 nm) light. Because RLUC does not require ATP for activity and is active in a range of heterologous hosts that includes bacteria, fungi, animals, and plants, new uses continue to be developed for this enzyme (Paulmurugan *et al*., 2003; Xu *et al*., 2007).

In its native organism, RLUC associates with a green fluorescent partner protein, as well as with a coelenterazine-binding protein, which is thought to deliver one molecule of substrate to RLUC upon exposure to calcium ions (Ward and Cormier, 1979). Because these partners are absent upon expression of RLUC in heterologous host cells, re-engineering of the RLUC sequence might improve undesirable properties such as enzymatic inactivation in the presence of substrate that results in light being emitted as a brief flash. While a short half-life of the enzyme might be beneficial for time-resolved gene expression studies, this property limits the suitability of the enzyme for protein-interaction studies based on bioluminescence resonance energy transfer (BRET). Alterations in the K_m, V_{max}, or other characteristics may also be beneficial.

Several high-resolution crystal structures in the presence or absence of the coelenterazine ligand have been solved for the calcium-dependent EF-hand photoproteins, aequorin and obelin (Head *et al*., 2000; Liu *et al*., 2000; Vysotski *et al*., 2003; Deng *et al*., 2004). Here, the coelenterazine reacts with molecular oxygen in a reaction coordinated by a catalytic triad of tyrosine (Y184 and Y190 in aequorin and obelin, respectively), tryptophan (W173 and W179), and histidine (H169 and H175). The Y190 residue stabilizes the hydroperoxy group of the oxidized coelenterazine via a hydrogen bond. In the strict sense, the term aequorin refers to this complex between the apo-aequorin polypeptide and the reaction intermediate. Upon calcium binding, H175 shifts position thus triggering a proton relay that deprotonates first Y190 and subsequently the hydroperoxy group of the reaction intermediate. The resulting peroxy-coelenterazine anion then reacts as a nucleophile to form a dioxetanone ring. This highly unstable intermediate spontaneously decarboxylates, yielding one molecule of carbon dioxide and the electronically excited state of coelenteramide, which relaxes to the ground state by emission of a photon. Typically, the coelenteramide is thought to be deprotonated at the R1 hydroxyl group (phenolate anion), likely due to a nearby histidine residue (H22). Under these conditions, photon emission will be in the blue range (470-490 nm; Deng *et al*., 2004; Vysotski *et al*., 2004). However, if coelenteramide remains protonated, i.e. neutral, it emits a photon of purple light (~400 nm; Deng *et al*., 2004; Vysotski and Lee, 2004; Liu *et al*., 2006). Spent aequorin is not immediately able to catalyze oxidation of a second coelenterazine substrate molecule. Instead, removal of the coelenteramide product and binding of a fresh substrate molecule require the concomitant removal and binding of calcium (Shimomura and Johnson, 1975), at least *in*

vitro.

Because RLUC uses the same substrate as apo-aequorin, yields the same products, and emits a photon with similar spectral characteristics as aequorin and obelin, the reaction mechanisms are expected to be similar (Matthews *et al*., 1977a and b). For example, the alternative substrate *bisdeoxycoelenterazine* (trade name, DeepBlue C) lacks the p-hydroxyl group on the R1 ring and, as would be expected by analogy with obelin, emits at 405 nm rather than around 480 nm. Aequorin can also function as a calcium-dependent luciferase (Inouye and Sasaki, 2007). The active site of apo-aequorin is highly hydrophobic and has three sets of triads consisting of tyrosine, histidine, and tryptophan. One of the triads functions as the catalytic triad and two others are involved in substrate binding (Head *et al*., 2000). However, RLUC itself is not calcium dependent. Therefore, RLUC may not possess a residue equivalent to Y190, the residue that stabilizes the hydroperoxy-coelenterazine intermediate in obelin. More importantly, RLUC and aequorin are not homologous to each other. Instead, RLUC is clearly homologous with bacterial haloalkane dehalogenases of the LinB family (Loening *et al*., 2006 and 2007b), thus joining the bacterial dioxygenases Hod and Qdo as an oxygenase derived from an α/β hydrolase ancestor (Frerichs-Deeken *et al*., 2004). Crystal structures of *Sphingomonas paucimobilis* LinB and related enzymes, which share above 42% of amino acid sequence identity with RLUC, show the characteristic fold of the α/β hydrolase superfamily (PDB ID, 1IZ8; Marek *et al*., 2000; Oakley *et al*., 2004) with a catalytic triad consisting of an aspartic acid in the nucleophile elbow, glutamic acid, and a histidine as a catalytic base (Loening *et al*., 2007a). Haloalkane dehalogenases including LinB can cleave a bond between carbon and halogen in

haloalkane molecules, thus producing inorganic halide ions and alcohols as byproducts (Holmquist, 2000; Oakley *et al*., 2004). In the catalytic triad of the haloalkane dehalogenase of *Xanthobacter autotrophicus,* whose mechanism has been well studied (reviewed in Holmquist, 2000), D124 functions as a nucleophile, H289 as a general base, and D260 as a catalytic acid. The substrate, 1.2-dichloroethane, binds to W175 and W125 in the active site, followed by the attack of D124 on the carbon-halogen bond. The intermediate alkyl-enzyme complex is attacked by a nucleophilic water molecule that interacts with histidine 289 interacting with D260. The nucleophilic water attack results in producing a tetrahedral oxyanion intermediate, which decomposes releasing a halogen and an alcohol molecule from the active site. The three equivalent catalytic triad residues reside in LinB are D108, H272, and E132 (Hynkova *et al*., 1999). They are conserved and functionally important in RLUC (Loening *et al*., 2006). Most recently, crystal structures of a stabilized form of RLUC carrying eight to ten amino acid substitutions (RLUC8) have been solved with and without the coelenteramide product (PDB ID, 2PSD 2PSE, 2PSF, 2PSH, 2PSJ; Loening *et al*., 2007a). These structures confirm the overall α/β hydrolase fold and the arrangement of the putative catalytic triad residues at the bottom of the active site cavity. Conformational differences between the solved crystal structures of RLUC depending on the crystallization conditions and also on the presence or absence of the reaction product suggest considerable flexibility of a surface-exposed α-helical section near the entrance to the active site as well as variations in the residues lining the active site per se. The coelenteramide product is seen on the flank of the outer portion of the active site (PDB ID, 2PSJ; Loening *et al*., 2007a). Only the para-hydroxyl on the R1-ring of the coelenteramide product is in

hydrogen-bonding distance to the putative catalytic triad. Meanwhile, the former reactive center of the product, the C2 carbon of the central heterocyclic ring, lies distal to the putative catalytic triad residues where its position is on the flank of the outer portion of the active site. Its position was interpreted as indicative of a non-productive binding mode (Loening *et al*., 2007a).

In this work, I have used the solved crystal structures of RLUC together with homology modeling and subsequent docking studies to make testable predictions about the active site of RLUC, the residues facilitating entry of coelenterazine into the active site, positioning of the substrate, as well as potential residues responsible for catalysis and spectral properties. These predictions were tested by site-directed mutagenesis and expression of recombinant RLUC enzyme as well as using pharmacological inhibitors. Moreover, I applied random mutagenesis with the goal of improving specific enzymatic parameters of RLUC, including the apparent k_{cat} and resistance against loss of activity. These alterations may enhance the utility of RLUC for BRET and other applications.

III-3. Results

In an attempt to build a hypothesis for how the native RLUC enzyme might position the coelenterazine substrate in preparation for catalysis, and in the absence of a crystal structure for RLUC, I initially generated a homology model using SwissModel ProModII (Schwede *et al*., 2003) based on the solved crystal structures of the bacterial haloalkane dehalogenase *Sphingomonas paucimobilis* LinB (Oakley *et al*., 2004) (PDB ID, 1IZ8A, 1K6EA, 1IZ7A, 1MJ5A; Fig. III-1A). The protein sequence identity between

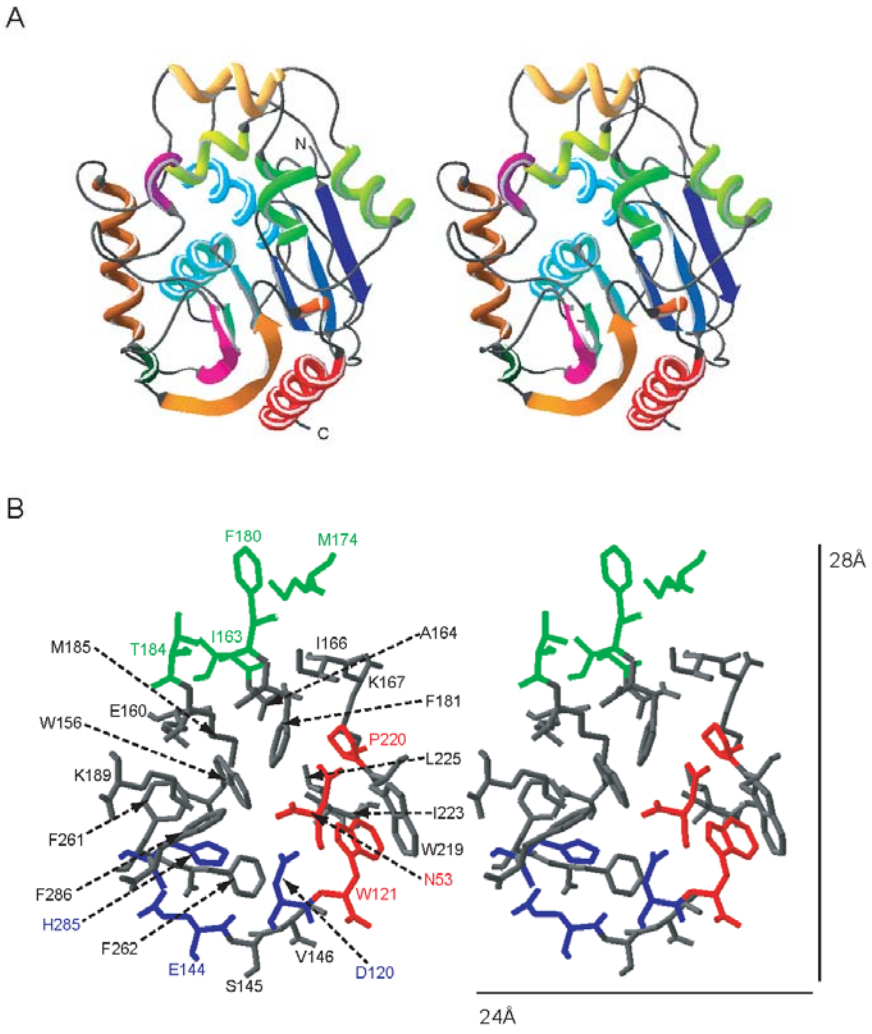

Figure III-1. Homology model and predicted active site of *Renilla* luciferase (RLUC)

(A) Stereoview of the overall fold looking down onto the cap motif with the gateway. (B) Active site residues identified using a 1.6Å probe. Color coding illustrates groups of residues that may be functionally related and many of them were subjected to mutagenesis. Blue represents the conserved catalytic triad. Red represents three other residues thought to be involved in substrate binding. Green represents the residues forming the narrow gateway, which is the main pocket of discrepancy between the model and the crystal structures.

LinB and RLUC is 42%. The root mean square deviation (rmsd) between the alpha carbon backbone, excluding loops, of the RLUC model and the LinB structure (262 out of 275 residues) was 0.34Å, suggesting a highly parsimonious model. A very similar model was obtained using the MOE software (Chemical Computing Group, Inc., Montreal, Canada) and in an independent study (Loening *et al*., 2006). According to the homology model, the active site is made up of 26 residues, of which 9 are aromatic, 17 are hydrophobic, and 9 are hydrophilic (Fig. III-1B). The outer portion of the active site is largely hydrophobic, while most of its more hydrophilic residues reside in the inner portion. The recently solved crystal structure of RLUC8 in the absence of product (Loening *et al*., 2007a) is also similar to our model (rmsd with PDB ID, 2PSD was 1.0Å over 254 residues excluding several large surface loops), validating the strategy of using a homology model to guide our mutagenesis approach. The catalytic triad of the LinB dehalogenase consists of D, E and H (Hynkova *et al*., 1999). All three residues are conserved and essential in RLUC although it is an oxygenase (Loening *et al*., 2006). Our model, in line with the crystal structures, suggests that these residues, D120, E144, and H285, lie close together at the bottom of the binding cavity in an almost identical spatial configuration as in LinB (Fig. III-2A).

III-3-1. Docking simulations

There is an entrance for coelenterazine in the flexible cap domain. The gateway of RLUC8 (Loening *et al*., 2007a) consists of W156, I159, D162, I165, M174, F180, V185 (M in RLUC), K189, F261 and F262 in the crystal structures (PDB ID, 2PSD and

Figure III-2. RLUC protein structure displays and substrate docking simulations (A) Overlay comparison between the catalytic triad and other active site residues of *Sphingomonas* haloalkane dehalogenase, LinB (PDB ID, IZ7A; red), the corresponding residues in the wild-type RLUC homology model (green), and the RLUC8 crystal structure (PDB ID, 2PSD; blue; Loening *et al*. 2007a). (B) Coelenterazine; oxygen and nitrogen are colored red and blue respectively. Carbon and selected hydrogen are gray and white. (C-E) Docking simulations of coelenterazine to the lower portion of the RLUC active site including the putative catalytic triad. Hydrogen bonds are symbolized by dashed green lines. (C-D) Docking of native coelenterazine (C) and the reaction intermediate, 2-hydroperoxy-coelenterazine (D) against the RLUC homology model. Note interactions between the hydroperoxy group and active site residues N53, W121, and P220. (E) Docking of the reaction intermediate, 2-hydroperoxy-coelenterazine was performed with the RLUC crystal structure obtained after exposure to substrate (PDB ID, 2PSJ). In this alternative docking simulation the reaction intermediate is suspended by hydrogen bonds between the R1 and R3 hydroxyls to N53 and the backbone of F262, respectively, while the reactive center is juxtaposed to the catalytic triad.

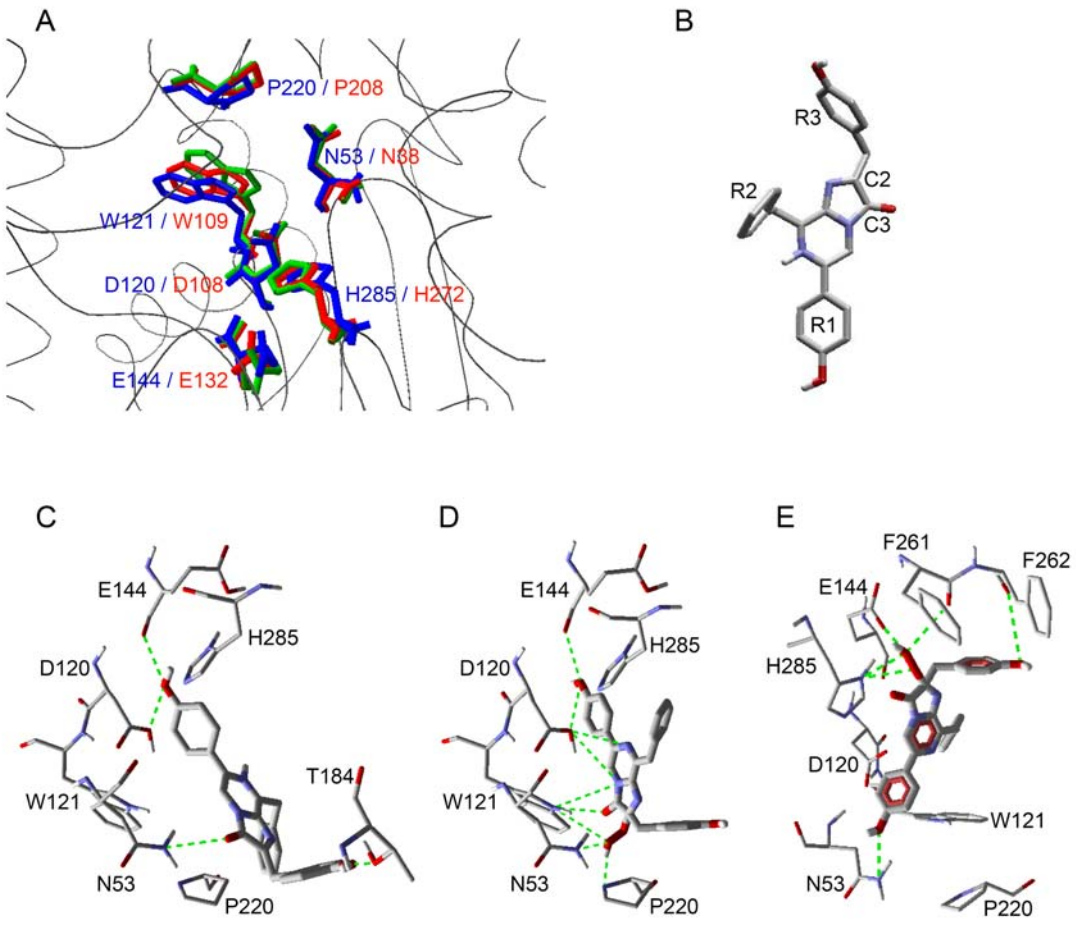

Figure III-2. Continued.

2PSJ). W156, I159, D162, F261, and F262 are flexible, however, the others are not, indicating that the size of the gateway may be dynamically changed by the location of the flexible residues on the gateway. To suggest important residues involved in the bioluminescence reaction, I performed docking simulations with our model and the crystal structures. Although the catalytic triad and several other residues in the active site were well conserved (Fig. III-1A), RLUC protein adopted a variety of structures (Loening *et al*., 2007a). In the docking simulations with the homology model, the hydroxyl group on the R1 ring of coelenterazine interacted with both D120 and E144 while the hydroxyl group on the R3 ring was bound to T184 (Fig. III-2C). When water was included in the docking simulation the results were similar except that the R1 hydroxyl group bound to H285 via a water molecule (not shown). Meanwhile, coelenterazine's reactive center, i.e. the C2 carbon, which initially reacts with oxygen, and the C3 carbonyl, which is eliminated in the form of CO_2, were docked in hydrogen-bonding distance to N53 (Fig. III-2C). It is unclear whether the oxidation of coelenterazine occurs inside or outside of the active site. Likewise, the hydroperoxy group of the reaction intermediate had the potential to hydrogen bond with N53, W121, and P220 (Fig. III-2D). Coincidentally, the same three residues are implicated in coordination of the eliminated halide anion in the LinB dehalogenase (Oakley *et al*., 2004). Similar results were obtained when 2-hydroperoxy-coelenterazine was docked to the crystal structures of RLUC8 that was obtained in the absence of substrate (PDB ID, 2PSD and 2PSF; not shown). Crystal structures of RLUC8 differ substantially with respect to the width of the gateway (Fig. III-3; Loening *et al*., 2007a), a situation previously observed with the equivalent surface helix in the cap domain of LinB

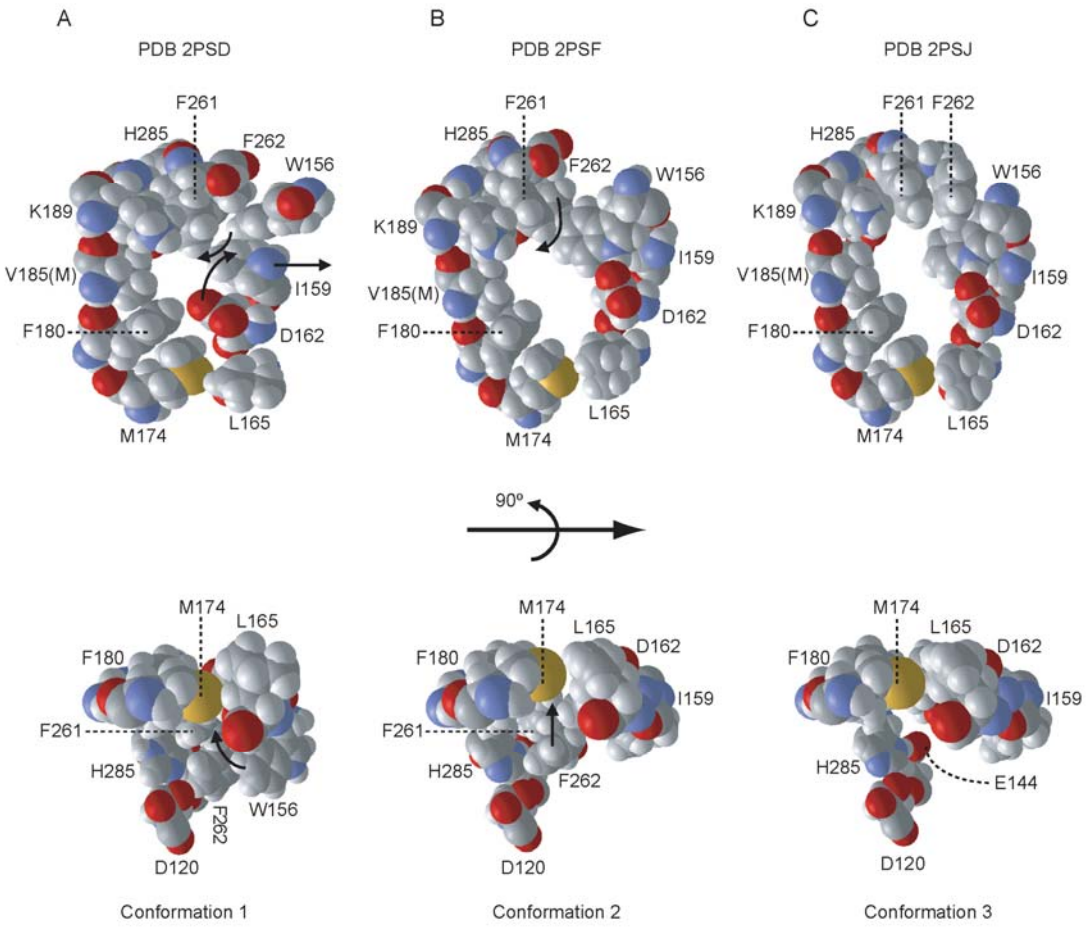

Figure III-3. Space filling residues of the gateway into the active site in three different crystal structures of RLUC8 presented in Loening *et al*. 2007a. 2PSD and 2PSF were crystallized without coelenterazine but 2PSJ was co-crystallized with coelenterazine. The upper panels show a top-down view of the gateway and the corresponding lower panels are side views that include the catalytic triad residues H285, D120 and E144. Note the flexibility in the positions of the residues forming the right half of the gateway (arrows). Accession numbers of the structures in the Protein Data Bank are indicated. Structure 2PSJ was obtained in the presence of the reaction product (not shown). Blue, red, and yellow represent nitrogen, oxygen, and sulfur atoms, respectively. M185 in RLUC is V185 in RLUC8.

(Streltsov *et al*., 2003). When docking was performed with the crystal structure that was obtained after exposing RLUC8 to substrate (PDB ID, 2PSJ), which has a wider gateway, most docking models showed the reactive center of coelenterazine juxtaposed to the putative catalytic triad residues, E144, and H285, as well as the backbone carbonyl of F261, while the R1 hydroxyl group interacted with N53 and the R3 hydroxyl group interacted with F262 (Fig. III-2E). These different, yet highly reproducible docking models represent two distinct hypotheses concerning the roles of the putative catalytic triad consisting of D120, E144, and H285 on the one hand and the triad consisting of N53, W121, and P220 on the other. In the following, these hypotheses were further tested by site-directed mutagenesis, drug inhibition, and scanning of emission spectra.

III-3-2. Inhibitor studies

Several enzymes that rely on a catalytic histidine are sensitive to diethylpyrocarbonate (DEPC) treatment, and H285 among ten histidines in the entire RLUC sequence is the only histidine in the RLUC active site. RLUC enzyme purified from *E. coli* was also inactivated by low concentrations of DEPC (IC_{50} at 2 μM substrate was 220 nM; kI was 160 nM) consistent with a role for H285 in RLUC catalysis (Fig. III-4A). For comparison, RLUC was also sensitive to Woodward Reagent K (Fig. III-4B). Because this reagent modifies acidic residues in a hydrophilic environment, the most likely target residue may be D162 (Fig. III-3). The serine/cysteine-reactive compound, PMSF (phenylmethylsulfonylfluoride) also inactivated RLUC (Fig. III-4C), perhaps by targeting S145 or S263, which lies near H285.

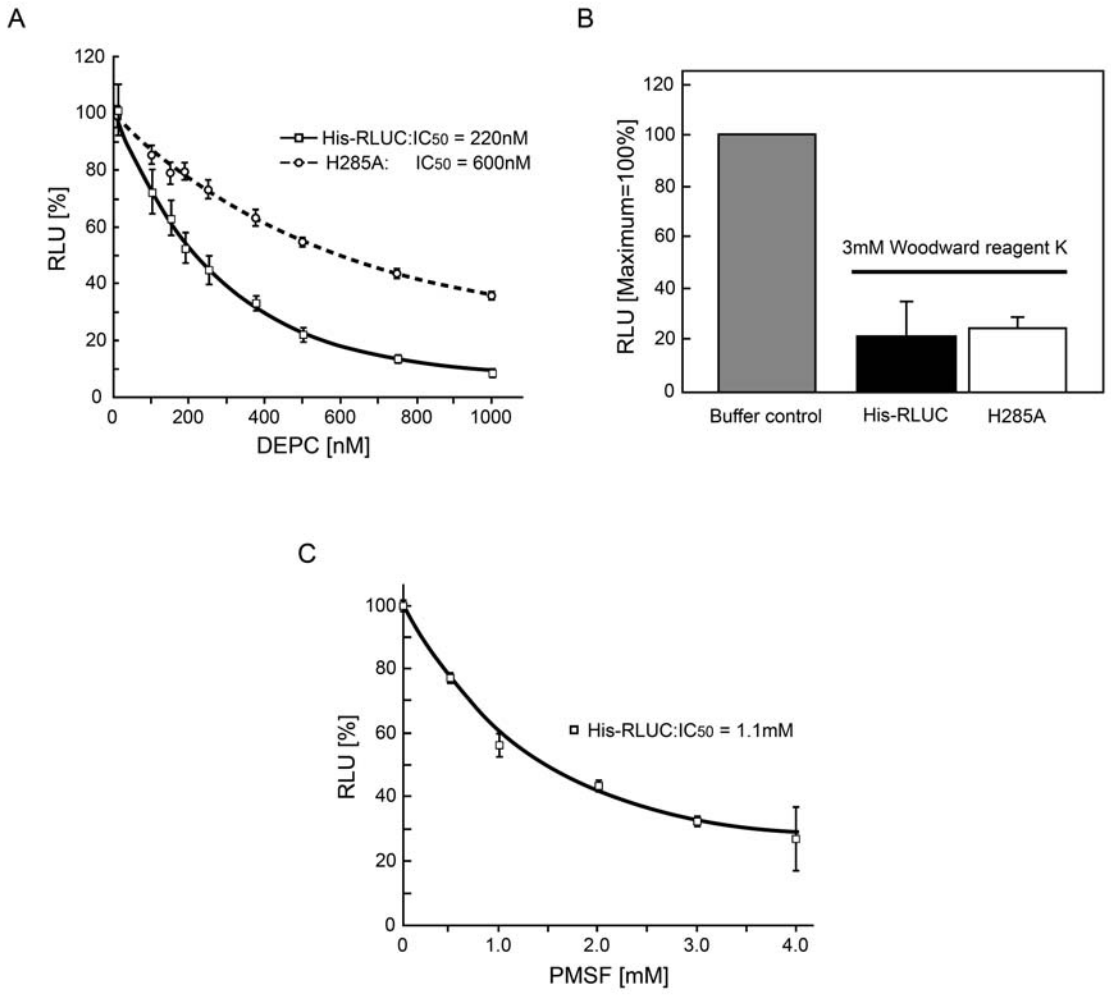

Figure III-4. Inhibitor studies of RLUC (A) DEPC. (B) Woodward Reagent K. (C) PMSF. Error bars represent standard error from n=3 repeats. Assays were performed with 10 nM RLUC, preincubated with inhibitor at the indicated concentration for 30 minutes. Substrate concentration was 2 μM. In (A), the activity of each protein in the absence of inhibitor was normalized to the peak value for ease of comparison. The H285A mutant has 11% of wild type activity (Table 1).

Table 1. RLUC enzyme activity of site-directed mutants

Mutant	Activity ± SD (% of wild type)
Wild type	100
Conserved triad residues	
D120E	1.1 ± 0.95
D120F	None detected
D120Y	None detected
E144D	5.6 ± 3.8
E144F	None detected
E144Y	None detected
H285A	11.3 ± 1.9
H285D	None detected
H285K	None detected
H285N	0.1 ± 0.05
“Empty vector”	< 0.001 (None detected)
Gateway residues	
F180Y	61.6 ± 5.1
F180C	14.3 ± 3.2
F180T	5.4 ± 1.7
F261A	None detected
F261S	None detected*
M185G	16.7 ± 0.8*
Other residues	
I140L	113 ± 11
P157R	101 ± 9
E160N	27.2 ± 2.5
A164W	73 ± 8
T184C	62.7 ± 10.4
T184F	46.1 ± 10.9
K189D	24.7 ± 0.1
K193S	54.8 ± 11.5*
I223W	0.2 ± 0.1
K308I	47.5 ± 9.4*
I163F	Not expressed in BL21
F180Y, I163F	11.0 ± 2.7

Values are *in vivo* luminescence activities from 1 mL of *E. coli* strain BL21 after induction of RLUC with IPTG for 1 h in the presence of 2 μM native coelenterazine. Activities were determined immediately after substrate addition as well as 10 min later, and the higher value is presented here. Asterisks indicate that activities of these mutants were determined with purified protein and compared to purified wild type RLUC. SD represents standard deviation (n=3).

III-3-3. Site directed mutagenesis of the putative catalytic triad

Based on the docking simulations, two sets of catalytic triads were postulated (Fig. III-2D and E). One consists of D120, E144, and H285 the other of N53, W121, and P220. Residues D120, E144, and H285 were subjected to individual site-directed mutagenesis. Residue D120 represents the “nucleophile elbow” (Holmquist, 2000) in the catalytic triad of the α/β hydrolase fold. When expressed in *E. coli*, D120E retained only 1% of wild type activity, and more drastic changes to F or Y caused complete inactivation. Tyrosine was chosen because the catalytic triad of apo-aequorin contains a critical tyrosine residue. Likewise, for E144 the conservative change, E144D, had low activity while changes to bulky aromatic side chains caused complete inactivation (Table 1). For comparison, mutation of another acidic residue near the active site, E160N, retained substantial activity. Taken together, and confirming similar mutagenesis results presented elsewhere (Loening *et al*., 2006), D120 and E144 must play important roles in catalysis.

Mutations of H285 to D, K, or N caused complete or nearly complete inactivation of RLUC (Table 1). However, the H285A mutation of RLUC retained partial activity. The H285A mutant protein was also less sensitive to DEPC (Fig. III-4A), underscoring that H285 is the residue most sensitive to DEPC inactivation and is important for efficient catalysis. In the hydrolases, the equivalent histidine often functions as an essential general base. For example, a similar H to A substitution in the LinB hydrolase results in a completely inactive protein (Hynkova *et al*., 1999). Aequorin, which is not related to hydrolases, also possesses a catalytic histidine (H169), whose mutation to alanine

reduces activity to 1% (Ohmiya and Tsuji, 1993).

In the coelenterazine-utilizing luciferases as well as in the photoproteins obelin and aequorin, light emission at 470 nm is usually attributed to a negatively charged phenolate anion in which the p-hydroxyl on the R1 ring of coelenteramide is deprotonated, while emission at 400 nm is attributed to the neutral coelenteramide (Hart *et al*., 1979; Shimomura, 1995; Ohmiya and Hirano, 1996; Vysotski and Lee, 2004). RLUC luminesces at 470 nm but also displays a weak shoulder near 400 nm (Fig. III-5A and 6; Matthews *et al*., 1977a). The substrate analog *bisdehydroxycoelenterazine* lacks the p-hydroxyl on the R1 ring and can therefore not form a phenolate anion. Accordingly, DeepBlue C luminesces with a peak near 400 nm (Fig. III-5A; Hart *et al*., 1979). In the Ca^{2+}-discharged aequorin, deprotonation on the R1 ring is mediated by one of the histidine/ tryptophan/ tyrosine triads (Vysotski *et al*., 2003). Aequorin generally lacks a 400 nm shoulder but aequorin with a Y82F mutation does have a shoulder, which is attributed to less efficient deprotonation when F replaces Y82. *Vice versa*, obelin, which naturally carries F at the equivalent position, has a 400 nm shoulder, but the F88Y mutant does not (Stepanyuk *et al*., 2005). According to the hypothetical substrate configuration in Fig. III-2C and D, H285 or other residues nearby might play a role as a proton acceptor for the R1 hydroxyl, thus ensuring formation of a phenolate that emits at 470 nm. This hypothesis predicts that nonpolar substitutions at these positions should enhance the 400 nm shoulder in RLUC. However, on the contrary, the H285A mutation displayed a loss of the shoulder (Fig. III-5A). Similar results were obtained for the weak luminescence of E144D and D120E (not shown). If H285 controlled the protonation state of the R1 hydroxyl, then its reaction with DEPC might enhance the 400 nm

Figure III-5. Luminescence spectra (A) Wild type RLUC (10 nM, 2 μM native coelenterazine or 40 nM with 4 μM DeepBlue C) was compared with the H285A mutant (100 nM, 3.1 μM native coelenterazine). Samples were scanned in triplicate from 350 nm to 600 nm at 1 nm per second and normalized to peak at 100%. Note that the spectra are distorted due to the loss of enzyme activity over the time of the scan (~5 minutes), a necessary condition for highlighting the emission spectrum around 400 nm. The presumptive structures underlying emission at 400 nm (neutral coelenteramide) and 470 nm (phenolate anion) are shown. Control experiments were performed with wild-type His-RLUC by initiating the scan at different wavelengths to confirm that the shoulder at 400 nm is not specific to the early phase of the luminescence reaction (Fig. III-6). (B) Wild type RLUC (His-RLUC) and the H285A mutant RLUC with 2 μM native coelenterazine were scanned at pH 7.2 and pH 6.0.

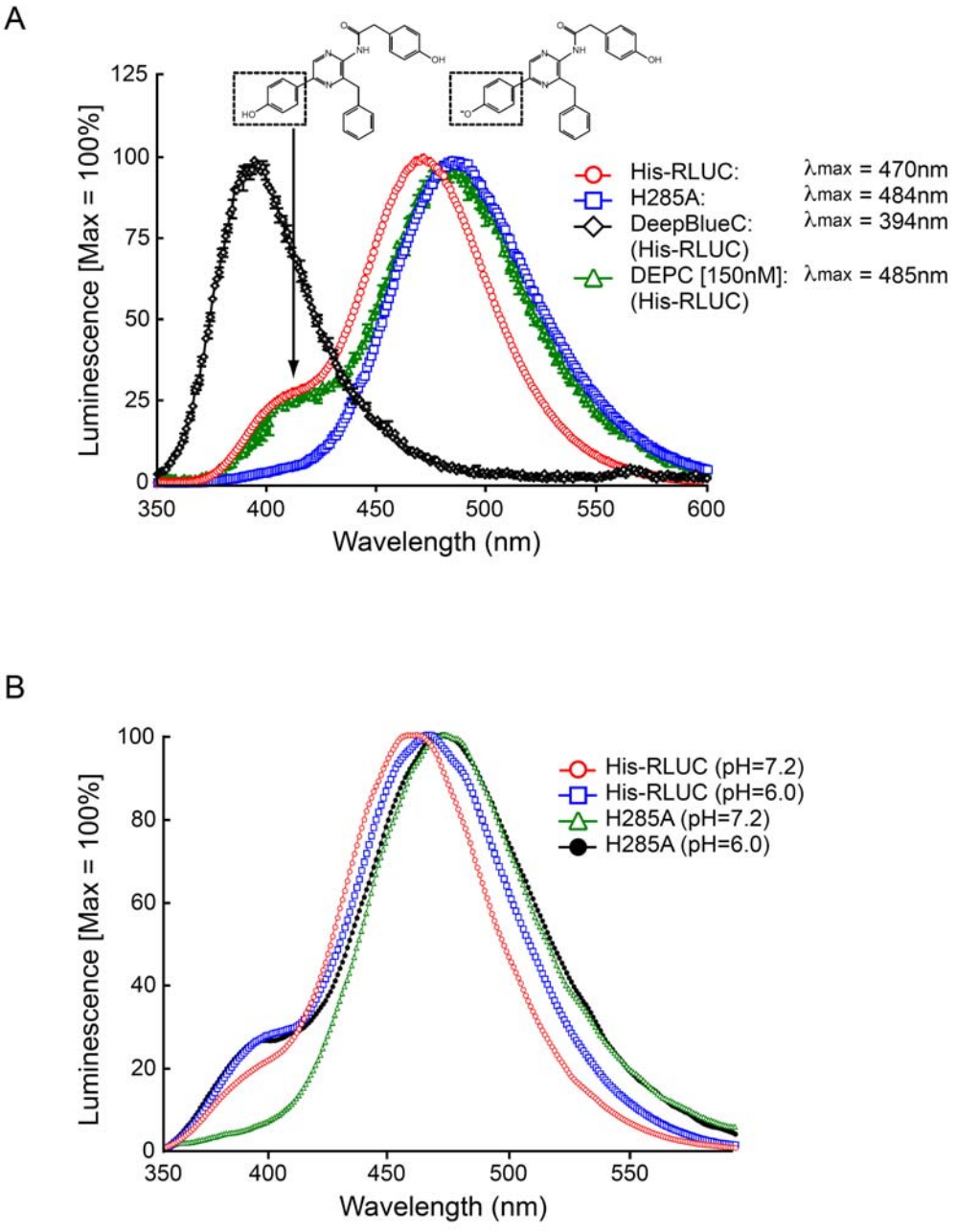

Figure III-5. Continued.

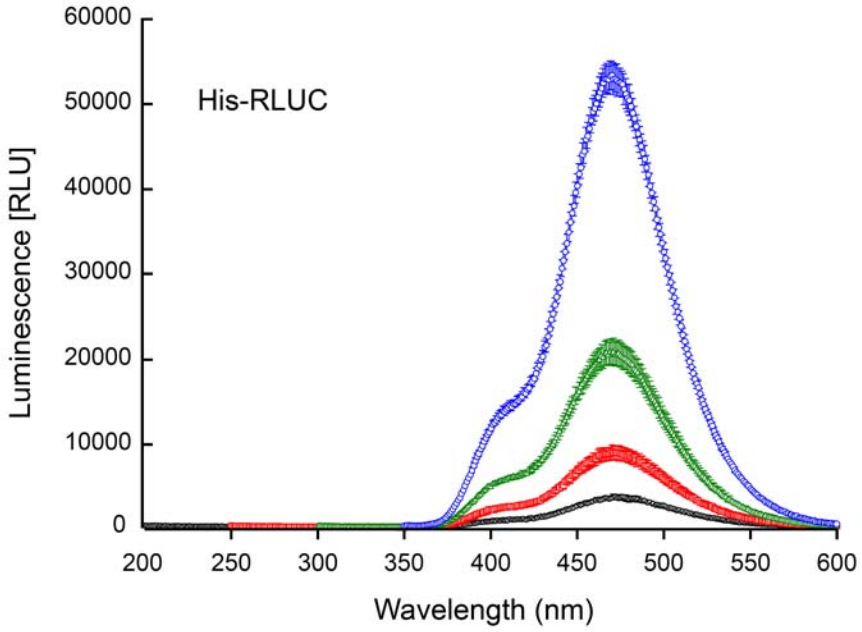

Figure III-6. Time delayed luminescence spectra of wild type RLUC

Luminescence spectra were collected for wild type RLUC at a speed of 1 nm/sec starting at different wavelengths between 350 and 200 nm. Despite the time delay required to reach the shoulder at 400 nm, the shoulder-to-peak ratio is the same. This result confirms that the shoulder is not associated with a transient intermediate seen only in the first few seconds of the enzymatic reaction. The emission spectra were scanned with 10 nM wild type RLUC purified in the presence of 2 μM coelenterazine.

shoulder, but this was not observed (Fig. III-5A). Moreover, one would predict that a pH below the pKa of histidine would favor protonation of the coelenteramide and thus increase the 400 nm shoulder; this trend was observed in the H285A mutant but not in the wild type where it would have been expected (Fig. III-5B). Taken together, although the model of coelenterazine with its R1 hydroxyl bound to the catalytic triad is typical in docking simulations with both our homology model as well as the crystal structure obtained in the absence of substrate (PDB ID, 2PSD), the spectroluminescence data are difficult to reconcile with the docking simulation postulated in Fig. III-2C.

III-3-4. Site directed mutagenesis of the triad, N53, W121, and P220

Site-directed mutagenesis was performed on residues N53, W121, and P220 with a randomized oligonucleotide with the goal of distinguishing whether these residues might interact with the reactive center of the substrate (Fig. III-2C and D) or the p-hydroxylated R1 ring (Fig. III-2E). For N53, the eight different substitutions tested caused varying loss of activity (R > Q,S > C,H,M > G > P; Table 2) anywhere between 0% of wild type (N53P) and 90% (N53R). Here, I briefly mention that almost all RLUC mutants described in this study accumulated to the same level after induction in *E. coli*. However, N53C accumulated exceptionally poorly (Fig. III-7A). RLUC mutants were examined in *E. coli in vivo* because the relative activities *in vivo* generally matched the activities obtained after purification of the His–tagged enzyme by nickel-affinity chromatography (Fig. III-8). If N53 functioned as a hydrogen-bonding partner for the R1 hydroxyl as postulated in Fig. III-2E then other hydrophilic residues, especially a basic

Table 2. Activities of active-site mutants, N53, W121, and P220

Mutant	Activity ± SD (% of wild type)
Wild type	100
Active site residues	
N53C	3.4 ± 2.1*
N53G	0.5 ± 0.4
N53H	2.1 ± 2.2
N53M	1.8 ± 1.0
N53P	None detected
N53Q	25.1 ± 3.6
N53R	90 ± 10
N53S	20.7 ± 7.9
W121A	26.8 ± 9.5
W121G	4.9 ± 2.6
W121R	1,1 ± 1.8
W121S	17.3 ± 8.1
W121Y	3.1 ± 1.5
P220C	72.7 ± 53.2
P220E	4.9 ± 3.9
P220F	15.7 ± 15.3
P220G	548 ± 167
P220L	500 ± 310
P220M	140 ± 121
P220Q	222 ± 44
P220S	55.4 ± 74.4
P220T	89.6 ± 17.4
P220V	70.5 ± 10.6

Values are *in vivo* luminescence activities from *E. coli* strain BL21(DE3) after induction of RLUC with IPTG. Activities were determined immediately after substrate addition as well as 10 min later, and higher value is presented here. Asterisk of N53C denotes that protein accumulates poorly in *E. coli*. In each measurement, luciferase activities of individual mutants were compared with the luciferase activity of wild type RLUC in *E. coli* (wild type=100%). Percentage of relative light unit (RLU) of mutant proteins is presented in Table 2 (n=3).

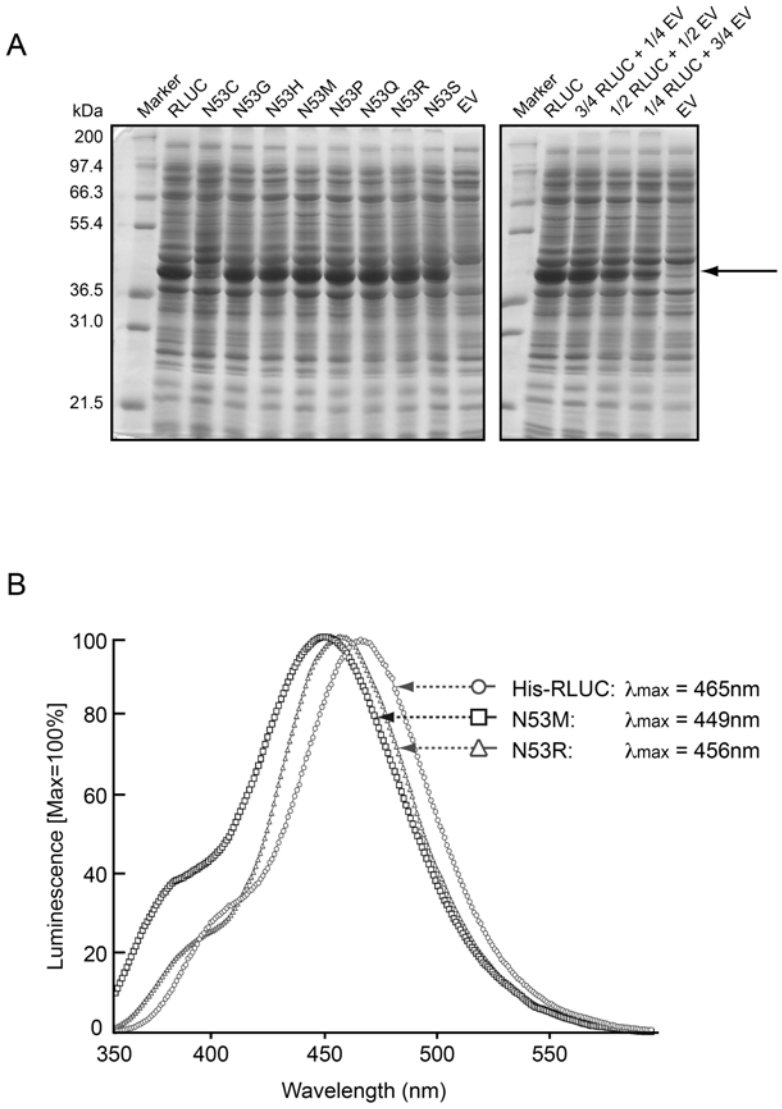

Figure III-7. Expression levels and luminescence spectra of representative mutant RLUC proteins (A) Coomassie Blue stained polyacrylamide gel demonstrating equal accumulation of wild type RLUC and several representative RLUC mutant proteins after 1 h of induction of expression with IPTG. The N53C mutant is a rare exception. A dilution series of RLUC extract in empty vector extract (EV) is shown on the right. Arrow points to recombinant RLUC. (B) Luminescence spectra of two mutations affecting residue N53. Conditions are as for Fig. III-5.

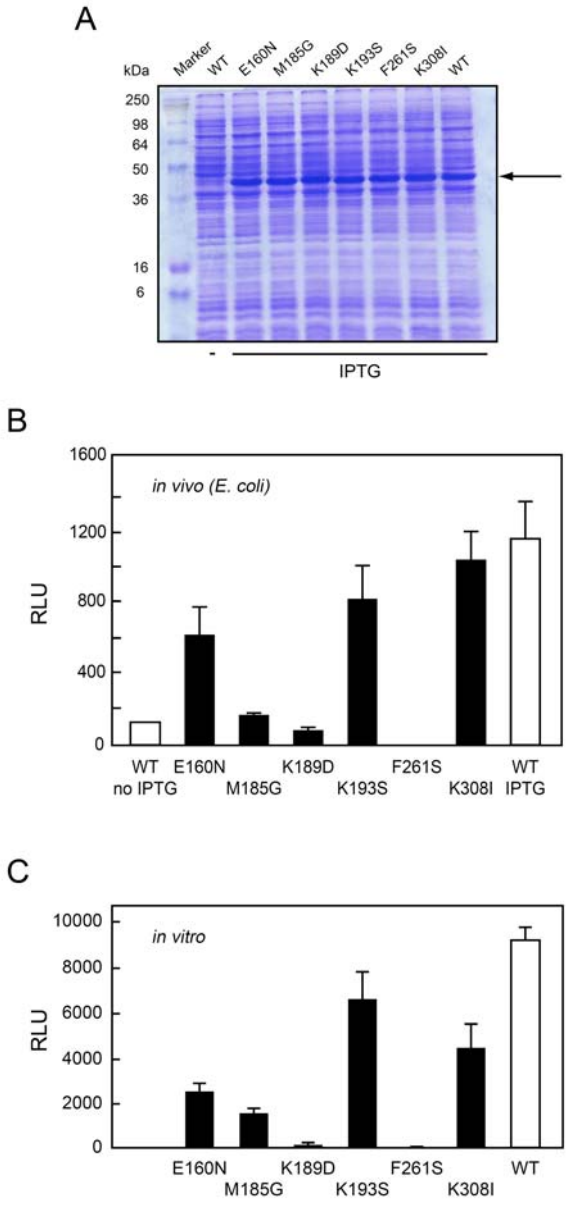

Figure III-8. Enzyme activities (relative light units) for wild type RLUC and selected mutants (A) Polyacrylamide gel for the RLUC expression strains shown in (B). (B) Values are *in vivo* luminescence activities from *E. coli* strain BL21 after induction of RLUC with IPTG. (C) Values are *in vitro* luminescence activities of purified proteins in the presence of coelenterazine substrate. Note the similarity between the activity profiles *in vivo* (B) and *in vitro* (C).

one, might be able to substitute partially, as was indeed observed. Furthermore, when the emission spectra of N53M (poor activity) and N53R (high activity) were compared with the wild-type enzyme, N53M had an enhanced shoulder at <400 nm and a blue-shifted emission maximum compared with N53R and His-RLUC. This result is consistent with the notion established with the Ca^{2+}-discharged aequorin that a less polar environment around the R1 ring causes more of the coelenteramide product to adopt the neutral state, which emits at 400 nm. Specifically, in the Ca^{2+}-discharged aequorin, a W86F mutation caused reduced luminescence, a strong shoulder at 400 nm, and blue-shifted emission (Ohmiya *et al*., 1992), which was attributed to the lack of a hydrogen bond between the R1 hydroxyl and F86. No such spectral shift was observed when W129 or W179, which interact with the reactive imidazolo-pyrazinone ring, were changed to phenylalanine (Ohmiya *et al*., 1992; Head *et al*., 2000).

Each of five substitutions at W121 (A, G, R, S, and Y) caused loss of activity between 75% (W121A) and 99% (W121R). The loss of activity with W121R compared to N53R might point to a role for W121 in guiding the R1 hydroxyl to interact with the N53 residue. The W121R mutation may hamper the proper positioning of the substrate in the active site. For comparison, ten different substitutions for P220 showed a wide range of activities (Table 2), generally indicating that other small or medium sized residues were tolerated or even beneficial at this position, but glutamic acid and phenylalanine were detrimental. Although initial LUC activities of P220G and L were lower than wild type RLUC, the LUC activities increased in *E. coli* after 10 min (Fig. III-9A). This observation did not result from the different level of the protein accumulation of P220G and P220L in *E. coli* (Fig. III-9A). One possibility to explain the phenomenon is that the enzymes of

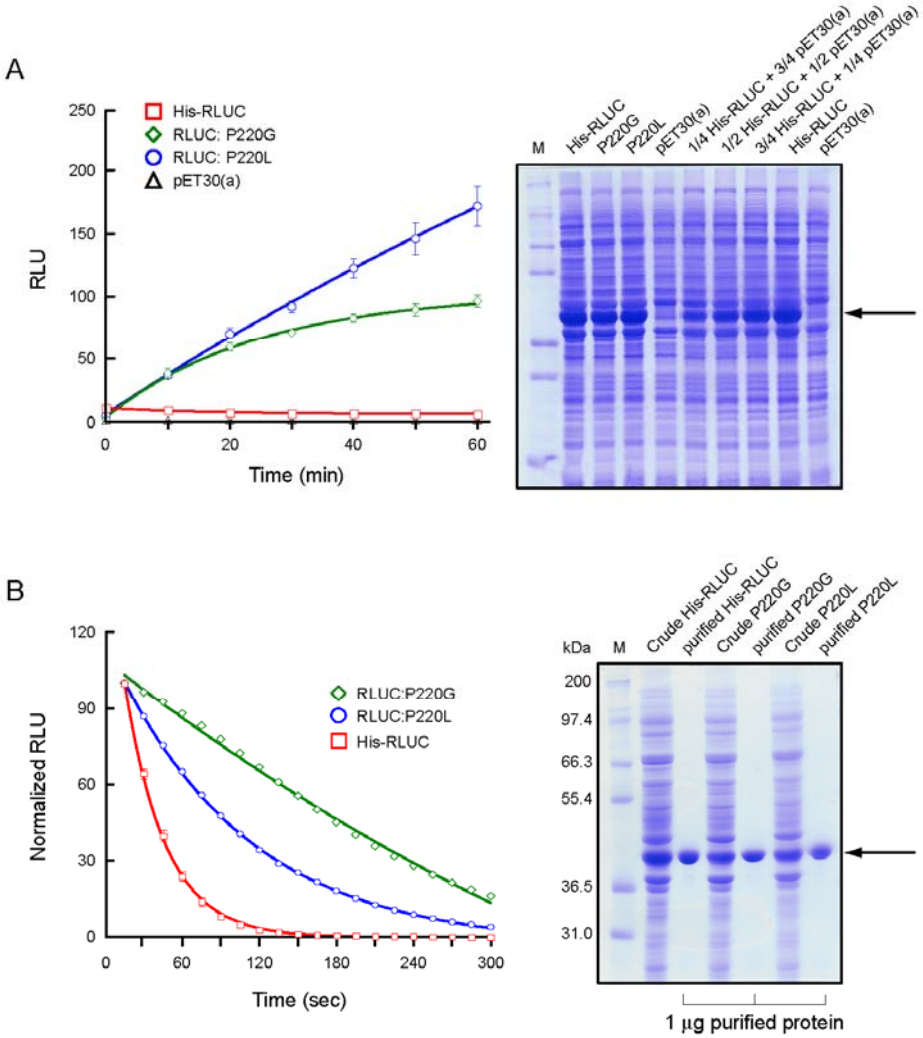

Figure III-9. Accumulation of luciferase activities of P220G and P220L in *E. coli* and increased stabilities *in vitro*

(A) Time course of *in vivo* luminescence in *E. coli* cells expressing wild type His-RLUC and two P220 mutants. Protein amounts were compared with serial dilution on a PAGE gel after the luciferase measurement had been taken. (B) Time course of the *in vitro* luminescence of wild type RLUC, P220G, and P220L. 10 nM protein purified was used for the stability test. The purity and the concentration were examined in the PAGE gel. Note the increased half-life of the P220G and P220L mutant proteins.

P220G and P220L may be much more stable than wild type RLUC. As a result, a larger fraction of protein molecules of P220G and P220L may catalyze substrate in *E. coli*, compared with wild type RLUC at indicated time points. To test this possibility, the *in vitro* stabilities of P220G and P220L were compared with wild type RLUC. While wild type RLUC exponentially lost LUC activity with a half-life of about 40 seconds (Fig. III-10), P220G and P220L showed a clear delay in the decay of their activities, indicating that P220G and P220L proteins were more stable than wild type (Fig. III-9B). Since the delayed decay of enzymatic activity does not by itself explain the increase in activity over time when the activities are measured in live cells, I cannot rule out another considerable factor such as a slow but gradual accumulation of coelenterazine inside the cell expressing P220G and P220L to explain the increased activities in *E. coli*.

Aside from mutations affecting the lower portion of the active site, I also examined a number of residues thought to compose the entrance to the active site (gateway; listed in Table 1). Among these, mutation of F180, which resides at the rim of the active site in all structures including our homology model, lost the LUC activity, suggesting that its strongly hydrophobic character might play a role in initial binding of the substrate. Alteration of F261 to serine or alanine completely disrupted RLUC activity, consistent with similar experiments presented elsewhere (Loening *et al*., 2006 and 2007b). Several additional mutations are presented for the record. Taken together, the active site mutagenesis data support the view that the oxygenase activity of RLUC relies on the catalytic triad inherited from a hydrolase ancestor and suggest that a pocket of N53 and W121 has been co-opted to function in substrate binding.

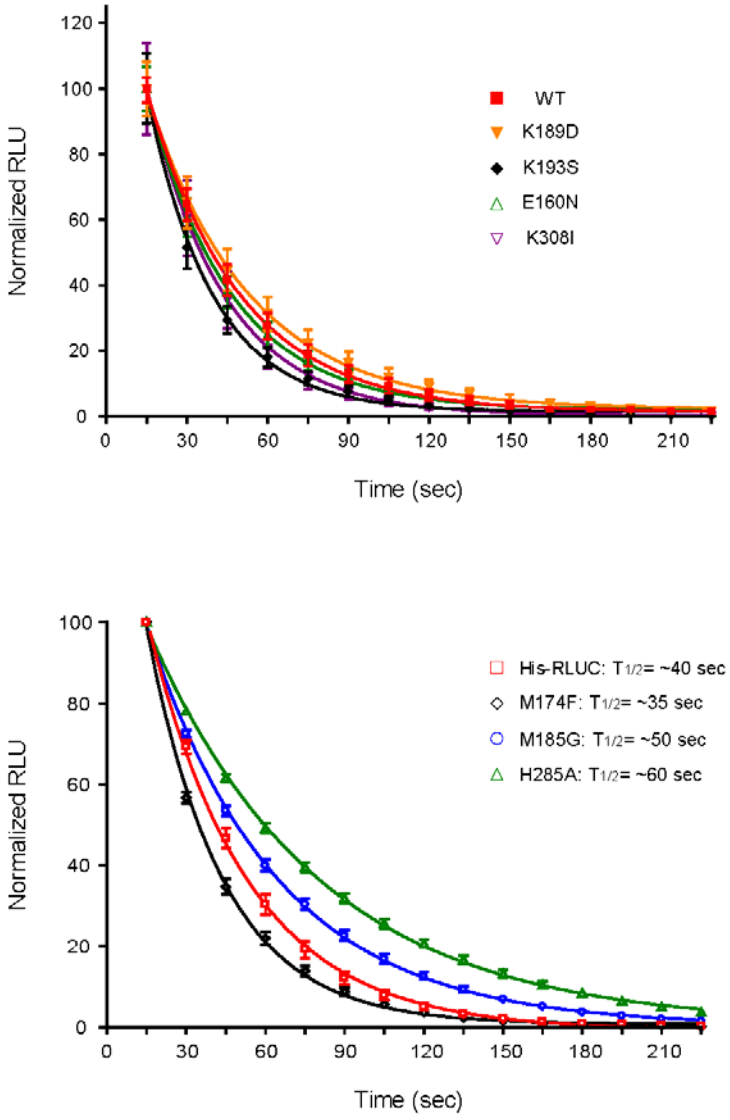

Figure III-10. *In vitro* stabilities of RLUC mutants

In vitro stabilities of selected mutants were compared with that of wild type RLUC. The half-life of wild type RLUC showed ~40 sec which is similar with the stabilities of most mutants. Although M185G and H285A lost LUC activities (listed in Table 1), their *in vitro* stabilities were slightly increased to a half-life of over 50 sec. For easy comparison, each measurement was normalized to the highest value (Max=100%).

III-3-5. Improved RLUC derivatives

Because most of the mutations introduced so far yielded reductions in RLUC enzyme activity, I employed random mutagenesis of the entire RLUC cDNA in order to identify mutations that altered the RLUC enzyme properties in a favorable direction (see Methods). A total of 1300 individual clones made by random mutagenesis were analyzed. I searched for mutants with an increased peak of light emission in *E. coli*, and also for mutants with increased stability of light emission over time. The M185G mutant emerged from this screen and was of interest since the half-life increased from 40 seconds to ~50 sec (Fig. III-10). Independently, M185V was identified as a mutation that increased the stability of enzyme activity in animal serum and the ability to luminesce using the substrate *bisdeoxycoelenterazine* (Loening *et al*., 2006). Two additional mutants were selected and sequenced. The activity of the purified proteins was compared to wild type His-RLUC. Preliminary tests showed that the activities of V267I and K189V were elevated over His-RLUC (Table 3) and K189V appeared to have a reduced K_m. Valine 267 lies outside of the active site, as do most if not all of the eight mutations constituting the RLUC8 mutant (Loening *et al*., 2006), while K189 lies on the gateway to the active site. The emission peak of K189V was very similar to wild type RLUC and no significant increase in emission at 400 nm was seen. It suggests that the amount of a neutral coelenteramide in the active site of K189V may be similar as wild type RLUC since the emission spectrum is not changed near the shoulder at which the neutral coelenteramide luminesces (Fig. III-11). However, the emission spectrum of V267I showed two major peaks with the prominent blue-shifted shoulder of 390 nm and

Table 3. Activities of mutants selected for improved enzymatic activity.

Mutant	Name	Condition	Activity ± SD
Native RLUC cDNA			
none	His-RLUC	*in vitro*[1)]	100
V267I		*in vitro*	163 ± 33
K189V		*in vitro*	128 ± 16
K189V+V267I	RLUC+	*in vitro*†	317 ± 82
M185V+K189V+V267I	SuperRLUC	*in vitro*†	411 ± 113
Condon-optimized RLUC cDNA			
none	His-hRLUC*	*in vivo*[2)]	100
K189V	hRLUC:K189V	*in vivo*	175 ± 70
M185V+K189V	hRLUC:MK	*in vivo*	425 ± 120
M185V+K189V+V267I	SuperhRLUC	*in vivo*	475 ± 130

1) *In vitro* activities are initial luminescence values upon addition of substrate (2 μM coelenterazine). 2) *In vivo* activities are luminescence activities from *E. coli* strain BL21 without IPTG induction (2 μM coelenterazine). † indicates the LUC activities were compared under 3 μM coelenterazine. * shows that hRLUC is a human codon-optimized version of the RLUC cDNA encoding the wild type protein sequence (n=3).

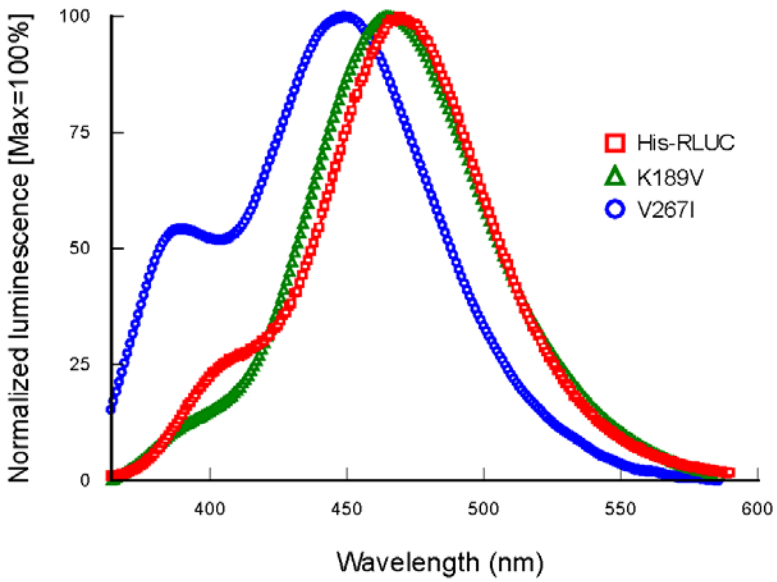

Figure III-11. Emission scanning of selected single mutants with improved enzymatic properties. While the shoulder of V267I at ~400 nm was increased and the blue shifted emission maximum was detected, the emission spectrum of K189V was essentially unchanged.

the blue-shifted maximum of 450 nm (Fig. III-11). Additionally, the spectrum for M185G showed an emission peak at 473 nm while the shoulder didn't change (not shown).

The beneficial mutations K189V and V267I were combined to generate a double mutant, named as RLUC+. The two mutations appeared to act additively, yielding a two-fold to three-fold increase in relative light units, compared to wild type RLUC (Table 3). Interestingly, the change in spectral characteristics previously seen for V267I (Fig. III-11) was suppressed in RLUC+, indicating that the active site of V267I might be reorganized by introduction of K189V (Fig. III-12B). I combined the mutations in RLUC+ with M185V (Loening *et al*., 2006), which yielded a further increase in light emission over RLUC+ (SuperRLUC; Table 3). Neither RLUC+ nor SuperRLUC had an altered K_m (Fig. III-13A). However, the luminescence of SuperRLUC had a two-fold longer half-life *in vitro* compared to wild type RLUC (Fig. III-12A) while the emission spectrum of SuperRLUC was similar to His-RLUC (Fig. III-12B). RLUC is known to be inhibited by aggregation at high concentrations of substrate (above 3 uM; Matthews *et al*., 1997b). SuperRLUC was less sensitive to substrate inhibition (Fig. III-13B). The right panel of Figure III-13A shows the purity of the preparation and serves as a control for protein quantification. Attempts to further enhance RLUC activity by including the P220G mutation remained unsuccessful. In conclusion, the combination of molecular docking and site-directed mutagenesis has provided some insight, which is identification of candidates of catalytic residues, into the molecular mechanisms whereby *Renilla* luciferase interacts with its substrate, coelenterazine. It is clear that the catalytic mechanism employed by RLUC must differ substantially from the one established for aequorin. All residues D120, E144, and H285 are conserved with the catalytic triad of the ancestral α/β hydrolase and play

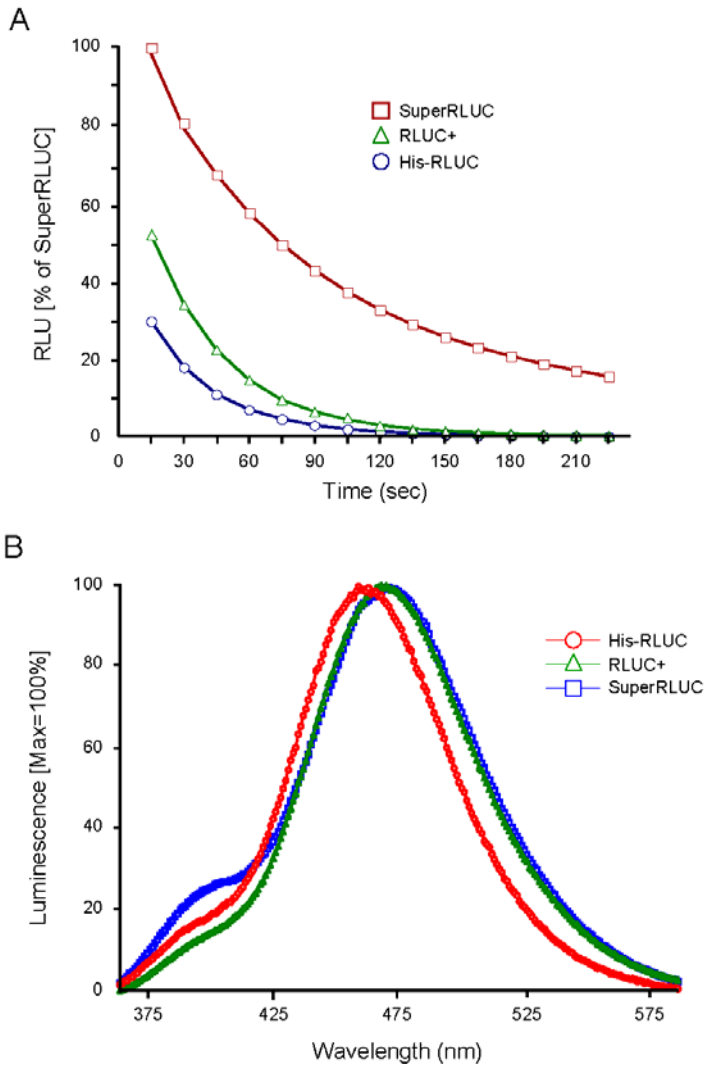

Figure III-12. Increased *in vitro* stability of SuperRLUC and its emission maximum

(A) Time course of the *in vitro* luminescence of His-RLUC and selected mutants. Enzyme and substrate concentrations were 10 nM and 2 uM respectively in PBS buffer, pH 7.2. Absolute activities (listed in Table 3) were normalized for better comparison (first time-point = 100). (B) Emission scanning of double and triple mutants. The emission spectra were similar to wild type RLUC.

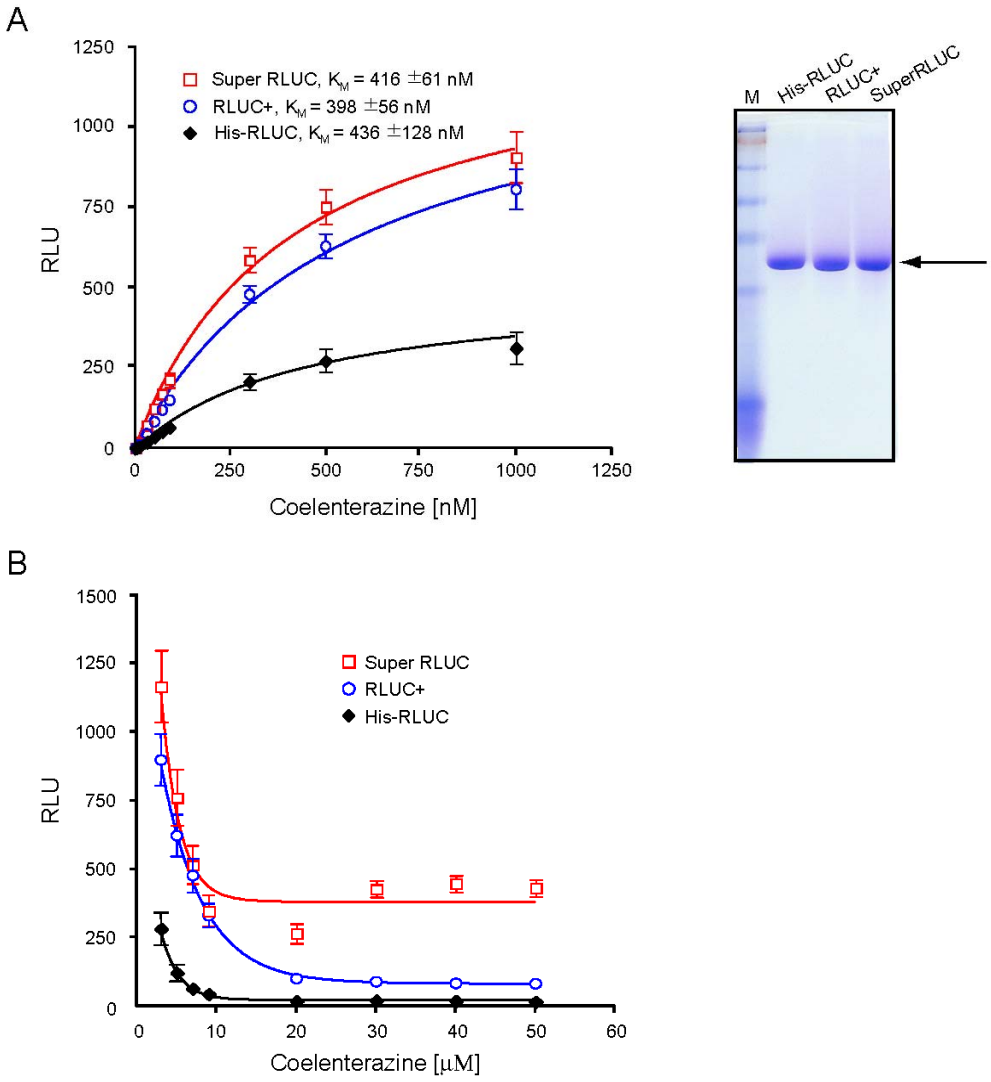

Figure III-13. Enzyme kinetics of optimized RLUC proteins (A) Derivation of K_m values. The K_m for wild type was similar to previously published data such as 210 nM (coelenterazine *h*; Matthews *et al*., 1977a) and 300 nM (Hoshino *et al*., 2007). Wild type His-RLUC, RLUC+ and SuperRLUC were purified by nickel affinity chromatography and run on a polyacrylamide gel at the right panel. (B) Inhibition of RLUC activity by high substrate concentration. Arrow indicates purities and molecular sizes of extracted proteins.

an important role for bioluminescence reaction although individual functions of the residues in RLUC may not be same as those of α/β hydrolases. Optimizations of the intensity of photon emission and towards more stable light emission over time in the continued presence of substrate may prove useful for adaptation of RLUC as a reporter in heterologous host cells.

III-4. Discussion

The combined data from molecular docking simulations, pharmacological inhibitors, site directed mutagenesis, and luminescence spectroscopy extend previously published structure function results (Loening *et al*., 2006). Although the active sites of RLUC and aequorin are both rich in aromatic residues, RLUC does not possess a spatial arrangement of catalytic triad residues analogous to that in aequorin, suggesting that the catalytic mechanism employed by RLUC must be different from aequorin and obelin. In detail, D120, E144, and H285 of RLUC appear to play an important role as a catalytic triad in the bioluminescence reaction whereas the catalytic triad of aequorin and obelin consists of Y184 (Y190 of obelin), W173 (W179), and H169 (H175). Instead, several active site residues in the evolutionarily related dehalogenase, LinB, including those forming the catalytic triad (D120, E144, and H285 in RLUC) and also N53, W121, and P220 are completely conserved in RLUC, including in their spatial arrangement. Meanwhile, the great majority of RLUC's gateway residues (Fig. III-3) are different in LinB (not shown) and show considerable variation between the homology model and the various crystal structures, which may point to dynamic flexibility in this portion of the

enzyme. Moreover, RLUC is not a calcium dependent luciferase, suggesting a different regulation of the bioluminescence reaction. Based on the molecular docking simulation and the mutagenesis experiment, E144, F261, and H285 directly interacted with the 2-hydroperoxyl group on the 2-hydroperoxyl coelenteramide intermediate, while N53 bound to the hydroxyl group of the R1 side ring. The R1 ring of coelenterazine is important for the enzyme reaction because RLUC cannot catalyze efficiently *bisdehydroxycoelenterazine*, which lacks the hydroxyl group of the R1 ring (Fig. I-4B; Loening *et al*., 2006). Thirteen coelenterazine variants are commercially available (Fig. I-4A). Generally, most variants showed low activities, compared with the native coelenterazine, and the R3 modifications affected the enzyme activities but not the emission maximum. Coelenterazine *hcp,* which carries modifications of both the R2 and the R3 ring, affected both the emission peak and activity. Interestingly, the emission maximum of coelenterazine *e* was red-shifted whereas coelenterazine *hcp* and DeepBlue C were blue-shifted (Fig. I-4B).

In the calcium-stimulated photoproteins, the oxidative decarboxylation reaction utilizes histidine as a general base. I propose that H285 functions in a similar capacity in RLUC, for the following reasons. First, RLUC was strongly inactivated by the histidine-reactive compound, DEPC (Fig. III-4A) whereas H285A showed a mild inactivation, indicating that H285A is more resistant to DEPC compared to wild type. The residual sensitivity of the H285A mutant to DEPC clearly shows that other functionally important histidines are also being modified. Interestingly, four out of ten histidines in RLUC (H119, H128, H133, and H142) lie near the two acidic catalytic residues (D120 and E144) and although neither is exposed to the active site cavity, their reaction with DEPC might

contribute to the residual inhibition of the H285A mutant by DEPC. Second, the drop in RLUC activity below the pH optimum at 7.2 (Matthews *et al*., 1977b) is consistent with a titratable histidine. Third, mutation of H285 to most other residues caused loss of activity, as did mutation of D120 and E144. And finally, molecular docking simulations suggested that RLUC can suspend the substrate on its R1 and R3 rings using hydrogen bonds to defined residues, possibly N53 and F262, in such a fashion that the reactive center of coelenterazine with its C2 and C3 ring atoms becomes juxtaposed to H285 and the remaining catalytic triad residues. Such a docking model was also plausible for the reaction intermediate, 2-hydroperoxy-coelenterazine (Fig. III-2E).

Ancillary evidence is that RLUC is expected to bind the R1 hydroxyl group in such a way as to facilitate its deprotonation into a phenolate anion, which gives rise to the emission peak at around 470 nm. While H285 could potentially perform this role, the presence of two acidic residues nearby does not make this scenario very likely and the luminescence spectrum of the H285A mutant was inconsistent with such a role (Fig. III-5). If, as seems more likely, the R1 hydroxyl of coelenterazine is bound by N53, it is unclear which residue causes its deprotonation in the majority of cases or whether coelenteramide may luminesce in its amide anion form (Shimomura, 1995) rather than as a phenolate anion, a hypothesis that does not require a proton acceptor near the R1.

That said, certain considerations potentially argue against the notion that H285 forms a component of the catalytic triad. For one, the H285A mutant retains ~11% of activity suggesting that another residue can substitute as a base, if poorly. However, the Ca^{2+}-discharged aequorin with an H-to-A mutation also retains low but detectable activity, around 1% of wild type (Ohmiya and Tsuji, 1993). Another consideration is that one X-

ray structure in the presence of the reaction product, coelenteramide, shows the reaction product near the surface of the active site rather than engaged with the proposed catalytic triad (PDB ID, 2PSJ). However, Loening and coworkers already pointed out that this position might represent a non-productive binding mode (Loening *et al*., 2007a). For example, it does not explain why active site residues such as D120, E144, W121, and N53 are important for function and, moreover, why mutations that ought to disrupt the hydrogen bonds with coelenteramide in the surface position had only mild effects on enzymatic activity (Loening *et al*., 2007a). Furthermore, our spectroscopic results (Fig. III-5) were difficult to reconcile with a hydrogen bond between the R1 hydroxyl and H285, a feature that the reaction product in PDB ID, 2PSJ shares with our disfavored docking model (Fig. III-2C).

A peculiar feature of the RLUC structure is the variation in the arrangement of surface residues near the gateway to the active site. The only crystal structure that allowed coelenterazine's reactive center to be docked to the catalytic triad was PDB ID, 2PSJ (with coelenteramide removed; Fig. III-2E; Loening *et al*., 2007a). This conformation has a wide gateway and a bowl-shaped active site, with the side chain of F262 flipped out of the active site, thus exposing H285 and E144 (Fig. III-3), while another conformation (PDB ID, 2PSD) possesses a narrow gateway and a vase-shaped active site, in which the side chains of both F262 and W156 are packed into the active site cavity to cover E144 and H285. Although the structure with the bowl-shaped active site appears consistent with our model, whether coelenterazine encounters RLUC with a vase-shaped or a bowl-shaped active site is unknown. However, it would be premature to argue that the only conformation of RLUC able to engage the substrate as predicted

by our model is a conformation that can only be seen once RLUC has reacted with the substrate. Instead, I point out that the structure in PDB ID, 2PSF, which was obtained without substrate, does have a fully open gateway, although F262 is still flipped into the active site. These results point to considerable flexibility in the conformation of RLUC, some of which may be driven by substrate binding.

In summary, while additional work is needed to clarify the mechanism of action of *Renilla* luciferase, there is now a framework on which additional mutagenesis of the enzyme with the goal of enhancing its activity in heterologous expression systems can be conducted. BRET applications, in particular, would benefit from such improvements, in the interest of reducing protein expression levels of RLUC-tagged proteins, shorten measurement times, and improve spatial resolution, especially for BRET imaging (Xu *et al*., 2007; Coulon *et al*., 2008). In this regard, although most mutations studied here compromised enzymatic activity (Table 1), both P220G and P220L are of interest because their *in vivo* activities were elevated five-fold over wild type after 10 min incubation with the substrate (Table 2). Furthermore, P220G and P220L were much more stable than wild type RLUC *in vitro* (Fig. III-9B), suggesting that increased activities of P220G and P220L in *E. coli* might partly result from the increased stabilities of P220G and P220L.

RLUC+ and SuperRLUC generated by protein engineering showed increased luciferase activities, however, spectral characteristics and substrate affinities of both mutants didn't show statistically significant difference in comparison with wild type RLUC (Fig. III-12B; Fig. III-13A). Additionally, SuperRLUC was more resistant to substrate inhibition (Fig. III-13B). Considering all benefits of SuperRLUC, SuperRLUC can replace

regular RLUC for BRET to investigate *in vivo* protein-protein interactions since the efficiency of the resonance energy transfer in the BRET system depends on the spectral overlap between the emission maximum of an energy donor and the absorption spectrum of an energy acceptor as well as the quantum yield of an energy donor. Moreover, the luciferase activity of SuperhRLUC, a codon optimized SuperRLUC, was much higher than wild type hRLUC in *E. coli* as shown in comparison of SuperRLUC with RLUC (Table 3). According to a preliminary result of the luciferase activity of SuperhRLUC in transgenic *Arabidopsis*, the luciferase activity of SuperhRLUC is higher than that of hRLUC, indicating that the benefits of SuperhRLUC may be useful for improvement of BRET upon the employment of SuperhRLUC as an energy donor. The utility of these and other mutations for enhancing RLUC activity is currently under investigation.

III-5. Materials and Methods

III-5-1. Site directed mutagenesis and other recombinant DNA techniques

The wild type *Renilla reniformis* luciferase cDNA obtained from plasmid pBS-35S:RLUC-attR (GeneBank accession No. AY995136; Subramanian *et al*., 2006) was subcloned into the expression vector pET30(a) as an *Nco* I - *Bam*H I fragment, thus adding an N-terminal histidine tag and linker sequence (Fig. III-14A and B). Site directed mutagenesis was performed using the Quickchange procedure (Stratagene, La Jolla, CA). The *E. coli* strain was BL21(DE3). Mutations were confirmed by DNA sequencing,

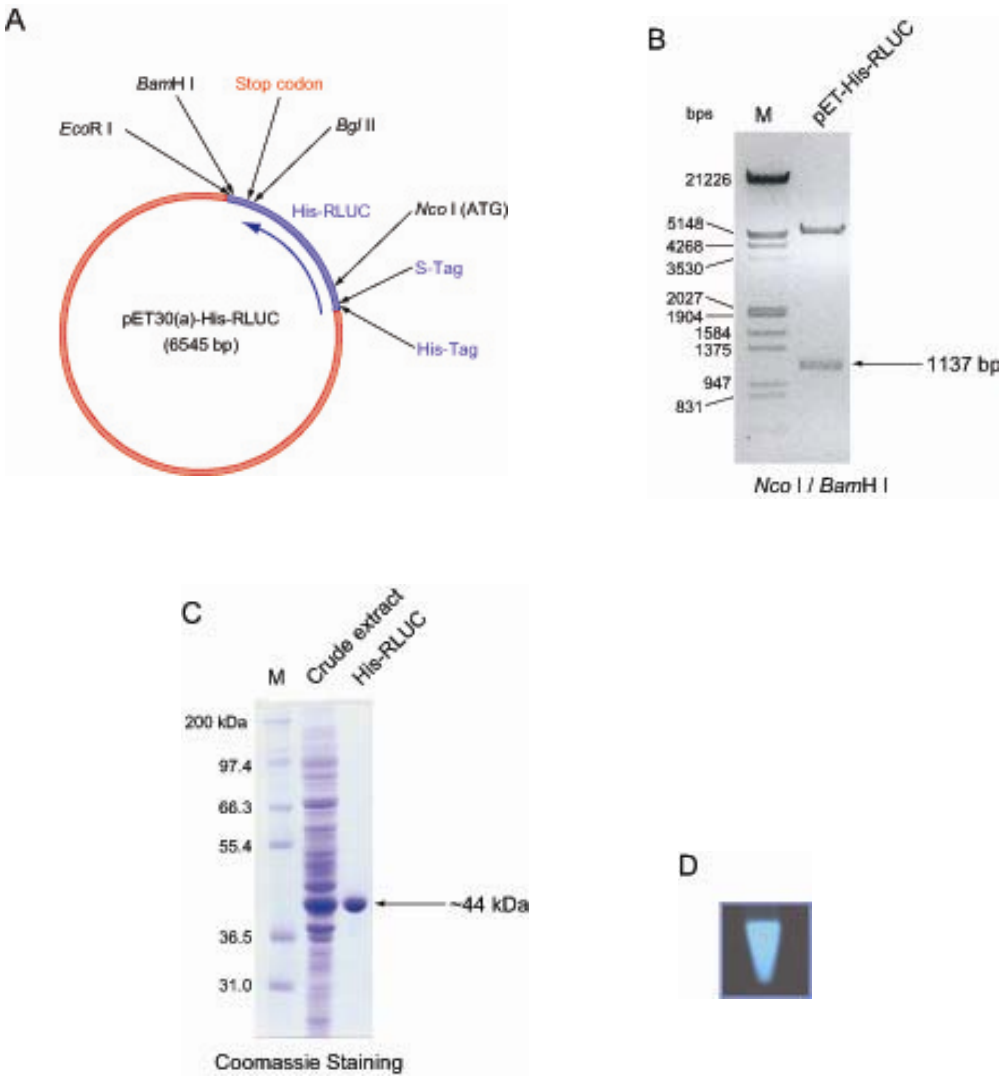

Figure III-14. Construction and purification of recombinant His-RLUC

(A) Expression vector map of pET30(a)-His-RLUC. The regular RLUC cDNA was cloned between *Nco* I and *Bam*H I restriction site (See methods). (B) The reading frame of His-RLUC was confirmed by sequencing and restriction digestion. (C) Recombinant His-RLUC was expressed and purified in *E. coli* BL21(DE3) strain. (D) His-RLUC activity was confirmed by *in vitro* bioluminescence. 1 μg His-RLUC purified through a nickel affinity column was used for the reaction.

including resequencing of the entire RLUC coding region to guard against unintended secondary mutations. For several codon positions, mutagenesis was performed using a mutagenic oligonucleotide pool in which all four bases were allowed at all three codon position (site-directed random mutagenesis). In this case, approximately 90 *E. coli* transformants were picked from the library, grown in LB in a white 96-well microtiter plate (Packard, Meriden, CT) to an optical density of about 1. Colonies were prescreened for RLUC activity *in vivo* by adding 2 uM coelenterazine to the culture medium, mixing, and luminescence was recorded in a PolarStar luminescence microplate reader for 3 sec per well (BMG Labtech, Durham, NC) alongside the original wild type RLUC strain and non-transformed *E. coli*. Colonies representing high, medium, and low RLUC levels were saved and the mutations identified by DNA sequencing. For random mutagenesis, the RLUC cDNA was amplified using an error-prone PCR procedure, GeneMorpho®II Random Mutagenesis (Stratagene, La Jolla, CA) following the manufacturer's protocol. A library of 1300 putative mutant clones was surveyed for RLUC activity in the PolarStar plate reader and candidate clones with elevated RLUC activity were identified. To reconfirm the elevated LUC activity, the individual colony was grown to OD 0.6 and then the recombinant protein was induced with 1 mM IPTG treatment for 1 hour at 30°C. The LUC activity was measured in the TD20/20 luminometer (Turnerdesigns, Sunnyvale, CA) after addition of 2 μM of native coelenterazine (Biotium, Hayward, CA) and the mutation identified by DNA sequencing. Subsequently, mutations were also introduced into a human codon-optimized RLUC cDNA (GeneBank accession No. AAK53368; Packard, Meriden, CT).

III-5-2. Docking simulations

For the docking simulations, molecular structures of native coelenterazine and 2-hydroperoxy-coelenteramide were drawn by the MOE program (Chemical Computing Group, Inc., Montreal, Canada). The homology model of RLUC and the crystallographic structures (PDB ID, 2PSD and 2PSJ) were used for multiple docking simulations using the MOLEGRO/MolDock program (Thomsen and Christensen, 2006). The volume of the individual active site was estimated by this program with the 1.6Å probe. Generally, individual docking simulations were performed from 10 to 100 repeats and every possible docking model was analyzed by moldock scores and hydrogen bonds. After multiple docking simulations, consistent docking simulations among the best-fitted predictions were used for the development of the hypotheses.

III-5-3. Expression and purification of RLUC

RLUC expression in *E. coli* strain BL21(DE3)pLysS was induced with 1 mM IPTG for 3 h hours at 30°C. The accumulation of RLUC *in E. coli* was routinely checked by cell lysis and gel electrophoresis and Coomassie Blue-staining. With just one exception (N53C and I163F), all site-directed mutants tested accumulated to similar levels. RLUC was purified from the soluble cytosolic fraction over a nickel column (Fig. III-14C) (His-Bind Kit; Novagen, Darmstadt, Germany) following standard procedures that included sonication, centrifugation of cell debris at 12,000 rpm for 10 minutes at 4°C, and filtration of the supernatant through a 0.45 micron filter to prevent clogging of resin. Protein was

affinity purified according to the manufacturer's protocol and eluted with elution buffer (1 M imidazole, 0.5 M NaCl, 20 mM Tris-HCl, pH 7.9). After elution, RLUC was dialyzed overnight against 2l of phosphate buffered saline (PBS; pH 7.2) in order to remove inhibitory imidazole (Inouye and Sasaki, 2007). Protein concentration was determined using the BCA assay (Pierce, Rockford, IL) with BSA as a standard. Alternatively, the protein concentration of preparations that were free of imidazole was measured by UV-absorbance using an extinction coefficient of 65,040 $M^{-1}Cm^{-1}$ (Mach *et al*., 1992). Purified RLUC protein was stored in PBS buffer with 50% glycerol at –70°C in small aliquots or stored at 4°C for up to 2 weeks. Western blotting was performed using a commercial monoclonal antibody (Chemicon, Temecula, CA).

III-5-4. Kinetics of RLUC enzyme activity

Enzyme assays were conducted using freshly purified RLUC enzyme at a concentration of 10 nM or as otherwise indicated in 1ml PBS (pH 7.2). 250X stock solution of native coelenterazine substrate in ethanol was diluted to the indicated concentration (final ethanol concentration, 0.8%), the solution was mixed by tapping to ensure a maximal supply of oxygen, and the luminescence activity was recorded in the TD20/20 luminometer. Because luciferase activity drops sharply over time, the first 5-second luminescence reading was taken as a measure of enzyme activity. The K_m values of wild type RLUC and selected mutants were calculated according to standard Michaelis-Menten theory using Prism software (GraphPad Software, Inc., San Diego, CA) from at least 3 repeat measurements. Several independent protein preparations

yielded similar K_m values.

III-5-5. Drug inhibition

Diethyl pyrocarbonate (DEPC; sigma, St. Louis, MO) and Phenylmethanesulfonyl fluoride (PMSF; sigma) were resolved with ethanol and isopropyl alcohol, respectively. N-ethyl-5-phenylisoxazolium-3´-sulphonate (Woodward's reagent K; Sigma) was added in 50 mM HEPES (pH 6.0). All inhibitors were prepared freshly before used. 10 nM protein purified was pre-incubated with an indicated inhibitor at room temperature for 30 min and then the luciferase activity was measured by TD20/20. Indicated substrate was added just before the measurement.

III-5-6. Emission spectra

Every bioluminescence spectrum was recorded under the same condition as the enzyme assay using a spectroluminometer (Photon Technology International, Inc., Birmingham, NJ), except that the assay volume was 2 ml. Native coelenterazine substrate was 2 uM (ethanol concentration, 0.8%). Protein concentration was 10 nM purified enzyme or as otherwise indicated. Generally, the emission spectrum was analyzed with the Felix32 software (Photon Technology International, Inc., Birmingham, NJ). All spectra were recorded at 1 nm per second.

CHAPTER IV.

CONCLUDING REMARKS

An emerging technology, Bioluminescence Resonance Energy Transfer (BRET), which is able to investigate *in vivo* protein-protein interactions in real time and with minimal invasiveness, has been further developed and upgraded. Although BRET is a similar technique as FRET, the enzymatically generated resonance energy simplifies the experimental procedures by eliminating the need for an excitation light source. This avoids photobleaching and minimizes undesired light signaling events that would be triggered by an external light source for fluorescence excitation. Adapting BRET to explore the light signaling events, BRET-plants; that is, plants expressing one RLUC-tagged and one YFP-tagged protein were generated by simultaneous dual T-DNA transformation, followed by the luminometer-based BRET assay. The resonance energy transfer was observed in two heterodimers, STH-RLUC and YFP-COP1 on the one hand as well as RLUC-HYH and YFP-HY5 on the other. In addition, the homodimerization of BRET-tagged HY5 supported the previous structural result (Yoon *et al*., 2007).

Previously, the standard protocol of the BRET experiment was established in the context of a transient transformation assay (Subramanian *et al*., 2004a). In Chapter II, the procedure of simultaneous dual T-DNA delivery was explained to generate BRET plants. Simultaneous dual T-DNA delivery has several advantages. The experimental time scale for generating BRET plants is reduced because the agrobacterial strains containing two different BRET expression cassettes are used for plant transformation. Furthermore, the two individual BRET expression cassettes can be separated by genetic segregation in the next generation since the two expression cassettes may not be genetically unlinked. The upgraded protocol may be helpful to guide new users of BRET towards successful research.

Chapter III provided new information on the enzymatic characteristics of *Renilla* luciferase (RLUC). Although the limited information about the reaction mechanism has been available, for the formulation of testable hypotheses about the reaction mechanism of RLUC, I performed computational analyses such as homology modeling of RLUC and the docking simulation with coelenterazine. The hypotheses were furthermore confirmed by mutagenesis, pharmacological inhibition, and luminescence spectroscopy.

In the crystal structure of RLUC8 carrying eight mutations (PDB ID, 2PSD; Loening *et al*., 2007a), six parallel β strands (β3-8), two antiparallel β strands (β1 and 2), and six α helices are folded as the α/β-hydrolase domain, on top of which there is a cap domain with three α helices, which form the substrate entrance (Loening *et al*., 2007a; Woo *et al*., 2008). The flexibility of the cap domain may result from the segment from W153 to I163, which showed high B-factors in the crystallography (Loening *et al*., 2007a). The active site of RLUC consists of a cavity that extends toward the middle of RLUC. In *Sphingomonas paucimobilis* LinB, Asp, Glu, and His serve as the catalytic triad for the hydrolytic dehalogenation of the haloalkane substrate, producing inorganic halide ions and alcohols as byproducts (Holmquist, 2000; Oakley *et al*., 2004). Results presented here suggest the equivalent residues, D120, E144, and H285, in RLUC are conserved not only structurally but also functionally in a similar capacity.

RLUC may have at least three different conformations (Fig. III-3). Coelenterazine must be located at the hydrophobic active site during the bioluminescence reaction and then the position of *Renilla* oxyluciferin may be rapidly changed to the secondary position where *Renilla* oxyluciferin exists near the gateway (Loening *et al*., 2007a). It is possible that the secondary position of byproduct, *Renilla* oxyluciferin, may be one of

positions in the middle of the dissociation of byproduct since a RLUC molecule can turn over around 100 coelenterazine molecules, indicating that the oxyluciferin should be released from the active site after bioluminescence reaction (Woo and von Arnim, in preparation). As proposed in Chapter III, the simulation showed that the 2-hydroperoxy group in the reaction intermediate may interact with E144, H285, and F261 while the para-hydroxyl group in the R1 hydroxy benzene and the hydroxyl group in the R3 ring may be engaged with N53 and F262, respectively. The putative binding position of the intermediate is agreement with mutagenesis results, showing that most mutants at those residues lose their activities (Woo *et al*., 2008). Taken all together, the understanding of the reaction mechanism may provide important insight for selection of new targets for mutagenesis. For example, if hydrophobicity in the active site is increased by protein engineering, water molecules may be excluded from the active site, resulting in the reduction of water-mediated resonance energy loss during bioluminescence reaction, as was observed for the active site of FLUC (Nakatsu *et al*., 2006). It is a speculative but quite promising scenario for next approach to identify improved RLUCs.

Renilla luciferase (RLUC) is being used in a variety of biological fields for gene expression assays, protein interaction studies, and *in vivo* biosensor applications (Bhaumik and Gambhir, 2002; De and Gambhir, 2005; Subramanian *et al*., 2006; Xu *et al*., 2007; Chan *et al*., 2008; Coulon *et al*., 2008). The broad range of applications of RLUC justifies the effort to generate new RLUC derivatives with improved enzymatic characteristics. For isolation of beneficial RLUC variants, random mutagenesis was employed to select new mutations that enhanced the intensity of photon emission and yielded more stable light emission over time. Two mutations, K189V and V267I, showed

increased affinity and activity, respectively. Including a previously reported mutation (M185V; Loening *et al*., 2006), a new triple mutant (SuperRLUC) was identified with advantageous enzymatic properties, such as increased k_{cat}, increased half-life, and higher resistance to high-concentration substrate inhibition. In parallel with SuperRLUC, it was found that mutations of proline 220 extended the half-life of photon emission, which yielded brighter signals when expressed in *E. coli*. Integration of the useful mutations into the codon-optimized RLUC, hRLUC, may expand the utilities of *Renilla* luciferase as a reporter protein, biosensor, or resonance energy donor of bioluminescence resonance energy transfer in heterologous host cells. New benefits from the isolated derivatives will be examined for our next challenge to capture BRET images at the subcellular level *in planta*.

REFERENCES

Abraham, E., Rigo, G., Szekely, G., Nagy, R., Koncz, C., and Szabados, L. (2003). Light-dependent induction of proline biosynthesis by abscisic acid and salt stress is inhibited by brassinosteroid in Arabidopsis. Plant Mol Biol **51,** 363-372.

Afolabi, A.S., Worland, B., Snape, J.W., and Vain, P. (2004). A large-scale study of rice plants transformed with different T-DNAs provides new insights into locus composition and T-DNA linkage configurations. Theor Appl Genet **109,** 815-826.

Ahmad, M., Lin, C., and Cashmore, A.R. (1995). Mutations throughout an Arabidopsis blue-light photoreceptor impair blue-light-responsive anthocyanin accumulation and inhibition of hypocotyl elongation. Plant J **8,** 653-658.

Anderson, J.M., and Cormier, M.J. (1973). Lumisomes, the cellular site of bioluminescence in coelenterates. J Biol Chem **248,** 2937-2943.

Ang, L.H., and Deng, X.W. (1994). Regulatory hierarchy of photomorphogenic loci: allele-specific and light-dependent interaction between the HY5 and COP1 loci. Plant Cell **6,** 613-628.

Ang, L.H., Chattopadhyay, S., Wei, N., Oyama, T., Okada, K., Batschauer, A., and Deng, X.W. (1998). Molecular interaction between COP1 and HY5 defines a regulatory switch for light control of Arabidopsis development. Mol Cell **1,** 213-222.

Bhaumik, S., and Gambhir, S.S. (2002). Optical imaging of Renilla luciferase reporter gene expression in living mice. Proc Natl Acad Sci U S A **99,** 377-382.

Branchini, B.R., Southworth, T.L., Murtiashaw, M.H., Wilkinson, S.R., Khattak, N.F., Rosenberg, J.C., and Zimmer, M. (2005). Mutagenesis evidence that the partial reactions of firefly bioluminescence are catalyzed by different conformations of the luciferase C-terminal domain. Biochemistry **44,** 1385-1393.

Campbell, A.K. (1974). Extraction, partial purification and properties of obelin, the calcium-activated luminescent protein from the hydroid Obelia geniculata. Biochem J **143,** 411-418.

Castillon, A., Shen, H., and Huq, E. (2007). Phytochrome interacting factors: central players in phytochrome-mediated light signaling networks. Trends Plant Sci **12,** 514-521.

Chan, C.T., Paulmurugan, R., Gheysens, O.S., Kim, J., Chiosis, G., and Gambhir, S.S. (2008). Molecular imaging of the efficacy of heat shock protein 90 inhibitors in living subjects. Cancer Res **68,** 216-226.

Clough, S.J., and Bent, A.F. (1998). Floral dip: a simplified method for Agrobacterium-mediated transformation of Arabidopsis thaliana. Plant J **16,** 735-743.

Conti, E., Franks, N.P., and Brick, P. (1996). Crystal structure of firefly luciferase throws light on a superfamily of adenylate-forming enzymes. Structure **4,** 287-298.

Cormier, M.J., Hori, K., and Karkhanis, Y.D. (1970). Studies on the bioluminescence of Renilla reniformis. VII. Conversion of luciferin into luciferyl sulfate by luciferin sulfokinase. Biochemistry **9,** 1184-1189.

Coulon, V., Audet, M., Homburger, V., Bockaert, J., Fagni, L., Bouvier, M., and Perroy, J. (2008). Subcellular imaging of dynamic protein interactions by bioluminescence resonance energy transfer. Biophys J **94,** 1001-1009.

Datta, S., Hettiarachchi, C., Johansson, H., and Holm, M. (2007). SALT TOLERANCE HOMOLOG2, a B-box protein in Arabidopsis that activates transcription and positively regulates light-mediated development. Plant Cell **19,** 3242-3255.

De, A., and Gambhir, S.S. (2005). Noninvasive imaging of protein-protein interactions from live cells and living subjects using bioluminescence resonance energy transfer. Faseb J **19,** 2017-2019.

de Wet, J.R., Wood, K.V., Helinski, D.R., and DeLuca, M. (1985). Cloning of firefly luciferase cDNA and the expression of active luciferase in Escherichia coli. Proc Natl Acad Sci U S A **82,** 7870-7873.

Deng, L., Markova, S.V., Vysotski, E.S., Liu, Z.J., Lee, J., Rose, J., and Wang, B.C. (2004). Crystal structure of a Ca2+-discharged photoprotein: implications for mechanisms of the calcium trigger and bioluminescence. J Biol Chem **279,** 33647-33652.

Deng, L., Vysotski, E.S., Liu, Z.J., Markova, S.V., Malikova, N.P., Lee, J., Rose, J., and Wang, B.C. (2001). Structural basis for the emission of violet bioluminescence from a W92F obelin mutant. FEBS Lett **506,** 281-285.

Deng, X.W., Caspar, T., and Quail, P.H. (1991). cop1: a regulatory locus involved in light-controlled development and gene expression in Arabidopsis. Genes Dev **5,** 1172-1182.

Deng, X.W., Matsui, M., Wei, N., Wagner, D., Chu, A.M., Feldmann, K.A., and Quail, P.H. (1992). COP1, an Arabidopsis regulatory gene, encodes a protein with both a zinc-binding motif and a G beta homologous domain. Cell **71,** 791-801.

Fankhauser, C., and Chory, J. (1997). Light control of plant development. Annu Rev Cell Dev Biol **13,** 203-229.

Fogel, M., and Hastings, J.W. (1972). Bioluminescence: mechanism and mode of control of scintillon activity. Proc Natl Acad Sci U S A **69,** 690-693.

Folta, K.M., and Spalding, E.P. (2001a). Unexpected roles for cryptochrome 2 and phototropin revealed by high-resolution analysis of blue light-mediated hypocotyl growth inhibition. Plant J **26,** 471-478.

Folta, K.M., and Spalding, E.P. (2001b). Opposing roles of phytochrome A and phytochrome B in early cryptochrome-mediated growth inhibition. Plant J **28,** 333-340.

Fraga, H. (2008). Firefly luminescence: A historical perspective and recent developments. Photochem Photobiol Sci **7,** 146-158.

Franks, N.P., Jenkins, A., Conti, E., Lieb, W.R., and Brick, P. (1998). Structural basis for the inhibition of firefly luciferase by a general anesthetic. Biophys J **75,** 2205-2211.

Frerichs-Deeken, U., Ranguelova, K., Kappl, R., Huttermann, J., and Fetzner, S. (2004). Dioxygenases without requirement for cofactors and their chemical model reaction: compulsory order ternary complex mechanism of 1H-3-hydroxy-4-oxoquinaldine 2,4-dioxygenase involving general base catalysis by histidine 251 and single-electron oxidation of the substrate dianion. Biochemistry **43,** 14485-14499.

Gyula, P., Schafer, E., and Nagy, F. (2003). Light perception and signalling in higher plants. Curr Opin Plant Biol **6,** 446-452.

Hart, R.C., Matthews, J.C., Hori, K., and Cormier, M.J. (1979). Renilla reniformis bioluminescence: luciferase-catalyzed production of nonradiating excited states from luciferin analogues and elucidation of the excited state species involved in energy transfer to Renilla green fluorescent protein. Biochemistry **18,** 2204-2210.

Hastings, J.W. (1971). Light to Hide by: Ventral Luminescence to Camouflage the Silhouette. Science **173,** 1016-1017.

Head, J.F., Inouye, S., Teranishi, K., and Shimomura, O. (2000). The crystal structure of the photoprotein aequorin at 2.3 A resolution. Nature **405,** 372-376.

Hink, M.A., Bisselin, T., and Visser, A.J. (2002). Imaging protein-protein interactions in living cells. Plant Mol Biol **50,** 871-883.

Holcik, M., Graber, T., Lewis, S.M., Lefebvre, C.A., Lacasse, E., and Baird, S. (2005). Spurious splicing within the XIAP 5' UTR occurs in the Rluc/Fluc but not the betagal/CAT bicistronic reporter system. Rna **11,** 1605-1609.

Holm, M., Hardtke, C.S., Gaudet, R., and Deng, X.W. (2001). Identification of a structural motif that confers specific interaction with the WD40 repeat domain of Arabidopsis COP1. Embo J **20,** 118-127.

Holm, M., Ma, L.G., Qu, L.J., and Deng, X.W. (2002). Two interacting bZIP proteins are direct targets of COP1-mediated control of light-dependent gene expression in Arabidopsis. Genes Dev **16,** 1247-1259.

Holmquist, M. (2000). Alpha/Beta-hydrolase fold enzymes: structures, functions and mechanisms. Curr Protein Pept Sci **1,** 209-235.

Hori, K., Nakano, Y., and Cormier, M.J. (1972). Studies on the bioluminescence of Renilla reniformis. XI. Location of the sulfate group in luciferyl sulfate. Biochim Biophys Acta **256,** 638-644.

Hoshino, H., Nakajima, Y., and Ohmiya, Y. (2007). Luciferase-YFP fusion tag with enhanced emission for single-cell luminescence imaging. Nat Methods **4,** 637-639.

Hu, C.A., Delauney, A.J., and Verma, D.P. (1992). A bifunctional enzyme (delta 1-pyrroline-5-carboxylate synthetase) catalyzes the first two steps in proline biosynthesis in plants. Proc Natl Acad Sci U S A **89,** 9354-9358.

Hu, C.D., Chinenov, Y., and Kerppola, T.K. (2002). Visualization of interactions among bZIP and Rel family proteins in living cells using bimolecular fluorescence complementation. Mol Cell **9,** 789-798.

Hynkova, K., Nagata, Y., Takagi, M., and Damborsky, J. (1999). Identification of the catalytic triad in the haloalkane dehalogenase from Sphingomonas paucimobilis UT26. FEBS Lett **446,** 177-181.

Indorf, M., Cordero, J., Neuhaus, G., and Rodriguez-Franco, M. (2007). Salt tolerance (STO), a stress-related protein, has a major role in light signalling. Plant J **51,** 563-574.

Inouye, S., and Sasaki, S. (2007). Imidazole-assisted catalysis of luminescence reaction in blue fluorescent protein from the photoprotein aequorin. Biochem Biophys Res Commun **354,** 650-655.

Inouye, S., Watanabe, K., Nakamura, H., and Shimomura, O. (2000). Secretional luciferase of the luminous shrimp Oplophorus gracilirostris: cDNA cloning of a novel imidazopyrazinone luciferase(1). FEBS Lett **481,** 19-25.

Kang, B., Grancher, N., Koyffmann, V., Lardemer, D., Burney, S., and Ahmad, M. (2008). Multiple interactions between cryptochrome and phototropin blue-light signalling pathways in Arabidopsis thaliana. Planta.

Karkhanis, Y.D., and Cormier, M.J. (1971). Isolation and properties of Renilla reniformis luciferase, a low molecular weight energy conversion enzyme. Biochemistry **10,** 317-326.

Kim, H.J., Kim, Y.K., Park, J.Y., and Kim, J. (2002). Light signalling mediated by phytochrome plays an important role in cold-induced gene expression through the C-repeat/dehydration responsive element (C/DRE) in Arabidopsis thaliana. Plant J **29,** 693-704.

Kim, W.Y., Fujiwara, S., Suh, S.S., Kim, J., Kim, Y., Han, L., David, K., Putterill, J., Nam, H.G., and Somers, D.E. (2007). ZEITLUPE is a circadian photoreceptor stabilized by GIGANTEA in blue light. Nature **449,** 356-360.

Koo, J.A., Schmidt, S.P., and Schuster, G.B. (1978). Bioluminescence of the firefly: key steps in the formation of the electronically excited state for model systems. Proc Natl Acad Sci U S A **75,** 30-33.

Landy, A. (1989). Dynamic, structural, and regulatory aspects of lambda site-specific recombination. Annu Rev Biochem **58,** 913-949.

Li, L., Hong, R., and Hastings, J.W. (1997). Three functional luciferase domains in a single polypeptide chain. Proc Natl Acad Sci U S A **94,** 8954-8958.

Lippuner, V., Cyert, M.S., and Gasser, C.S. (1996). Two classes of plant cDNA clones differentially complement yeast calcineurin mutants and increase salt tolerance of wild-type yeast. J Biol Chem **271,** 12859-12866.

Liu, Z.J., Vysotski, E.S., Chen, C.J., Rose, J.P., Lee, J., and Wang, B.C. (2000). Structure of the Ca2+-regulated photoprotein obelin at 1.7 A resolution determined directly from its sulfur substructure. Protein Sci **9,** 2085-2093.

Liu, Z.J., Stepanyuk, G.A., Vysotski, E.S., Lee, J., Markova, S.V., Malikova, N.P., and Wang, B.C. (2006). Crystal structure of obelin after Ca2+-triggered bioluminescence suggests neutral coelenteramide as the primary excited state. Proc Natl Acad Sci U S A **103,** 2570-2575.

Lloyd, J.E. (1965). Aggressive Mimicry in Photuris: Firefly Femmes Fatales. Science **149,** 653-654.

Loening, A.M., Fenn, T.D., and Gambhir, S.S. (2007a). Crystal structures of the luciferase and green fluorescent protein from Renilla reniformis. J Mol Biol **374,** 1017-1028.

Loening, A.M., Wu, A.M., and Gambhir, S.S. (2007b). Red-shifted Renilla reniformis luciferase variants for imaging in living subjects. Nat Methods **4,** 641-643.

Loening, A.M., Fenn, T.D., Wu, A.M., and Gambhir, S.S. (2006). Consensus guided mutagenesis of Renilla luciferase yields enhanced stability and light output. Protein Eng Des Sel **19,** 391-400.

Lorenz, W.W., McCann, R.O., Longiaru, M., and Cormier, M.J. (1991). Isolation and expression of a cDNA encoding Renilla reniformis luciferase. Proc Natl Acad Sci U S A **88,** 4438-4442.

Luker, G.D., Bardill, J.P., Prior, J.L., Pica, C.M., Piwnica-Worms, D., and Leib, D.A. (2002). Noninvasive bioluminescence imaging of herpes simplex virus type 1 infection and therapy in living mice. J Virol **76,** 12149-12161.

Mach, H., Middaugh, C.R., and Lewis, R.V. (1992). Statistical determination of the average values of the extinction coefficients of tryptophan and tyrosine in native proteins. Anal Biochem **200,** 74-80.

Marek, J., Vevodova, J., Smatanova, I.K., Nagata, Y., Svensson, L.A., Newman, J., Takagi, M., and Damborsky, J. (2000). Crystal structure of the haloalkane dehalogenase from Sphingomonas paucimobilis UT26. Biochemistry **39,** 14082-14086.

Markova, S.V., Vysotski, E.S., Blinks, J.R., Burakova, L.P., Wang, B.C., and Lee, J. (2002). Obelin from the bioluminescent marine hydroid Obelia geniculata: cloning, expression, and comparison of some properties with those of other Ca2+-regulated photoproteins. Biochemistry **41,** 2227-2236.

Matthews, J.C., Hori, K., and Cormier, M.J. (1977a). Purification and properties of Renilla reniformis luciferase. Biochemistry **16,** 85-91.

Matthews, J.C., Hori, K., and Cormier, M.J. (1977b). Substrate and substrate analogue binding properties of Renilla luciferase. Biochemistry **16,** 5217-5220.

Minko, I., Holloway, S.P., Nikaido, S., Carter, M., Odom, O.W., Johnson, C.H., and Herrin, D.L. (1999). Renilla luciferase as a vital reporter for chloroplast gene expression in Chlamydomonas. Mol Gen Genet **262,** 421-425.

Miyawaki, A., Llopis, J., Heim, R., McCaffery, J.M., Adams, J.A., Ikura, M., and Tsien, R.Y. (1997). Fluorescent indicators for Ca2+ based on green fluorescent proteins and calmodulin. Nature **388,** 882-887.

Moncrief, N.D., Kretsinger, R.H., and Goodman, M. (1990). Evolution of EF-hand calcium-modulated proteins. I. Relationships based on amino acid sequences. J Mol Evol **30,** 522-562.

Morse, D., Milos, P.M., Roux, E., and Hastings, J.W. (1989). Circadian regulation of bioluminescence in Gonyaulax involves translational control. Proc Natl Acad Sci U S A **86,** 172-176.

Nagaoka, S., and Takano, T. (2003). Salt tolerance-related protein STO binds to a Myb transcription factor homologue and confers salt tolerance in Arabidopsis. J Exp Bot **54,** 2231-2237.

Nakajima, Y., Kobayashi, K., Yamagishi, K., Enomoto, T., and Ohmiya, Y. (2004). cDNA cloning and characterization of a secreted luciferase from the luminous Japanese ostracod, Cypridina noctiluca. Biosci Biotechnol Biochem **68,** 565-570.

Nakamura, H., Wu, C., Murai, A., Inouye, S., and Shimomura, O. (1997). Efficient bioluminescence of bisdeoxycoelenterazine with the luciferase of a Deep-sea shrimp Oplophorus. Tetrahedron Lett **38,** 6405-6406.

Nakatsu, T., Ichiyama, S., Hiratake, J., Saldanha, A., Kobashi, N., Sakata, K., and Kato, H. (2006). Structural basis for the spectral difference in luciferase bioluminescence. Nature **440,** 372-376.

Neff, M.M., and Chory, J. (1998). Genetic interactions between phytochrome A, phytochrome B, and cryptochrome 1 during Arabidopsis development. Plant Physiol **118,** 27-35.

Oakley, A.J., Klvana, M., Otyepka, M., Nagata, Y., Wilce, M.C., and Damborsky, J. (2004). Crystal structure of haloalkane dehalogenase LinB from Sphingomonas paucimobilis UT26 at 0.95 A resolution: dynamics of catalytic residues. Biochemistry **43,** 870-878.

Ohmiya, Y., and Tsuji, F.I. (1993). Bioluminescence of the Ca(2+)-binding photoprotein, aequorin, after histidine modification. FEBS Lett **320,** 267-270.

Ohmiya, Y., and Hirano, T. (1996). Shining the light: the mechanism of the bioluminescence reaction of calcium-binding photoproteins. Chem Biol **3,** 337-347.

Ohmiya, Y., Ohashi, M., and Tsuji, F.I. (1992). Two excited states in aequorin bioluminescence induced by tryptophan modification. FEBS Lett **301,** 197-201.

Okamoto, O.K., Liu, L., Robertson, D.L., and Hastings, J.W. (2001). Members of a dinoflagellate luciferase gene family differ in synonymous substitution rates. Biochemistry **40,** 15862-15868.

Osterlund, M.T., Hardtke, C.S., Wei, N., and Deng, X.W. (2000). Targeted destabilization of HY5 during light-regulated development of Arabidopsis. Nature **405,** 462-466.

Otto-Duessel, M., Khankaldyyan, V., Gonzalez-Gomez, I., Jensen, M.C., Laug, W.E., and Rosol, M. (2006). In vivo testing of Renilla luciferase substrate analogs in an orthotopic murine model of human glioblastoma. Mol Imaging **5,** 57-64.

Oyama, T., Shimura, Y., and Okada, K. (1997). The Arabidopsis HY5 gene encodes a bZIP protein that regulates stimulus-induced development of root and hypocotyl. Genes Dev **11,** 2983-2995.

Paulmurugan, R., and Gambhir, S.S. (2003). Monitoring protein-protein interactions using split synthetic renilla luciferase protein-fragment-assisted complementation. Anal Chem **75,** 1584-1589.

Penfield, S., Josse, E.M., Kannangara, R., Gilday, A.D., Halliday, K.J., and Graham, I.A. (2005). Cold and light control seed germination through the bHLH transcription factor SPATULA. Curr Biol **15,** 1998-2006.

Ridgway, E.B., and Ashley, C.C. (1967). Calcium transients in single muscle fibers. Biochem Biophys Res Commun **29,** 229-234.

Saijo, Y., Sullivan, J.A., Wang, H., Yang, J., Shen, Y., Rubio, V., Ma, L., Hoecker, U., and Deng, X.W. (2003). The COP1-SPA1 interaction defines a critical step in phytochrome A-mediated regulation of HY5 activity. Genes Dev **17,** 2642-2647.

Sawa, M., Nusinow, D.A., Kay, S.A., and Imaizumi, T. (2007). FKF1 and GIGANTEA complex formation is required for day-length measurement in Arabidopsis. Science **318,** 261-265.

Schultz, L.W., Liu, L., Cegielski, M., and Hastings, J.W. (2005). Crystal structure of a pH-regulated luciferase catalyzing the bioluminescent oxidation of an open tetrapyrrole. Proc Natl Acad Sci U S A **102,** 1378-1383.

Schwede, T., Kopp, J., Guex, N., and Peitsch, M.C. (2003). SWISS-MODEL: An automated protein homology-modeling server. Nucleic Acids Res **31,** 3381-3385.

Seliger, H.H., and McElroy, W.D. (1964). The Colors Of Firefly Bioluminescence: Enzyme Configuration And Species Specificity. Proc Natl Acad Sci U S A **52,** 75-81.

Seo, H.S., Yang, J.Y., Ishikawa, M., Bolle, C., Ballesteros, M.L., and Chua, N.H. (2003). LAF1 ubiquitination by COP1 controls photomorphogenesis and is stimulated by SPA1. Nature **423,** 995-999.

Shimomura, O. (1995). Cause of spectral variation in the luminescence of semisynthetic aequorins. Biochem J **306 (Pt 2),** 537-543.

Shimomura, O., and Johnson, F.H. (1975). Regeneration of the photoprotein aequorin. Nature **256,** 236-238.

Sibout, R., Sukumar, P., Hettiarachchi, C., Holm, M., Muday, G.K., and Hardtke, C.S. (2006). Opposite root growth phenotypes of hy5 versus hy5 hyh mutants correlate with increased constitutive auxin signaling. PLoS Genet **2,** e202.

Spurlock, B.O., and Cormier, M.J. (1975). A fine structure study of the anthocodium in Renilla mulleri. Evidence for the existence of a bioluminescent organelle, the luminelle. J Cell Biol **64,** 15-28.

Stacey, M.G., Hicks, S.N., and von Arnim, A.G. (1999). Discrete domains mediate the light-responsive nuclear and cytoplasmic localization of Arabidopsis COP1. Plant Cell **11,** 349-364.

Stacey, M.G., Kopp, O.R., Kim, T.H., and von Arnim, A.G. (2000). Modular domain structure of Arabidopsis COP1. Reconstitution of activity by fragment complementation and mutational analysis of a nuclear localization signal in planta. Plant Physiol **124,** 979-990.

Stefan, E., Aquin, S., Berger, N., Landry, C.R., Nyfeler, B., Bouvier, M., and Michnick, S.W. (2007). Quantification of dynamic protein complexes using Renilla luciferase fragment complementation applied to protein kinase A activities in vivo. Proc Natl Acad Sci U S A **104,** 16916-16921.

Stepanyuk, G.A., Golz, S., Markova, S.V., Frank, L.A., Lee, J., and Vysotski, E.S. (2005). Interchange of aequorin and obelin bioluminescence color is determined by substitution of one active site residue of each photoprotein. FEBS Lett **579,** 1008-1014.

Streltsov, V.A., Prokop, Z., Damborsky, J., Nagata, Y., Oakley, A., and Wilce, M.C. (2003). Haloalkane dehalogenase LinB from Sphingomonas paucimobilis UT26: X-ray crystallographic studies of dehalogenation of brominated substrates. Biochemistry **42,** 10104-10112.

Subramanian, C., Xu, Y., Johnson, C.H., and von Arnim, A.G. (2004a). In vivo detection of protein-protein interaction in plant cells using BRET. Methods Mol Biol **284,** 271-286.

Subramanian, C., Kim, B.H., Lyssenko, N.N., Xu, X., Johnson, C.H., and von Arnim, A.G. (2004b). The Arabidopsis repressor of light signaling, COP1, is regulated by nuclear exclusion: mutational analysis by bioluminescence resonance energy transfer. Proc Natl Acad Sci U S A **101,** 6798-6802.

Subramanian, C., Woo, J., Cai, X., Xu, X., Servick, S., Johnson, C.H., Nebenfuhr, A., and von Arnim, A.G. (2006). A suite of tools and application notes for in vivo protein interaction assays using bioluminescence resonance energy transfer (BRET). Plant J **48,** 138-152.

Thompson, E.M., Nagata, S., and Tsuji, F.I. (1989). Cloning and expression of cDNA for the luciferase from the marine ostracod Vargula hilgendorfii. Proc Natl Acad Sci U S A **86,** 6567-6571.

Thomsen, R., and Christensen, M.H. (2006). MolDock: a new technique for high-accuracy molecular docking. J Med Chem **49,** 3315-3321.

Torii, K.U., McNellis, T.W., and Deng, X.W. (1998). Functional dissection of Arabidopsis COP1 reveals specific roles of its three structural modules in light control of seedling development. Embo J **17,** 5577-5587.

Tsien, R.Y. (1998). The green fluorescent protein. Annu Rev Biochem **67,** 509-544.

Ugarova, N.N., Maloshenok, L.G., Uporov, I.V., and Koksharov, M.I. (2005). Bioluminescence spectra of native and mutant firefly luciferases as a function of pH. Biochemistry (Mosc) **70,** 1262-1267.

Venisnik, K.M., Olafsen, T., Loening, A.M., Iyer, M., Gambhir, S.S., and Wu, A.M. (2006). Bifunctional antibody-Renilla luciferase fusion protein for in vivo optical detection of tumors. Protein Eng Des Sel **19,** 453-460.

Villalobos, V., Naik, S., and Piwnica-Worms, D. (2007). Current state of imaging protein-protein interactions in vivo with genetically encoded reporters. Annu Rev Biomed Eng **9,** 321-349.

Viviani, V.R., Arnoldi, F.G., Neto, A.J., Oehlmeyer, T.L., Bechara, E.J., and Ohmiya, Y. (2008). The structural origin and biological function of pH-sensitivity in firefly luciferases. Photochem Photobiol Sci **7,** 159-169.

von Arnim, A., and Deng, X.W. (1996). Light Control Of Seedling Development. Annu Rev Plant Physiol Plant Mol Biol **47,** 215-243.

von Arnim, A.G., and Deng, X.W. (1993). Ring finger motif of Arabidopsis thaliana COP1 defines a new class of zinc-binding domain. J Biol Chem **268,** 19626-19631.

von Arnim, A.G., and Deng, X.W. (1994). Light inactivation of Arabidopsis photomorphogenic repressor COP1 involves a cell-specific regulation of its nucleocytoplasmic partitioning. Cell **79,** 1035-1045.

von Arnim, A.G., Osterlund, M.T., Kwok, S.F., and Deng, X.W. (1997). Genetic and developmental control of nuclear accumulation of COP1, a repressor of photomorphogenesis in Arabidopsis. Plant Physiol **114,** 779-788.

Vysotski, E.S., and Lee, J. (2004). Ca2+-regulated photoproteins: structural insight into the bioluminescence mechanism. Acc Chem Res **37,** 405-415.

Vysotski, E.S., Liu, Z.J., Markova, S.V., Blinks, J.R., Deng, L., Frank, L.A., Herko, M., Malikova, N.P., Rose, J.P., Wang, B.C., and Lee, J. (2003). Violet bioluminescence and fast kinetics from W92F obelin: structure-based proposals for the bioluminescence triggering and the identification of the emitting species. Biochemistry **42,** 6013-6024.

Wannlund, J., DeLuca, M., Stempel, K., and Boyer, P.D. (1978). Use of 14C-carboxyl-luciferin in determining the mechanism of the firefly luciferase catalyzed reactions. Biochem Biophys Res Commun **81,** 987-992.

Ward, W.W., and Cormier, M.J. (1979). An energy transfer protein in coelenterate bioluminescence. Characterization of the Renilla green-fluorescent protein. J Biol Chem **254,** 781-788.

Watkins, N.J., and Campbell, A.K. (1993). Requirement of the C-terminal proline residue for stability of the Ca(2+)-activated photoprotein aequorin. Biochem J **293 (Pt 1),** 181-185.

Wilson, T., and Hastings, J.W. (1998). Bioluminescence. Annu Rev Cell Dev Biol **14,** 197-230.

Woo, J.C., Howell, M.H., and von Arnim, A.G. (2008). Structure-function studies on the active site of the coelenterazine-dependent luciferase from Renilla. Protein Sci **17,** 725-735.

Xu, X., Soutto, M., Xie, Q., Servick, S., Subramanian, C., von Arnim, A.G., and Johnson, C.H. (2007). Imaging protein interactions with bioluminescence resonance energy transfer (BRET) in plant and mammalian cells and tissues. Proc Natl Acad Sci U S A **104,** 10264-10269.

Xu, Y., Piston, D.W., and Johnson, C.H. (1999). A bioluminescence resonance energy transfer (BRET) system: application to interacting circadian clock proteins. Proc Natl Acad Sci U S A **96,** 151-156.

Yamaguchi, S., Smith, M.W., Brown, R.G., Kamiya, Y., and Sun, T. (1998). Phytochrome regulation and differential expression of gibberellin 3beta-hydroxylase genes in germinating Arabidopsis seeds. Plant Cell **10,** 2115-2126.

Yamauchi, Y., Ogawa, M., Kuwahara, A., Hanada, A., Kamiya, Y., and Yamaguchi, S. (2004). Activation of gibberellin biosynthesis and response pathways by low temperature during imbibition of Arabidopsis thaliana seeds. Plant Cell **16,** 367-378.

Yegutkin, G.G., Samburski, S.S., and Jalkanen, S. (2003). Soluble purine-converting enzymes circulate in human blood and regulate extracellular ATP level via counteracting pyrophosphatase and phosphotransfer reactions. Faseb J **17,** 1328-1330.

Yoon, M.K., Kim, H.M., Choi, G., Lee, J.O., and Choi, B.S. (2007). Structural basis for the conformational integrity of the Arabidopsis thaliana HY5 leucine zipper homodimer. J Biol Chem **282,** 12989-13002.

Yoshiba, Y., Kiyosue, T., Katagiri, T., Ueda, H., Mizoguchi, T., Yamaguchi-Shinozaki, K., Wada, K., Harada, Y., and Shinozaki, K. (1995). Correlation between the induction of a gene for delta 1-pyrroline-5-carboxylate synthetase and the accumulation of proline in Arabidopsis thaliana under osmotic stress. Plant J **7,** 751-760.

Yu, X., Shalitin, D., Liu, X., Maymon, M., Klejnot, J., Yang, H., Lopez, J., Zhao, X., Bendehakkalu, K.T., and Lin, C. (2007). Derepression of the NC80 motif is critical for the photoactivation of Arabidopsis CRY2. Proc Natl Acad Sci U S A **104,** 7289-7294.

Yu, Y.A., Timiryasova, T., Zhang, Q., Beltz, R., and Szalay, A.A. (2003). Optical imaging: bacteria, viruses, and mammalian cells encoding light-emitting proteins reveal the locations of primary tumors and metastases in animals. Anal Bioanal Chem **377,** 964-972.

VITA

Jongchan Woo was born at Youngil-County in Gyeongsangbuk-Do, South Korea on July 30, 1970. He went to Kyonggi University in 1990 and enlisted in the Korean Air Force from 1991 to 1993. After his military service, he received a B.S. in Biology in 1997. He served his internship at the National Veterinary Research and Quarantine Service in 1997. In 1998, he went to Seoul National University, and then earned a M.S. in Biology in 2000. From 2002 to 2008, he has been in Ph.D. program of the Department of Botany at the University of Tennessee, Knoxville and is going to receive a Ph.D. degree in May 2008.

Currently, Jongchan is a postdoctoral fellow appointee in Rockefeller University, New York, NY.